Cholesterol transbilayer distribution and its impact on microdomains in the mammalian cell plasma membrane

Kevin Courtney

A thesis submitted to the
Faculty of Graduate and Postdoctoral Studies
in partial fulfillment of the requirements for the
Doctorate in Philosophy degree in Biochemistry

Department of Biochemistry, Microbiology and Immunology
Faculty of Medicine
University of Ottawa

Abstract

The plasma membrane (PM) of live cells has a striking phospholipid asymmetry between bilayer leaflets, yet the purpose of this fundamental structure remains elusive. It is also unknown whether and how this phospholipid asymmetry impacts on the lateral organization of the PM, such as microdomains or lipid rafts that are thought to facilitate specific protein-protein interactions. Here, we generated asymmetric giant unilamellar vesicles (GUVs) and found that microdomain formation is inhibited by outer leaflet very long acyl chain (24:0) sphingomyelin (SM), the primary sphingolipid species in mammalian cells. Interestingly, although cholesterol is believed to associate favourably with SM, molecular dynamic (MD) simulations of asymmetric membranes indicate a strong preference for cholesterol in the inner leaflet when 24:0 SM is in the outer leaflet, as well as, interdigitation of 24:0 SM acyl chain across the centre of the bilayer. We thus hypothesized that the outer leaflet-localized 24:0 SM interdigitates across the leaflets of the bilayer and facilitates cholesterol enrichment in the inner leaflet. Indeed, we obtained evidence that, in asymmetric unilamellar vesicles with 24:0 SM exclusively in the outer leaflet, 75-80% of cholesterol was partitioned into the inner leaflet, which was correlated with the disappearance of microdomains in GUVs. Importantly, in live cell PM, where 24:0 sphingolipids are the predominant species and exclusively in the outer leaflet, cholesterol was similarly enriched in the cytoplasmic leaflet. SM with shorter acyl chains such as 16:0, a minor species in mammalian cells, failed to generate cholesterol asymmetry and promoted microdomains in both symmetric and asymmetric GUVs. Furthermore, we generated live mammalian cells with either 16:0 or 24:0 SM and analyzed submicron domains in these cells, using density-dependent FRET of GPI-anchored proteins. Indeed, 16:0 SM cells are capable of forming submicron domains. The 24:0 SM cells, by contrast, are nearly devoid of

submicron domains, as are unmodified control cells. Moreover, we silenced ceramide synthase 2 (CerS2), the enzyme that generates very long acyl chain sphingolipids. We found that silencing CerS2 alters diffusional properties of membrane proteins, consistent with enhanced microdomain formation. Together, our results establish a surprising and central role of very long acyl chain sphingolipids in regulating membrane lateral organization, including in the native plasma membrane, by creating cholesterol asymmetry. We propose that sphingolipid asymmetry functions to dynamically regulate microdomains in live cells.

Acknowledgements

I am grateful to my supervisor, Dr. Xiaohui Zha, for providing guidance and expertise throughout my time at the University of Ottawa. I am also grateful for the opportunity to work with each of the members of the Zha lab, past and present. I am very appreciative of Dr. Alexander Sorisky who provides excellent support and advice. Furthermore, Dr. Sorisky's lab members, Dr. AnneMarie Gagnon and Anne Landry were very helpful both technically and intellectually throughout my degree. I am also grateful for the collaborative work in producing molecular dynamics simulation data with Himanshu Khandelia, Weria Pezeshkian and John Ispen from the MEMPHYS, Center for Biomembrane Physics at the University of Southern Denmark. Throughout the degree research, I had several thesis advisory committee members, Drs. Jay Baltz, Alexander Sorisky, John Pezacki, Nuch Tanphaichitr and John Baenziger. Each of them were excellent advisors and helpful in the progression of my work. I also received, much appreciated, guidance from Dr. John Presley from McGill University. From an administrative perspective, I also really appreciated Victoria Stewart in the biochemistry department, who was a very kind and excellent resource.

Table of contents

Abbreviations

16:0 SM	N-palmitoyl-D-*erythro*-sphingosylphosphorylcholine
24:0 SM	N-lignoceroyl-D-*erythro*-sphingosylphosphorylcholine
24:1 SM	N-nervonoyl-D-*erythro*-sphingosylphosphorylcholine
αCD	Alpha cyclodextrin
βCD	Beta-cyclodextrin
γCD	Gamma-cyclodextrin
ABCA1	ATP-binding cassette transporter A1
ABCG1	ATP-binding cassette transporter G1
AC	Alternating current
ACAT2	Acetyl-coenzyme A acetyltransferase 2
AFM	Atomic force microscopy
ApoA1	Apolipoprotein A1
ApoB100	Apolipoprotein B100
bSM	Brain sphingomyelin
CD	cyclodextrin
CerS	ceramide synthase
CERT	Ceramide transfer protein
CFP	Cyan fluorescent protein
CHOL	Cholesterol
CTL	Cholestatrienol
DC	Direct current
DHE	Dehydroergosterol
DiIC16	1,1'-dihexadecyl-3,3,3',3'-tetramethylindocarbocyanine perchlorate

DiIC18	1,1'-dioctadecyl-3,3,3',3'-tetramethylindocarbocyanine perchlorate
DLS	Dynamic light scattering
DMEM	Dulbecco's modified eagle medium
DMPC	1,2-dimyritoyl-*sn*-glycero-3-phosphocholine
DPH	l,6-diphenyl-l,3,5-hexatriene
DSPC	1,2-distearoyl-*sn*-glycero-3-phosphocholine
DOPC	1,2-dioleoyl-*sn*-glycero-3-phosphocholine
DOPE	1,2-dioleoyl-*sn*-glycero-3-phosphoethanolamine
DPPC	1,2-dipalmitoy-*sn*-glycero-3-phosphocholine
DPPE	1,2-dipalmitoy-*sn*-glycero-3-phosphoethanolamine
DRM	Detergent resistant membrane(s)
ELOVL	Elongation of very long chain fatty acids
ER	Endoplasmic reticulum
eSM	Egg sphingomyelin
FCS	Fluorescence correlation spectroscopy
FLIM	Fluorescence lifetime imaging microscopy
FMMP	Formyl-methionyl (sulphone) methyl phosphate;
FRAP	Fluorescence recovery after photobleaching
FRET	Förster resonance energy transfer
GFP	Green fluorescent protein
GPI-anchored protein	Glycosylphosphatitylinositol-anchored protein
GUV	Giant unilamellar vesicle
HDL	High density lipoprotein
HMG-CoA	3-hydroxy-3-methylglutaryl-coenzyme A

HP-αCD	Hydroxypropyl alpha-cyclodextrin
INSIG	Insulin induced gene
IDL	Intermediate density lipoprotein
ITO	Indium tin oxide
LCAT	Lecithin-cholesterol acyltransferase
LDL	Low density lipoprotein
lo	Liquid ordered
ld	Liquid disordered
LUV	Large unilamellar vesicle
LXR	Liver X receptor
M+FB1	Myriocin and fumonisin b1
MLV	Multilamellar vesicle
NADPH	Nicotinamide adenine dinucleotide phosphate
NAP	Naphtho[2,3-*a*]pyrene
NBD-DOPE	1,2-dioleoyl-*sn*-glycero-3-phosphoethanolamine-N-(7-nitro-2-1,3-benzoxadiazol-4-yl
NBD-DPPE	1,2-dipalmitoyl-*sn*-glycero-3-phosphoethanolamine-N-(7-nitro-2-1,3-benzoxadiazol-4-yl
ORP	OSBP-related protein
OSBP	Oxysterol binding protein
PA	Phosphatidic acid
PBS	Phosphate buffered saline
PC	Phosphatidylcholine
PH domain	Pleckstrin homology domain
POPC	1-palmitoyl-2-oleoyl-*sn*-glycero-3-phosphocholine
POPE	1-palmitoyl-2-oleoyl-*sn*-glycero-3-phosphoethanolamine

POPS	1-palmitoyl-2-oleoyl-*sn*-glycero-3-phosphoserine
PE	Phosphatidylethanolamine
PG	Phosphatidylglycerol
PI	Phosphatidylinositol
PM	Plasma Membrane
PS	Phosphatidylserine
RCT	Reverse cholesterol transport
Rho-DOPE	Lissamine™ rhodamine B 1,2-dioleoyl-*sn*-glycero-3-phosphoethanolamine
Rho-DPPE	Lissamine™ rhodamine B 1,2-dipalmitoyl-*sn*-glycero-3-phosphoethanolamine
SCAP	SREBP-cleavage-activating-protein
SREBP	Sterol regulatory element binding protein
StAR	Steroidogenic acute regulatory protein
STARD4	StAR-related lipid transfer protein 4
START	StAR-related lipid transfer
SUV	Small unilamellar vesicle
SM	Sphingomyelin
TBS	Tris buffered saline
TLC	Thin layer chromatography
Thy-1	Thymocyte differentiation antigen 1
TLC	Thin layer chromatography
TLR4	Toll-like receptor 4
Tm	Lipid melting temperature/ transition temperature
TMA-DPH	1-(4-(trimethylamino)phenyl)-6-phenylhexa-1,3,5-triene
TNBS	Trinitrobenzene sulfonic acid

TX-100	Triton X-100
VAP	Vesicle associated membrane protein-associated protein
VLAC	Very long acyl chain
VLDL	Very low density lipoprotein
YFP	Yellow fluorescent protein

List of Figures

List of Tables

Chapter 1 - Introduction

1.1 - Overview

The proteins and phospholipids of the mammalian cell plasma membrane are long known to be maintained asymmetrically across the bilayer. The partitioning of cholesterol between leaflets of the plasma membrane, however, is still debated. Contrary to proteins and phospholipids, cholesterol can easily flip-flop between the leaflets in a bilayer membrane, which imposes technical challenges to determine cholesterol in a leaflet specific fashion. Because of this, previous attempts to determine the cholesterol bilayer distribution in mammalian cells were contradictory and often poorly supported by experimental evidence. More recently, an alternative strategy has been published using fluorescent analogues of cholesterol, which suggested that native cholesterol may be primarily located in the inner leaflet of the PM (Mondal et al., 2009; Schroeder et al., 1991). Although this result is based on sterols with minor structural modifications, the idea that cholesterol could be mostly in the inner leaflet would have significant implications for structure and organization of the PM. We thus wondered if native cholesterol is similarly partitioned in live cells and how this asymmetry is maintained, which served as the basis for the thesis project. In particular, cholesterol is thought to promote the formation of ordered lateral microdomains in the PM. The current models of microdomain formation, however, overlook two unique characteristics of the PM, namely (a) phospholipid asymmetry and (b) the abundance sphingolipids with very long acyl chains. We thus aimed to develop a method to characterize cholesterol partitioning between leaflets and apply it to mammalian cells. Furthermore, we also aimed to understand the mechanisms that govern cholesterol partitioning and the subsequent consequences of cholesterol asymmetry. We indeed observed that membrane cholesterol can

be highly asymmetric between the bilayer leaflets and this is governed by very long acyl chain (VLAC) sphingomyelin (SM), such as 24:0 SM. When VLAC sphingolipids reside in the outer leaflet of the unilamellar vesicles or the PM, cholesterol is mostly found in the inner or cytoplasmic leaflet. Importantly, by creating cholesterol asymmetry, the VLAC sphingolipids suppress membrane microdomains in both GUVs and live mammalian cells. Conversely, altering the acyl chain length of sphingolipids to 16:0 SM, a common SM used in model membrane studies, enhanced microdomains, which is also correlated with an even cholesterol partitioning between leaflets. This work, therefore, establishes for the first time that cholesterol is mostly in the cytoplasmic leaflet of the PM in the live cells and that sphingolipid acyl chain length is critical for the lateral organization of the PM.

1.2 - Membrane lipids

The mammalian cell is an entity defined by a limiting bilayer lipid membrane, or the plasma membrane. It is also compartmentalized, within the plasma membrane, into specialized organelles by limiting endo-membranes (Diekmann and Pereira-Leal, 2013). In addition to this structural role, the membranes participate in maintaining cellular homeostasis by regulating protein-protein interactions, cell signalling and trafficking of cargo throughout the cell (Lingwood and Simons, 2010; Simons and Ikonen, 1997). The majority of lipids in a membrane, such as the glycerophospholipids, are composed of a hydrophilic head that is covalently linked to a glycerol backbone and anchored into the membrane by two hydrocarbon chains of varying lengths (Fahy et al., 2005). As a result, these lipids are amphipathic and can self-assemble into a membrane bilayer by sequestering the acyl chains away from the surrounding environment (Israelachvili et al., 1977). There are over 500 unique lipid species in mammalian cells. The phospholipids can be subdivided into groups

based on their hydrophilic constituent, or head group (Quehenberger et al., 2010). The most abundant lipids in mammalian cells are phosphatidylcholines (PC), which represent a high percentage of lipid in all membrane compartments (Gerl et al., 2012). The other major groups of membrane lipids are phosphatidylethanolamine (PE), phosphatidylserine (PS), phosphatidylinositol (PI), phosphatidic acid (PA) and phosphatidylglycerol (PG) (Gerl et al., 2012). Other membrane lipids are also present, but in low abundance (Quehenberger et al., 2010). The structures of lipids that are most relevant to this thesis are summarized in **Table 1**.

Another major class of lipids, which primarily reside in the plasma membrane, are the sphingolipids. In contrast to the phospholipid glycerol backbone, the core feature of the sphingolipid group is the sphingoid backbone, such as sphingosine (Chen et al., 2010). Sphingosine structurally resembles a 16 or 18 carbon monoacylglycerol (single acyl chain lipid) and is the precursor to many sphingolipids (Gault et al., 2010). During sphingolipid synthesis, sphingosine can be modified with the addition of a head group moiety and/or a single fatty acid chain of various lengths to form a structure analogous to glycerophospholipids (Chen et al., 2010). Acylated sphingolipids are also primarily categorized by their head group constituent. The most abundant mammalian sphingolipid is sphingomyelin (SM), which contains a phospho-choline head group similar to PC. Other major sphingolipids are glycosphingolipids and ceramides (Gerl et al., 2012). Glycosphingolipids are characterized by one or more sugar residues as a head group, whereas, ceramides contain a hydroxyl group (Chen et al., 2010). Although in low abundance, ceramide-1-phosphate or lyso-sphingolipids, such as sphingosine-1-phosphate are also important lipid constituents that have been shown to act as second messengers (Gomez-Munoz, 2004; Spiegel and Kolesnick, 2002).

Lipid structure	Technical name and abbreviation
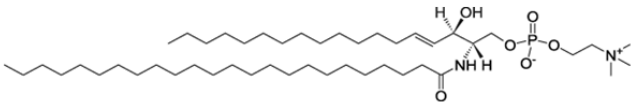	**N-lignoceroyl-D-*erythro*-sphingosylphosphorylcholine (24:0 SM)**
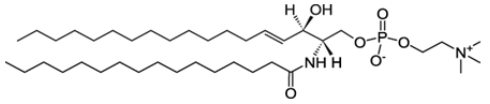	**N-palmitoyl-D-*erythro*-sphingosylphosphorylcholine (16:0 SM)**
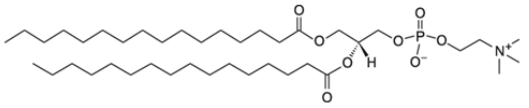	**1,2-dipalmitoyl-*sn*-glycero-3-phosphocholine (DPPC)**
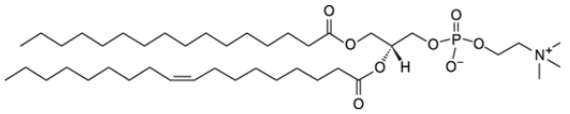	**1-palmitoyl-2-oleoyl-*sn*-glycero-3-phosphocholine (POPC)**
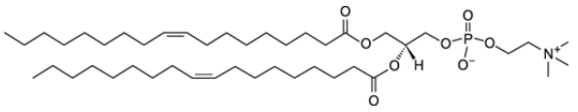	**1,2-dioleoyl-*sn*-glycero-3-phosphocholine (DOPC)**
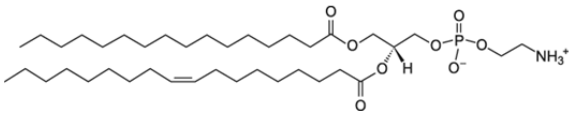	**1-palmitoyl-2-oleoyl-*sn*-glycero-3-phosphoethanolamine (POPE)**
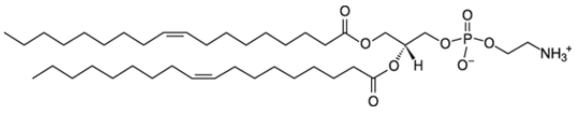	**1,2-dioleoyl-*sn*-glycero-3-phosphoethanolamine (DOPE)**
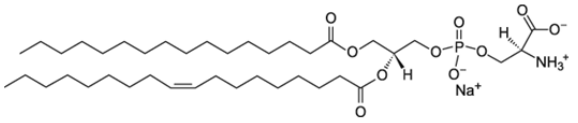	**1-palmitoyl-2-oleoyl-*sn*-glycero-3-phospho-L-serine (POPS)**
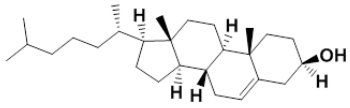	**Cholesterol**

Table 1 – Structures of common mammalian cell lipids. The structures of the lipids discussed throughout this thesis are summarized. Each lipid structure is accompanied by the chemical name and the associated abbreviation.

The glycerophospholipids and the sphingolipids can also both be subdivided into classes based on the structure of their acyl chains. Each acyl chain, also referred to as a tail or fatty acid, is commonly composed of a hydrocarbon chain of even numbers ranging from 4 to 28 carbons long (Fahy et al., 2005). The fatty acid contains carboxyl group on one end (alpha) and a terminal methyl group on the other (omega). The acyl chains can also contain one or more double bonds, or unsaturations, that introduces a kink in the otherwise straight (saturated) configuration, which alters the physical properties (Fahy et al., 2005). For the purpose of describing the length and degree of unsaturation of a lipid acyl chain, a widely adopted shorthand notation is used in this thesis. For example, an acyl chain that is 18 carbon long with one double bond is written as 18:1. The convention of this numbering system begins counting the carbon atoms from the carboxyl end of the acyl chain. The most common site of a double bond in a phospholipid chain occurs at the 9th carbon in the chain, relative to the carboxyl end. Another common notation is also used to describe the location of a double bond in the chain, relative to the omega end (Fahy et al., 2005). This notation is largely associated with polyunsaturated acyl chains such as an omega-3 fatty acid.

In addition to the glycerophospholipids and sphingolipids, another highly abundant cellular lipids is cholesterol (Maxfield and van Meer, 2010; Van Meer et al., 2008). In contrast to the structures of other major lipids, cholesterol is characterized by a structure that has a hydroxyl head group, three six-sided hydrocarbon rings, one five-sided ring and a hydrocarbon tail (Xu et al., 2005). Although cholesterol is primarily hydrophobic, the hydroxyl group makes cholesterol amphipathic and facilitates a parallel orientation with other lipids in a bilayer. Cholesterol is an important membrane constituent that modulates fluidity and reduces permeability of a lipid bilayer by intercalating with the other lipids (Cooper, 1978). Cholesterol also acts a precursor for many sterol derivatives, such as vitamin

D, steroid hormones, oxysterols and bile salts (Maxfield and van Meer, 2010; Norman, 2012). Furthermore, cholesterol regulates a diversity of cell functions including vesicle trafficking and cell signalling, as well as, controlling lipogenesis (Norman, 2012; Simons and Gerl, 2010; Soccio and Breslow, 2004).

1.3 - Cholesterol in health and disease

The role of cholesterol in human health and disease began to be appreciated in the early 20th century when it became known that cholesterol is present in all human cells and also in high concentration in the blood (Campbell, 1925; Doree and Gardner, 1908). Cholesterol is an essential molecule in mammalian cells that can be produced or acquired entirely by de novo synthesis. The necessity for adequate cellular cholesterol levels can be demonstrated by genetic mutations in the cholesterol biosynthetic pathway. Smith–Lemli–Opitz syndrome, for example, is a hypocholesterolemic disorder caused by a mutation in the 7-dehydrocholesterol reductase (DHCR7) enzyme (Thurm et al., 2016). DHCR7 acts at the end of the cholesterol biosynthetic pathway and converts 7-dehydrocholesterol into cholesterol. The DHCR7 mutation causes the retention of a single additional double bond in the 7-dehydrocholesterol molecule, compared to cholesterol and results in a spectrum of neurological and cognitive impairments (Thurm et al., 2016; Waterham, 2002). Although mature cholesterol can be supplied in the diet, the blood brain barrier prevents the transfer of dietary cholesterol into the brain. The human brain, therefore, relies on local lipogenesis to produce cholesterol, which rationalizes a correlation between disturbed cholesterol biosynthesis and neurological disorders (Bjorkhem and Meaney, 2004). Mutations in DHCR7 also illustrate the importance of the precise structure of cholesterol in humans, which cannot be substituted with minimally modified structural analogues.

In order to ensure that sufficient cholesterol is present throughout the body, mammals have developed a sophisticated strategy to produce and deliver cholesterol to peripheral tissues by the circulatory system. To distribute both digested and newly synthesized cholesterol throughout the body, lipids are transported through the aqueous environments by binding to extracellular proteins that form water-soluble lipoprotein complexes (Hussain, 2014). These lipid-protein complexes are typically composed of a lipid and protein monolayer that surrounds a dense hydrophobic core of triacylglycerides and esterified cholesterol. Lipoproteins in circulation are categorized by relative density, determined by electrophoresis or density centrifugation, into five groups: chylomicrons, very low density lipoproteins (VLDL), intermediate density lipoproteins (IDL), low density lipoproteins (LDL) and high density lipoproteins (HDL) (Havel et al., 1955; Lamer et al., 2011; Macfarlane et al., 1997). The most widely studied lipoproteins are LDL and HDL. The balance of these two lipoproteins in the circulatory system is a clinical predictor for the development of human disease.

LDL plays a role in delivering lipid to peripheral tissues, which can be catabolized by beta oxidation for energy or stored for later use in cytosolic lipid droplets (Anderson et al., 1977). Currently, however, modern diets are nutrient dense and rich in cholesterol, which can result in a high level of circulating LDL in the blood. Excessive dietary consumption of cholesterol increases the deposition of lipid in the periphery tissues, including blood vessels, and is a risk factor for many diseases in human populations, such as coronary heart disease and stroke (Kinosian et al., 1994; Zhang et al., 2012). The underlying cause of human health risk associated with elevated circulating LDL is the formation of plaque in the artery wall, known as atherosclerosis (Hansson and Hermansson, 2011). The primary role of HDL, however, is to remove excess lipid from the PM of cells and deposit the lipids back in the

liver (Kozarsky et al., 1997). Once returned to the liver, cholesterol can be sent back into circulation by incorporation into a new lipoprotein particle, or catabolized by hydroxylation to form bile acids. This process of removing excess cholesterol from cells is referred to as reverse cholesterol transport (RCT) (Lewis and Rader, 2005). Circulating HDL, therefore, works against LDL and is inversely correlated with the progression of atherosclerosis (Camont et al., 2011). Maintaining an appropriate ratio of HDL/LDL, therefore, is important for avoiding diseases of excess cholesterol while still maintaining the basal cellular functions provided by cholesterol.

1.4 - Cholesterol biosynthesis

The enzyme acetyl-coenzyme A acetyltransferase 2 (ACAT2) initiates the first step in cholesterol biosynthesis by condensation of two acetyl-CoA molecules to form acetoacetyl-CoA (Lynen and Ochoa, 1953). A third acetyl-CoA molecule is then added to acetoacetyl-CoA by 3-hydroxy-3-methylglutaryl-coenzyme A (HMG-CoA) synthase to form HMG-CoA (Clinkenbeard et al., 1975; Reynolds et al., 1984). The next step in synthesis has been shown to be rate limiting, which uses nicotinamide adenine dinucleotide phosphate (NADPH) to form melavonate by the enzyme HMG-CoA reductase. As the rate limiting enzyme, HMG-CoA reductase has been the target of statins, one of the most widely administered drugs in the world to lower cholesterol in the circulation (Tobert, 2003). After the synthesis of melavonate, a series of 5 ATP consuming steps produces isopentenyl pyrophosphate, which is then converted to the isomer dimethylallyl pyrophosphate (Rilling et al., 1958). The following two steps in cholesterol synthesis pathway use two molecules of 3-isopentenyl pyrophosphate to form geranyl pyrophosphate, followed by synthesis of farnesyl pyrophosphate by farnesyl pyrophosphate synthase (Hugueney and Camara, 1990).

In addition to producing cholesterol, farnesyl pyrophosphate is diverted as substrate for multiple other products, such as coenzyme Q10 and the post-translational modifications of prenylated proteins. For cholesterol synthesis, squalene synthase uses NADPH to condense two molecules of farnesyl pyrophosphate to form squalene (Popjak et al., 1961; Rilling et al., 1958), which is then converted in a cyclization reaction by lanosterol synthase to form the first sterol molecule, lanosterol. Lanosterol is the precursor for mammalian steroid hormones and vitamin D (Baker et al., 1995). Formation of lanosterol is the first committed step in the cholesterol synthesis, which is followed by an additional 19 reactions and 9 enzymes to produce cholesterol. Further details are thoroughly summarized elsewhere (Risley, 2002).

Regulation of cellular cholesterol synthesis is accomplished by cholesterol sensing enzymes in the ER known as sterol regulatory element binding proteins (SREBPs) (Radhakrishnan et al., 2007; Radhakrishnan et al., 2004). SREBPs are responsible for the transcription of many lipid related genes that produce proteins, such as HMG-CoA synthase and reductase, fatty acid synthase and LDL-receptor (Wang et al., 1993). The full length SREBP proteins are localized in the ER, which keeps them in an inactive form (DeBose-Boyd et al., 1999). When total cell cholesterol levels are high, ER cholesterol is increased and SREBPs are retained in the ER by binding to another ER protein complex, SREBP-cleavage-activating-protein (SCAP) and insulin induced gene (INSIG) (Brown et al., 2002; Sun et al., 2007). When the cholesterol content is low, SREBPs, along with SCAP, are released from INSIG. This exposes a region of SCAP to bind COPII vesicles and facilitates delivery of SREBP and SCAP to the Golgi apparatus (DeBose-Boyd et al., 1999). At the Golgi, the SREBP/SCAP complex is acted upon by two proteases, site-1-protease and site-2-protease, which release the cytoplasmic portion of SREBP from the membrane bound

SREBP/SCAP complex (Cheng et al., 1999). The soluble cytoplasmic portion of SREBP then translocates to the nucleus where it functions as translation factor to activate target genes.

Conversely, the cell also has multiple mechanisms to limit the cholesterol content when sterol levels become too high. In addition to preventing SREBPs trafficking and maturation at the Golgi, INSIG also degrades HMG-CoA reductase when sterol levels are elevated (DeBose-Boyd, 2008; Radhakrishnan et al., 2007). High cholesterol in the ER induces HMG-CoA reductase to bind to INSIG, which leads to proteosomal degradation of the rate-limiting enzyme and subsequently inhibits cholesterol synthesis (Sever et al., 2003; Song et al., 2005). Another strategy to reduce cellular cholesterol content is through oxidation of cholesterol. When cholesterol is elevated, a portion of the cholesterol will be oxidized in the mitrochondria to form oxysterols, such as 22-hydroxycholesterol. Oxysterols act as a ligand for transcription factors, such as, liver X receptor (LXR) (Chen et al., 2007). Activation of LXR up-regulates genes that are involved in efflux of excess cholesterol from the cell. For example, upon binding of oxysterols to LXR, ATP-binding cassette transporters A1 and G1, are up-regulated and facilitate the transfer of cellular cholesterol to extracellular lipoprotein acceptors, such as apolipoprotein A1 and HDL (Costet et al., 2000; Schwartz et al., 2000). Moreover, elevated cholesterol in the cell can also be reduced by acylation, which will stored in lipid dense compartments, known as lipid droplets (Brown et al., 1979). Together, the interplay between cholesterol synthesis and inhibition or efflux of excessive cholesterol maintains the cellular cholesterol homeostasis.

1.5 - Cholesterol Trafficking

With the exception of the first few steps in the cytosol, the majority of the cholesterol synthesis reactions occur in the ER. However, ER is low in cholesterol (<5%), mainly due to a limited capacity to retain cholesterol by other phospholipids (Van Meer et al., 2008). After synthesis, cholesterol is trafficked to different compartments of the cell by both vesicular and non-vesicular carriers (Iaea and Maxfield, 2015). Cholesterol has is known to have increasing affinity to the membranes along the secretory pathway, which leads to a gradient of cholesterol concentrations in cells (Ikonen, 2008). For example, cholesterol is low in the ER, but higher in the Golgi. The highest concentration of cholesterol is found in the PM and endocytic recycling compartments (Mondal et al., 2009). The distribution of cholesterol is correlated with sphingolipid and saturated phospholipid content in these membranes; cholesterol is first to be enriched in the trans Golgi network, where the final steps of sphingolipid synthesis occur. This enables de novo cholesterol to travel against a concentration gradient to reach the PM (Mukherjee et al., 1998).

Vesicular transport of cholesterol occurs bi-directionally in the secretory (outward from the ER/ Golgi) and endosomal pathways (inward from the PM) (Ma and Chisholm, 2002). However, distinct cholesterol distributions among organelles must be actively maintained. It has been proposed that lipids are sorted during vesiculation to help maintain compartmentalization (Deng et al., 2016; Surma et al., 2012). The concept of vesicular lipid sorting lead to the term “lipid raft”, described below (Simons and Ikonen, 1997). For example, vesicles budding from the Golgi, which are destined for different compartments, use specific lipids to sort proteins into specialized vesicle carriers. Cholesterol and sphingolipids are known to be sorted from the bulk membrane into PM-destined vesicles that traffic PM proteins (Deng et al., 2016; Simons and Ikonen, 1997; Simons and Van Meer,

1988). Similarly, membranes are sorted within the endosomal system to recycle membrane receptors and deliver extracellular constituents to lysosomes, during which, cholesterol is maintained high in the endosomes and low in the lysosomal membrane (Lange et al., 1998; Mondal et al., 2009). This suggests that cholesterol is mostly sorted out of the late endosome and recycled to the PM before delivery of cargo to the lysosome.

Interestingly, although cholesterol is trafficked to and from the PM in vesicles, it has been shown that cholesterol is primarily transported throughout the cell by non-vesicular means. Inhibition of the secretory pathway by brefeldin A, for example, does not significantly prevent the delivery of newly synthesized cholesterol to the PM (Field et al., 1998). Although nearly insoluble in aqueous solution, cholesterol can move between membranes by two mechanisms: (1) lateral diffusion, mediated by lipid transfer proteins at membrane contact sites, and (2) inter-membrane exchange, mediated by soluble sterol binding proteins (Lev, 2010). Lateral diffusion of sterols is rapid (3.4 μm^2/second), which facilitates dispersal of newly synthesized cholesterol out of the ER (Hiramoto-Yamaki et al., 2014). With a large surface area and broad spread throughout the cell, the ER maintains membrane contact sites with every major cellular compartment, including the Golgi, mitochondria and the PM (Helle et al., 2013). This enables the movement of cholesterol and other lipids between compartments. A family of proteins, known as oxysterol binding proteins (OSBP) including also OSBP-related proteins (ORP), bind and move cholesterol and other oxygenated derivatives between adjacent membranes (Im et al., 2005; Ngo et al., 2010). OSBPs contain a C-terminal sterol binding domain that sequesters sterols into a hydrophobic pocket (Im et al., 2005). Many of the OSBPs also contain a pleckstrin homology (PH) binding domain, as well as, a FFAT motif (two phenylalanines in an acidic tract) (Ngo et al., 2010) that enable OSBPs to bridge between two membranes. The FFAT

motif allows OSBPs to bind and anchor to the ER resident proteins vesicle associated membrane protein-associated protein (VAP) A and B. At the same time, the PH domain can bind phosphatidylinositide lipids in another membrane, for example the PM. By simultaneously binding an ER protein and PM lipids, OSBPs stabilize membrane contact sites, which allow the OSBP sterol binding domains to transfer sterols between the adjacent membranes (Ngo et al., 2010).

In addition to membrane contact sites, many soluble sterol binding proteins have been identified that have been shown to greatly increase the rate of cholesterol movement between membrane compartments. Cholesterol is poorly soluble in aqueous solution, which makes unaided, spontaneous inter-membrane exchange unfavourable. Soluble sterol binding proteins have been shown to facilitate transport of cholesterol between each membrane compartment by shielding cholesterol into a hydrophobic pocket (Mesmin and Maxfield, 2009). Steroidogenic acute regulatory protein (StAR)-related lipid transfer (START) proteins, another major protein family, are soluble cytosolic proteins that bind sterols and enable rapid movement between membrane compartments (Garbarino et al., 2012). The START family of proteins is subdivided into 15 subgroups that share sequence homology. The START domain common among the family members contains a hydrophobic pocket that binds cholesterol and other lipids, such as PC and ceramide (Clark, 2012). The first and well-characterized START domain containing protein, StAR, facilitates the bioconversion of cholesterol into steroid hormones by delivering cholesterol from the outer to the inner mitochondrial membrane (Clark et al., 1994). Another well-characterized START protein, STARD4, is involved in maintaining cholesterol homeostasis by delivering cholesterol from the PM back to the ER (Garbarino et al., 2012; Mesmin et al., 2011). Overall, each group of START proteins shows a set of substrate and target membrane specificities. It is not clear,

however, if any START protein is specifically involved in trafficking cholesterol out of the ER to the PM.

Ultimately, it is a combination of cholesterol affinity for cellular membrane compartments, vesicular trafficking and non-vesicular trafficking that determines how cholesterol is distributed throughout the cell.

1.6 - Principles of lateral lipid phase separation in a membrane

Each membrane lipid exhibits unique physical properties based on their structural features, such as head group, acyl chain length and degree of acyl chain unsaturation (Shevchenko and Simons, 2010). These physical features determine how lipids interact together and whether they can mix together homogeneously. This is referred to as the lipid miscibility (or conversely, immiscibility). Two lipid species that may not mix well, for example, a long saturated lipid and a short unsaturated lipid, may be immiscible and cause the long lipids to organize together and separate from the shorter lipid. Each species of lipid also has a unique temperature that determines if the lipid is in a fluid or solid-like state. This is referred to as the transition temperature, or melting temperature (Tm). Lipid miscibility is greatly influenced by the temperature of the sample and the Tm of the lipids. For instance, if the temperature is above the transition temperature of all the lipids in a sample, then lipids are fluid and would have a greater tendency to be miscible. However, if the temperature of a sample is higher than the Tm of one lipid and below the Tm of another, then the two lipids may become immiscible and cause separation of the lipids into different phases (Veatch and Keller, 2003, 2005). Overall, depending on temperature, a membrane may be classified into three phases: gel phase (solid), liquid ordered (l_o) (some ordered, some disordered) or liquid disordered (l_d) (fluid) phase. In three-component model membranes, it has been

demonstrated that combining a saturated lipid with an unsaturated lipid, in the presence of cholesterol, can cause spontaneous phase separation into distinct ordered and disordered domains (Sankaram and Thompson, 1991). Although phase separation has been observed in the absence of cholesterol, immiscibility of saturated and unsaturated lipids is enhanced by cholesterol. The rigid, planar structure of the steroid ring allows cholesterol to engage in van der Waals interactions with saturated acyl chains (McIntosh et al., 1992). This interaction reduces the flexibility and mobility of the acyl chains and also straightens them, reinforcing the immiscibility with an unsaturated lipid. Therefore, cholesterol can greatly modify the physical properties of multicomponent lipid bilayer. Thorough characterization of three-component membrane systems have produced ternary lipid phase diagrams that predict the phase status of a membrane at a given composition (Veatch and Keller, 2003, 2005). It is postulated that lipid-mediated phase separation may similarly occur in the live cell PM.

1.7 - Plasma membrane microdomains

Previously, the PM was considered a homogeneous membrane bilayer at thermodynamic equilibrium (Singer and Nicolson, 1972). However, it is now clear that the mammalian cell PM is laterally heterogeneous where lipids and proteins could be organized into specialized functional domains (Brown and Rose, 1992). The term, lipid raft, was originally used to describe how polarized epithelial cells sort and deliver unique vesicle cargo from the Golgi to the apical and basolateral surfaces (Simons and Ikonen, 1997). Vesicles directed to the apical surface were enriched in sphingolipids, whereas, the basolateral surface received primarily PC rich vesicles. It was also noted that glycosylphosphatidylinositol (GPI) anchored proteins are preferentially concentrated in the apical membrane vesicles, suggesting that lipid and protein complexes are sorted together

before exiting the Golgi (Brown and Rose, 1992; Simons and Van Meer, 1988). Since the original hypothesis was proposed, the support for the existence of lipid-mediated membrane domains has come from multiple experimental methods, such as, the isolation of detergent resistant membranes, artificial model membranes, biochemical assays and live-cell fluorescence microscopy (Eisenberg et al., 2006; Schroeder et al., 1994; Sezgin et al., 2012).

In contrast to the notion that membranes are two dimensional solvents for membrane proteins, the lipid raft hypothesis postulates that membrane lipids actively form specific domains that regulate cellular functions. Over the years, this hypothesis has evolved considerably. Support for the lipid raft hypothesis began with biochemistry manipulations, such as membrane fractionation, which isolated membrane components that are resistant to detergent extraction. The PM was found to separate into light and heavy fractions by density gradient centrifugation (Demus, 1973). These light and heavy PM fractions contain distinct populations of PM proteins (Hoessli and Runggerbrandle, 1983). In continuation with the isolation of proteins by density centrifugation, it was found that detergents can extract specific sets of proteins (Hoessli and Runggerbrandle, 1985). For example, a subset of PM glycoproteins, including thymocyte differentiation antigen 1 (Thy-1), were found to form large lipid-protein complexes that are resistant to solubilization by the detergent, Triton X-100 (TX-100) (Draberova and Draber, 1993). Similarly, PM sphingolipids were also found to be resistant to detergent extraction (Hagmann and Fishman, 1982). The reproducible insolubility of a subset of PM proteins and lipids in TX-100, relative to the total PM content, is now referred to as detergent resistant membrane (DRM). The DRM complexes are believed to represent the isolation of lipid-mediated ordered membrane microdomains that exist in the native PM (London and Brown, 2000). Strikingly, detergent resistance required cholesterol in the membrane, which seemingly supported the lipid raft hypothesis. These

early experiments postulated that proteins and lipids in the PM may be organized into functional domains, as described by the lipid raft hypothesis. Although skepticism remains about the usefulness of DRMs (Morris et al., 2011), the properties of DRM are still actively investigated (van Gestel et al., 2016).

Experiments in model membranes also seem to be consistent with the lipid raft hypothesis. Lipid phase separation in model membranes could be readily achieved and postulated to provide insight into the properties of PM (Shimshick and McConnell, 1973). For example, atomic force microscopy (AFM) of two-component supported lipid bilayers provided the first direct visualization of phase separation: membranes were heterogeneous and contained small domains approximately 10 nm in size (Gliss et al., 1998). An alternative strategy was also developed around the same time, which used an unsupported membrane bilayer, known as giant unilamellar vesicles (GUV) (Angelova et al., 1992). Incorporating fluorescent probes into the GUVs that are sensitive to the lipid environment enabled real time visualization of co-existing lipid phases (Bagatolli and Gratton, 2000). This discovery led to a thorough characterization of how lipid composition affects domain formation in GUVs (Veatch and Keller, 2003).

A criticism of the two or three component lipid systems, either as supported bilayers or GUVs, is that they are an over-simplified version of the PM. This criticism, however, was partially addressed by the characterization of phase properties in PM derived vesicles. Giant plasma membrane vesicles (GPMV) can be isolated from live cells with similar protein and lipid content as the PM. These GPMVs can readily form microdomains analogous to three component GUVs (Baumgart et al., 2007a). Visualization of membrane phases in GPMVs was achieved by incorporation of fluorescent lipid probes, similar to GUVs, or by expression of fluorescent-tagged PM proteins (Baumgart et al., 2007b). As such, GPMVs greatly

supported the lipid raft theories by directly confirming that proteins predicted to partition into ordered domains in the PM do reside in ordered domains (Baumgart et al., 2007a). GPMVs showed that membranes with the complex protein and lipid composition of the PM can form microdomains. However, it remains a paradox why microdomains do not form in the unperturbed PM where GPMVs were isolated. Nevertheless, GPMVs have become a powerful model system to understand membrane organization that serve to bridge between pure lipid systems and the intact PM.

Additional support for the existence of membrane microdomains in cells has come from biochemical analyses that examine how PM cholesterol regulates protein-protein interaction. Given that membrane domains are thought to be cholesterol dependent, the most widely employed method of manipulating membrane microdomains is to increase or decrease cholesterol levels in the PM. Removal of cholesterol, either by blocking de novo synthesis with statins, or by acute extraction with a cholesterol acceptor, such as cyclodextrin, is believed to disrupt or prevent the formation of membrane domains. If cholesterol depletion will inhibit, and repletion will rescue, for example, a phosphorylation event, the process could potentially occur within lipid rafts (Lasserre et al., 2008). Some examples of lipid raft dependent processes are the T-cell receptor complex activation, phosphorylation of Akt (also known as protein kinase B) and toll-like receptor 4 (TLR4) signaling (Kabouridis et al., 2000; Zhu et al., 2010). Furthermore, cholesterol is necessary for viral infection (Popik et al., 2002; Takeda et al., 2003). Importantly, since not all PM protein interactions are sensitive to changes in cholesterol levels, it is speculated that cholesterol is involved in regulating a subset of specific protein interactions in the PM (Kenworthy et al., 2004).

With the definition continually evolving, lipid rafts are currently described as dynamic assemblies of protein and lipids that form domains rich in cholesterol and sphingolipids (Pike, 2006). Curiously, lipid rafts, postulated to form micron-scale domains in live cell PM, as found in GUVs or GPMVs, have not been observed. This discrepancy is rationalized by the arguments that rafts are transient and less than 200 nm in size, which precludes the possibility of detection by conventional fluorescence microscopy. In order to circumvent this limitation, advanced fluorescent microscopy strategies have been used to characterize membrane domains, such as fluorescence recovery after photobleaching (FRAP), Förster resonance energy transfer (FRET) and more recently, super resolution microscopy (Eggeling et al., 2009; Kenworthy, 2007; Sharma et al., 2004).

For membrane studies, FRAP methods typically involve expressing a membrane bound fluorescent protein or the incorporation of a lipophilic dye into the PM of cells to monitor the lateral diffusion rate (Kenworthy, 2007). Photobleaching a region of interest in the PM with a high intensity laser is then followed by the acquisition of a time series of images to record the return of fluorescent molecules to the region (recovery). This produces a diffusion coefficient for the protein or lipophilic dye that may be sensitive to manipulations, such as cholesterol depletion or repletion (Siggia et al., 2000). For example, a membrane microdomain-associated protein may exhibit restricted lateral mobility within a domain. However, depletion of cholesterol, which disperses the membrane microdomains, may result in significant increase in the diffusion rate of the protein due to unrestricted mobility (Crane and Tamm, 2004). Conversely, proteins that are not associated with membrane domains may not be affected by the cholesterol depletion and, therefore, the diffusion rate would remain unchanged between treatments (Kenworthy, 2007).

Another method that is commonly used to characterize membrane domains is FRET. FRET is particularly useful for sensing nanoscale proximity between donor and acceptor molecules (Stryer, 1978). With FRET, when the donor is excited, the emitted light from the donor can be absorbed by the acceptor nearby and subsequently re-emitted by the acceptor with a longer wavelength. This process is highly sensitive to the distance between the fluorophores (Fung and Stryer, 1978) and thus is effective to detect protein-protein interactions or densities. In order for FRET to occur, the donor and acceptor pair must be within 10 nm and the efficiency of energy transfer increases with closer proximity (Stryer, 1978). A common example of a widely used FRET pair is cyan fluorescent protein (CFP) and yellow fluorescent protein (YFP). FRET has been used to monitor the surface density of PM proteins (Fung and Stryer, 1978). When used with co-expressing proteins that are known to associate with membrane microdomains, such as CFP and YFP GPI-anchored proteins, FRET can be used to detect recruitment into cholesterol-dependent membrane microdomains (Rao and Mayor, 2005). FRET between two different fluorophores, such as CFP and YFP, is termed heteroFRET. FRET can also be performed with one fluorophore, which termed homoFRET (Raghupathy et al., 2015; Varma and Mayor, 1998). HomoFRET employs fluorophores with significant overlap between their own excitation and emission spectrum, such as green fluorescent protein (GFP) (Sharma et al., 2004; Varma and Mayor, 1998). When excited with polarized light, either horizontal or vertical, GFP could emit its regular fluorescence, which remains polarized (vertical). If the emitted light is absorbed by a nearby GFP, or energy transfer has occurred, this secondary emission will lose the original polarity (both vertical and perpendicular), which produces anisotropy. Thus by collecting emitted light in both parallel and perpendicular planes, the amount of energy transferred to the perpendicular plane can be determined. When FRET is occurring, light can be emitted from

parallel and perpendicular planes and reduce anisotropy. HomoFRET has successfully been used to monitor recruitment of GPI-anchored proteins into sub-optical membrane domains, or nanoclusters that would otherwise be undetectable using conventional microscopy (Raghupathy et al., 2015; Rao and Mayor, 2005).

Finally, an emerging new strategy is super resolution microscopy. Previously, membrane domains were considered to be too small and transient for direct visualization by microscopy due to limits in optical resolution (~200 nm). These new imaging strategies, such as stimulated emission depletion microscopy, fluorescence photoactivation localization microscopy or lattice light sheet microscopy have greatly improved resolution (10-50 nm) and are beginning to be applied to characterize membrane organization (Dean et al., 2016; Eggeling et al., 2009; Gudheti et al., 2013). Each system has benefits and limitations, summarized in reviews (Eggeling, 2015; Owen and Gaus, 2013). As the technologies continue to develop, the improvement in resolution and the speed of acquisition should facilitate direct imaging of membrane processes that occur in the range of tens of nanometres. Since the classical definition of PM microdomains, or lipid rafts, are thought to be in nanometre size range, it is conceivable that super resolution microscopy should be capable of detecting cholesterol-dependent membrane microdomains. Indeed, some attempts have been made in this regard (Eggeling et al., 2009; Gudheti et al., 2013). The application of super resolution microscopy should provide further insights as the technology continues to develop.

In summary, the membrane microdomain hypothesis has been supported by biochemistry experiments, model membrane studies and advanced fluorescence techniques. When considered in combination, it is known that (1) phospholipids can self-assemble and phase separate into ordered and disordered domains in a cholesterol dependent manner, as

shown by DRMs, GPMVs and GUVs, (2) interactions between subsets of proteins in the PM are influenced by the lipid content of the membrane, particularly cholesterol. However, definitive evidence supporting the presence of membrane microdomains in the live cell PM is lacking. Moreover, the precise nature of these domains is not completely understood.

1.8 - Plasma membrane transbilayer asymmetry

A unique feature of the mammalian cell PM, which may not have received due attention, is the bilayer asymmetry. The outer leaflet of the PM is primarily composed of SM and PC lipids, whereas the inner bilayer leaflet is mostly PE and PS (Murate 2016). This difference in lipids between the two leaflets is referred to as transbilayer or transmembrane asymmetry. Initial attempts to examine PM lipid asymmetry came from characterizing the transbilayer distribution of the aminophospholipids, PE and PS in erythrocytes (Bretscher, 1972a). Both PE and PS contain an amino residue in the head group that is reactive with formyl-methionyl methyl phosphate (FMMP) or trinitrobenzene sulfonic acid (TNBS). These membrane impermeable reagents can be added to the exterior of cells and the amount of lipid reacted can be quantified by spectroscopy or TLC. Treating human erythrocytes with FMMP found that the majority of PM PE and PS did not react unless the cells were lysed, suggesting that the aminophospholipids are primarily located in the inner leaflet (Bretscher, 1972b). Bretscher then correctly hypothesized that PE and PS make up the majority of the inner leaflet lipids, and assumed that the outer leaflet should be composed of PC and SM. Only a year later, this hypothesis was independently validated by a strategy that involved a series of phospholipases. Human erythrocytes were treated with phospholipase A_2 (PLA_2) and sphingomyelinase. PLA_2 is a bacterial enzyme that is specific to phospholipids, rather than sphingolipids, which cleaves one acyl chain from a lipid to release a fatty acid and a

lysophospholipid (Glaser et al., 1993). Sphingomyelinase, on the other hand, is a lipase specific to SM that cleaves the choline from the SM head group to produce ceramide and choline (Kornhuber et al., 2015). The results of PLA_2 and sphingomyelinase treatments found that 68% of PC and 85% of SM was localized to the outer bilayer leaflet of the erythrocyte PM. Furthermore, the lipases had no effect on the PE and PS content (Verkleij et al., 1973). When combining these lipase results with the FMMP reaction study, it confirms that the erythrocyte PM is composed of PC and SM in outer leaflet with PE and PS in the inner leaflet.

Interestingly, although the phospholipids and sphingolipids are well characterized to be transversely asymmetric in the PM, consensus on the cholesterol transbilayer distribution has been elusive (Murate and Kobayashi, 2016). Due to only a small hydrophilic hydroxyl head group, cholesterol is highly mobile between bilayer leaflets (half time < 1 second) (Bennett et al., 2009; Leventis and Silvius, 2001; Steck et al., 2002), referred to as cholesterol flip-flop. This rapid flip-flop rate has complicated attempts to quantify the steady-state partitioning of native cholesterol. The first attempts to quantify cholesterol partitioning in a mammalian cell PM were performed using freeze-fracture analysis (Fisher, 1976). This initial analysis fractured the bilayer into two halves, performed a lipid extraction and quantified the cholesterol content in each half by thin layer chromatography (TLC). It was concluded by this technique that more cholesterol was located in the outer leaflet of human erythrocytes. These data, however, showed wide variability based on the type of buffer used (equal distribution with PBS versus up to 3 times more in the outer leaflet with TBS), which questions the validity of the results. Two years later, the cholesterol transbilayer distribution in human erythrocytes was again quantified; however, the strategy was to monitor cholesterol partitioning by staining with the fluorescent probe, filipin. Filipin is a

histochemical stain that specifically binds to cholesterol. The authors generated erythrocyte ghost membranes (permeabilized and resealed cells) that were right-side-out, inside-out and unsealed. After filipin treatment, the amount of cholesterol present in the outer leaflet, inner leaflet and both leaflets, respectively, can then be quantified. It was found that cholesterol was evenly distributed between bilayer leaflets (Blau and Bittman, 1978). These results, however, are not particularly surprising considering the extensive amount of cellular manipulation involved in sample preparation.

As an alternative to the perturbing strategies of freeze-fracture analysis and filipin staining of erythrocyte ghosts, the distribution of cholesterol in the PM has also been investigated indirectly by inferring the cholesterol distribution through using fluorescent analogues, or other sterol derivatives with structural similarity. Some prominent examples of fluorescent sterols that have been used to understand cholesterol dynamics are boron dipyrromethene difluoride (bodipy)-cholesterol, cholestatrienol (CTL) and dehydroergosterol (DHE). Bodipy-cholesterol is a synthetic derivative of native cholesterol that has a fluorescent dye conjugated to the sterol ring in place of the acyl chain. This commercially available fluorescent sterol is amenable to conventional light microscopy without the need for specialized filters and is also highly photostable. Bodipy-cholesterol has been found to exhibit similar properties and tissue distributions, compared to cholesterol, and has been used to visualize sterol trafficking events (Holtta-Vuori et al., 2008; Wustner et al., 2016). Unfortunately, the addition of the large bodipy moiety would likely affect the dynamics of the sterol. In contrast to bodipy-cholesterol, CTL and DHE are intrinsically fluorescent molecules that are structurally more similar to cholesterol than bodipy-cholesterol. DHE is a naturally occurring and naturally fluorescent compound isolated from fungi (Ano et al., 2015). Compared to cholesterol, the CTL and DHE sterol rings contains two additional

double bonds, which can emit weak fluorescence with excitation near the UV range (Pourmousa et al., 2014). DHE also has an additional double bond and methyl group in the alkyl chain. The structure of CTL on the other hand, does not have alkyl chain modifications, making CTL structurally more similar to cholesterol than DHE. CTL, however, must be custom synthesized and is, therefore, less accessible. A disadvantage of both CTL and DHE is that the fluorescent excitation and emission is 320 nm and 370-400 nm, respectively. In addition to a low quantum yield, CTL and DHE analysis typically require specific fluorescence filter sets.

The leaflet-specific partitioning of these fluorescent analogues can be determined in the PM of live cells using a fluorescence quenching method. To do this, the fluorescent sterols are incorporated into cells and allowed to equilibrate with native cholesterol. This is then followed by the addition of a membrane impermeable fluorescence quencher into the media. The amount of PM fluorescence was then determined before and after the quencher. The reduction in fluorescence, as a consequence of the quencher, is then used to determine outer leaflet sterol fluorescence, relative to total PM fluorescence. Using this method, Mondal et al. (2009) quantified the sterol distribution in live Chinese hamster ovary cells and similar results were shown by another research group using human erythrocytes (Schroeder et al., 1991). Contrary to the freeze-fracture results, the fluorescent sterol data found that both CTL and DHE were primarily located in the inner bilayer leaflet (Mondal et al., 2009; Schroeder et al., 1991). It was then inferred that native cholesterol may also be transversely asymmetric and be enriched in the inner leaflet. Though potentially valid, the results of sterol fluorescence quenching have not been widely accepted. Structural modifications, although minor, could alter the physical properties and can affect how the sterol analogues interact with other components in the lipid environment. For example, the rate of sterol efflux from a

bilayer differs between cholesterol and fluorescent sterols (Ohvo and Slotte, 1996; Ohvo-Rekilä et al., 2000). Therefore, this indirect approach using a derivative may not represent the true native cholesterol distribution. As a result of conflicting literature, the cholesterol transbilayer distribution in the mammalian cell PM is still unresolved (Devaux and Morris, 2004; Murate and Kobayashi, 2016).

1.9 - Rationale and thesis proposal

The lipids and proteins that comprise the mammalian cell PM are distinct between the inner and outer leaflets of the bilayer (Devaux and Morris, 2004). Curiously, the distribution of cholesterol between bilayer leaflets is still not established even though cholesterol represents approximately 30-40 percent of the PM lipids and is involved in numerous cell functions. Cholesterol is believed to be integral in the formation of ordered membrane microdomains in the PM of live cells and, yet, the role of cholesterol asymmetry on membrane domain formation has not been studied. Understanding how cholesterol partitions between leaflets and the potential consequences of the cholesterol asymmetry was the primary focus of this thesis.

It has been suggested that cholesterol could concentrate in one leaflet over another in the bilayer due to differences in affinity for specific phospholipids in the individual leaflets (Yesylevskyy and Demchenko, 2012). However, characterizing the steady state cholesterol distribution between leaflets has represented a technical challenge, due to the rapid flip-flopping of cholesterol between leaflets. In order to overcome these limitations we hypothesized that if cholesterol flip-flop between bilayer leaflets could be stopped, we can then distinguish between the pools of cholesterol localized in each leaflet. We reasoned that cholesterol flip-flop is a form of Brownian motion and it could be sensitive to temperature. It

is, therefore, possible that cholesterol flip-flop could be greatly reduced or prevented if temperature is sufficiently low. Once cholesterol movement was prevented, we could then quantify cholesterol partitioning in each leaflet.

The objectives of this thesis are:

(**1**) Develop and optimize a protocol for determining cholesterol transbilayer distribution using a model membrane system.

(**2**) Apply above protocol to characterize cholesterol transbilayer distribution in the PM of live mammalian cells.

(**3**) Identify regulatory mechanisms for maintaining the cholesterol transbilayer distribution.

(**4**) Examine the impact of cholesterol transbilayer distribution on the lateral organization of membrane microdomains in the live mammalian cell PM.

The results of each of the objectives are described in the subsequent chapters of this thesis. Herein, a protocol is described that can quantify how cholesterol partitions between leaflets of a bilayer in both model membranes and the live cell PM. We identify that sphingolipid asymmetry can influence the cholesterol partitioning and, in particular, that sphingolipid acyl chain length is a key factor. We then proceed to characterize how sphingolipid acyl chain length influences the formation of membrane domains in model membranes and live cell PM. Altogether, this work suggests that 24:0 sphingolipids regulate the formation of membrane microdomains by governing the partitioning of cholesterol between bilayer leaflets.

Chapter 2 - Materials and Methods

Materials

Phospholipids and liposome accessories were purchased from Avanti Polar Lipids. Cholesterol, trinitrobenzene sulphonic acid (TNBS) and all cyclodextrins used were purchased from Sigma-Aldrich. Radiolabelled (^{3}H) cholesterol was purchased from Perkin Elmer. TMA-DPH was purchased from Molecular Probes. Naphtho[2,3-a]pyrene was purchased from Santa Cruz Biotechnologies. Thin layer chromatography plates were acquired from Cedarlane Laboratories. The transfection reagent, Attractene, was purchased from Qiagen. Platinum wire was purchased from Omega Engineering. All other materials and reagents were purchased from Fisher Scientific.

Cell culture

Adherent mammalian cells were cultured in 100 mm plastic dishes in Dulbecco's Modified Eagle Medium (DMEM) supplemented with 10% fetal bovine serum and 1 % antibiotics (penicillin and streptomycin). Cells were maintained in a 37 °C incubator with 5 % CO_2. Under certain experimental conditions, the culture media was changed to serum-free DMEM overnight, which was supplemented with 1 mg/mL bovine serum albumin.

LUV preparation

All lipids were stored as 50 mg/mL stocks in chloroform/methanol (95:5). 1 mM LUVs are generated by combining the desired lipid components followed by evaporating the organic solvent under nitrogen gas and subsequent vacuum desiccation for at least 60 minutes. In the case of symmetric ^{3}H-cholesterol labeled LUVs, trace amount of ^{3}H-cholesterol (~100 pmol/3 μmol phospholipid) was incorporated into the sample prior to

desiccation. Dried lipids were then resuspended in Medium 1 (20 mM HEPES, 150 mM NaCl, 5 mM KCl, 1 mM $CaCl_2$, 1 mM $MgCl_2$), subjected to 5 freeze/heat cycles and extruded through a 100 nm membrane to form 100 nm LUVs. For LUV isolation from the aqueous media, 1 mol% biotinylated-PE was added to lipid mixture above and resultant LUVs were incubated with streptavidin-coated agarose beads at 4 °C overnight. Unbound LUVs were removed by washing the beads 3 times with Medium 1.

For intermembrane exchange, two LUV populations (donor and acceptor) were similarly made with 30 % cholesterol. The donor population received trace ^{3}H-cholesterol, was biotinylated and bound to streptavidin beads to facilitate separation from unlabelled acceptor LUVs.

Determination of vesicle size and unilamellarity

Before proceeding with LUV characterizations, control experiments were performed to confirm if the LUVs were unilamellar (single bilayer) and if the population of vesicles was uniform. After extrusion through the 100 nm membrane, the size of the vesicle population was determined by light scattering analysis using a NanoSight LM10 (Malvern) system according to the manufacturer's instructions. To confirm that the vesicles were unilamellar, we quantified the aminophospholipids present in the outer leaflet of the vesicles by reaction with TNBS by following a previously published protocol (Nordlund et al., 1981). For this, extruded vesicles containing PE and PS were generated and treated with 1.5 % TNBS for 20 minutes in the dark. Subsets of the vesicles were lysed by Triton X-100 prior to the addition of TNBS to act as the positive control that reacts to completion. When TNBS reacts with aminophospholipids, an orange colour is produced. After incubation, the amount of reacted

TNBS was quantified and compared between positive control and the intact vesicles by reading the absorption of the same at 410 nm.

Temperature controlled flip-flop and outer leaflet cholesterol extraction

Cholesterol flip-flop in symmetric and asymmetric LUVs was controlled by reducing temperature to 0 °C (see **Appendix 1** for additional details). In order to successfully prevent flip-flop, the temperature of the cholesterol extraction procedure was stringently regulated by performing the experiments in a cold room and in an ice water bath, or 0 °C water bath containing 50 % ethylene glycol. Furthermore, to prevent incidental hand warming of the samples, all manipulation of the tubes was required to be carried out with utensils similarly maintained at 0 °C. At least one hour prior to the cholesterol extraction, samples, utensils and MCD media were pre-incubated at 0 °C. To initiate cholesterol extraction, 5 mM MCD was added to the medium to selectively remove cholesterol from the outer leaflet of the LUVs at 0 °C until cholesterol extraction reached a plateau. Similar experiments were also conducted in a 37 °C water bath. After incubation, the LUVs were separated from MCD containing medium by a brief centrifugation in 0 °C centrifuge within a cold room. The amounts of ^{3}H-cholesterol in the medium and in the LUVs are quantified by scintillation counting. Total ^{3}H-cholesterol was determined by lysing the same amount of ^{3}H-cholesterol labeled LUVs with 2% Triton X-100.

LUV intermembrane exchange

The assay was performed by mixing bead-bound ^{3}H-cholesterol donor LUVs with excess unlabelled acceptor LUVs (100-fold) at 37 °C, 0 °C or -5 °C in the presence of 1 mM βCD. Outer leaflet cholesterol is exchanged between populations, until equilibrium. Donor

and acceptor LUVs are isolated by 60 second centrifugation at 1000 x g and the amount of ^{3}H-cholesterol in the acceptor LUVs is quantified.

Erythrocyte intermembrane exchange

All erythrocyte work was approved by the Ottawa Health Sciences Network Research Ethics Board (#20140233-01H). Human erythrocytes were isolated from whole blood by centrifugation through Ficoll-Hypaque gradient solution. The erythrocytes were then washed 3 times with PBS containing 2 mM EDTA. 100 million washed erythrocytes were incubated with 20 μCi ^{3}H-cholesterol in 10 mL DMEM for at least 4 hours, subsequently biotinylated according to manufacturer's instructions (Fisher Scientific) and 100,000 cells were adhered to a streptavidin coated microplate. 100-fold excess unlabelled erythrocytes were added to the microplate wells in suspension with 1 mM βCD at 37 °C or -0 °C, until equilibrium. 75 μL of supernatant containing erythrocyte acceptor cells was removed at each time point and the amount of cholesterol transferred to the acceptors was determined by scintillation counting.

Asymmetric vesicles

Asymmetric LUVs with POPC, eSM or mSM introduced into the outer leaflet and DOPE, POPS, POPC (2:1:0.15) in the inner leaflet were generated by adapting a previously published protocol (Lin and London, 2014). Experiments were also conducted using POPC/POPS/POPE (1:1:1) as the inner leaflet. Briefly, 500 μL of 10 mM donor LUVs (POPC, eSM or mSM) were mixed with 100 μL 360 mM hydroxypropyl-α-cyclodextrin (HPα-CD) and vortexed for 2 hours at 55 °C. The donor-MCD solution was then mixed with 600 μL of 2 mM acceptor LUVs for 30 minutes at 55 °C to initiate outer leaflet lipid exchange. After the mixture had cooled to room temperature, the 1 mL solution was overlaid

onto 4 mL 10% sucrose in Medium 1 and centrifuged at 10 °C in an NVT-100 rotor for 40 minutes at 190,000 x g. The resulting asymmetric vesicle pellet was resuspended in 1mL Medium 1 and centrifugation was repeated followed by a final resuspension in 1 mL Medium 1. When examining the effect of transbilayer asymmetry on cholesterol partitioning, the 10 mM LUV donor contained 1% biotinyl-PE allowing for the final asymmetric vesicles to be bound to streptavidin agarose beads. ^{3}H-cholesterol was introduced into the asymmetric vesicles by incubation with 1 mM ^{3}H-cholesterol donor LUVs in the presence of 1 mM βCD at 37 °C followed by repeated washing to remove unincorporated ^{3}H-cholesterol. The cholesterol transbilayer distribution was determined by MCD mediated extraction, as described above.

Lipid Mass Spectrometry

Confirmation of outer leaflet lipid exchange in LUVs was performed by electrospray ionization tandem mass spectrometry (ESI-MS/MS). Asymmetric LUVs were generated as described above. The lipids were then extracted by the Bligh and Dyer method in the presence of internal standards including 1,2-dieicosanoyl-sn-glycero-3-phosphocholine (PC), N-heptadecanoy-sphingomyelin (SM), 1,2-ditetradecanoyl-sn-glycero-3-phosphoethanolamine (PE), and 1,2-ditetradecanoyl-sn-glycero-3-phosphoserine (PS). Lipid extracts from LUVs were then subjected to shotgun lipidomics in the negative ion mode using neutral loss scanning (NLS) for 50 amu (for PC), NLS for 87 amu (for PS), and product ion scanning for m/z 196 (for PE). Individual lipid molecular species were quantified by comparing the ion intensity of individual molecular species to that of the lipid class internal standard following corrections for type I and type II ^{13}C isotope effects.

Asymmetric vesicle TMA-DPH anisotropy

Fluorescence anisotropy measurements were performed using a Photon Technology International fluorometer and FeliX software. We generated symmetric SM/cholesterol and PC/PS/PE/cholesterol vesicles as described previously with the addition of 1 mol% TMA-DPH (Cheng et al., 2009). To generated asymmetric vesicles, SM/cholesterol was introduced into the outer leaflet of PC/PS/PE/cholesterol vesicles. During the asymmetry procedure no TMA-DPH was present in the SM/cholesterol donor vesicles. Outer leaflet TMA-DPH was then removed from PC/PS/PE/cholesterol vesicles during phospholipid exchange resulting in only inner leaflet labeling of asymmetric vesicles. Anisotropy was compared between symmetric, asymmetric and scrambled vesicles by excitation and emission at 365 nm and 425 nm, respectively.

Giant unilamellar vesicles

Symmetric GUVs containing 0.05 % rhodamine-DPPE were created by depositing 2.5 µL of 330 µM lipids dissolved in chloroform:methanol (95:5) onto two 3 cm long platinum wires positioned 3 mm apart (Juhasz et al., 2010). Detailed description of the GUV setup is described in **Appendix 2**. Organic solvent was evaporated away under a stream of nitrogen gas and then the wires were placed in a vacuum desiccator for at least 1 hour. The platinum wire was then submerged into approximately 1 mL of 30 mM sucrose solution at 70 ºC and connected to a digital PM5193 programmable synthesizer/ function generator producing an A/C sine wave at 10 Hz and 3 V for 90 minutes. For symmetric GUVs, the vesicles also contained 0.1 % NBD-DPPE. For microscopy purposes, the sucrose encapsulated vesicles were diluted into 30 mM glucose solution in order to settle the vesicles onto the bottom of a microscope dish.

Asymmetric giant unilamellar vesicles

Symmetric GUVs were initially generated and converted into asymmetric GUVs by outer leaflet lipid exchange by adapting a previously published protocol (Chiantia et al., 2011). 5 mM cholesterol containing outer leaflet donor lipids plus 0.1 % NBD-DPPE were dissolved in 30mM sucrose and incubated while vortexing for two hours at 55 ºC in 60 mM HPα-CD. DPPC/DOPC/Cholesterol (35:35:30) GUVs containing 0.05 % rhodamine-DPPE were then incubated in 20 mM of the HPα-CD/ donor lipid complex at 70 ºC for 30 minutes. To remove excess donor lipid and HPα-CD, the samples were washed in 30 mM glucose by passively filtering the sample through a membrane with 8 μm pores to collect purified GUVs. The resulting asymmetric GUVs were then transferred to a microscope dish.

Microscopy

All fluorescence images of GUVs were generated on a Nikon TE2000-E inverted fluorescent microscope with a 60x objective. Data was captured by 100-200 millisecond exposure with a Photometrics Cascade 512B CCD camera and Metamorph software. GUVs were found in the sample by searching the sample under low light conditions or by Differential Interference Contrast microscopy to avoid photo-oxidation effects. Post-acquisition editing was performed using ImageJ v1.43 software. FRAP analysis was performed on live cells using an inverted Leica BMI6000B microscope with a Quorum spinning-disk confocal system and Hamamatsu EM-CCD camera.

Fluorescence recovery after photobleaching

Fluorescence recovery after photobleaching analysis was performed on live HeLa cells transfected with shRNA targeting either CerS2 or a scramble control. Experiments were conducted 48 hours after transfection using an inverted Leica BMI6000B microscope and Quorum spinning-disk confocal system with temperature and humidified CO^2 regulation.

Cells were imaged with a 40x oil objective using 490 nm or 561 nm lasers with FITC and Texas-Red filter sets and captured with a Hamamatsu EM-CCD camera. Image acquisition was performed using MetaMorph software. All photobleaching experiments were conducted under identical conditions. An image sequence was acquired including 10-20 pre-bleach images and a complete post-bleach sequence (>60 seconds) acquired at a frame rate of 3-5 images/sec. A 305 μm^2 region of the plasma membrane was bleached with a 405 nm laser and the recovery at the centre of the bleach region was monitored overtime with 100-200 millisecond exposure per frame. An unbleached region of the plasma membrane, as well as, a background region was also monitored for each frame to normalize the recovery curves (Trinkle-Mulcahy et al., 2007). For analysis of diffusion in the plasma membrane, diffusion coefficients were determined using the diffuse program (described in Siggia *et al*. 2000), using the time-series of post-bleach images as input and a pre-bleach image as a reference for the cellular geometry (Ridsdale et al., 2006).

Cholesterol extraction from nucleated mammalian cells

HeLa cells were transfected with shRNA targeting either CerS2 or a scramble control by Attractene transfection reagent (Qiagen). Experiments were performed 48 hours after transfection. The cells were incubated with 1 μCi/mL ^{3}H-cholesterol supplemented into the media overnight prior to the experiment. After overnight incubation, the cells were washed with PBS 4 times to remove unincorporated ^{3}H-cholesterol and allowed to equilibrate for 5 hours in DMEM media supplemented with 10 % FBS. For outer leaflet cholesterol extraction, the cells were pre-incubated at 0 °C for one hour, followed by changing the media to 0 °C 10 mM MCD in DMEM or a DMEM negative control. After each time point, the media was removed and centrifuged at 2000 x g for 10 minutes and the amount of ^{3}H-

cholesterol in the supernatant was determined by scintillation counting. The adherent cells were then washed 3 times with ice cold PBS and harvested by scraping the cells in radioimmunoprecipitation assay buffer (RIPA) buffer. To determine total cell cholesterol content, a portion of cell lysate was measured by scintillation counting. The relative amount of outer leaflet cholesterol in the CerS2 knockdown and scramble control was then normalized to the maximal value of the scramble control samples to account for individual experimental variation.

Fluorescence resonance energy transfer

Fluorescence resonance energy transfer (FRET) was performed on HeLa cells co-transfected with mCFP- and mYFP- GPI-APs. Images were acquired with a Nikon TE2000-E inverted fluorescent microscope using a 60x objective. Data was captured a Cascade 512B CCD camera (Photometrics) and MetaMorph software (Universal Imaging). To quantify the crosstalk between CFP and YFP channels, cells were transfected with either mCFP or mYFP plasmids and imagined identically as FRET experiments. This generates crosstalk factors from CFP or YFP to the sensitized YFP channel, G_{CFP} or G_{YFP}. To measure the FRET, co-transfected cells were imagined with a 3-cube system: CFP_{ex}/CFP_{em} (I_{CFP}), CFP_{ex}/YFP_{em} (I_S) and YFP_{ex}/YFP_{em}(I_{YFP}). The true FRET signal, I_{FRET}, was calculated as following:

$$I_{FRET} = I_S - G_{CFP} \times I_{CFP} - G_{YFP} \times I_{YFP}$$

FRET efficiency, E (%), was derived as below:

$$E\ (\%) = I_{FRET} / (I_{FRET} + Q^* \times I_{CFP}) \times 100$$

*Q is the ratio of sensitized emission, I_{FRET}, to corresponding amount of donor (CFP) recovery in CFP_{ex}/CFP_{em} channel after YFP photobleaching using co-transfected HeLa cells.

The density of mCFP- and mYFP-GPI-AP in the HeLa cell PM was determined by imaging purified mCFP and mYFP protein in solution under identical conditions as the FRET experiments. Serial dilutions of the fluorescent proteins were imaged to produce a standard curve for fluorescent intensity as a function of protein concentration. The imaging volume was determined using the known pixel dimensions (xy) of the Cascade 512B CCD camera and by placing the fluorescent protein solutions between coverslips separated by 50 μm beads to standardize the focal depth (z). The standard curves for the soluble fluorescent protein densities were then used to interpolate the mCFP- and mYFP-GPI-AP protein densities from the FRET experiments.

The mCFP- and mYFP-GPI-APs expressing HeLa cells were treated with or without 50 μM myriocin and fumonisin B1 for 3 days to deplete the sphingolipids from the cells. The night before microscopy experiments, the media was changed to serum free media to prevent incorporation of exogenous lipids from the fatal bovine serum into the cells. In the morning, a subset of the cells was incubated with either 16:0 SM or 24:0 SM/γ-CD complex for 1 hour at 37 °C. Microscopy experiments were performed at approximately 12 °C. Each treatment was also accompanied by an additional dish treated with 0.2 % saponin for 30 minutes on ice before microscopy experiments. This was to compare the FRET change before and after depletion of cholesterol for each treatment.

FRET efficiency simulation

A Monte Carlo approach was used for simulations of density-dependent FRET using a program written in Fortran 95 and compiled using gfortran/gcc running in the command line interface of a computer running Mac OSX 10.8. The number of YFP and CFP molecules per 1000 nm X 1000 nm square were input. YFP and CFP molecules were assigned floating-

point coordinates at random within a square patch of simulated membrane using the Mersanne Twister pseudorandom number generator and units of nm. Molecules were not allowed to fall within 2.4 nm of other molecules, as this is the diameter of the GFP cylinder. Once molecules were placed, FRET efficiency (E) was calculated for each CFP to every YFP within 50 nm of the CFP using the equation $E = 1 / (1 + (r/R_0)^6$ where r is the distance between the centers of the two molecules and R_0 is 4.89 nm (Rizzo et al., 2006). At greater than 50 nm, $E < 1 \text{ X } 10^{-6}$, and FRET was not calculated for reasons of computational efficiency. Cumulative FRET efficiency from a CFP was calculated from the cumulative probability of FRET from this CFP molecule to all available YFPs.

$$1 - \prod_{YFPn} (1 - E\text{YFPn})$$

Total FRET efficiency was calculated as the mean efficiency of FRET from all CFPs included in the simulation. As expected (Fung and Stryer, 1978), total FRET efficiency depended only on the density of acceptor (YFP) included in the simulation and not on CFP density.

Thin layer chromatography

To confirm thorough depletion of sphingolipids by the myriocin and fumonisin b1 treatment, as well as, to test the efficiency of sphingomyelin supplementation, thin layer chromatography (TLC) was performed on lipid extracts from HeLa cells. After each treatment, HeLa cells were trypsinized and washed in PBS, followed by lipid extraction (Bligh and Dyer, 1959). Lipid extracts were loaded onto the TLC plate alongside purified lipid standards to compare sphingolipid levels in all treatments. The lipids were resolved on the plate by running in a chloroform/acetone/methanol/acetic acid/water (6:8:2:2:1) solvent

system. The lipids were visualized by incubating the plate in a solution of 0.03 % coomassie blue G, 30% methanol and 100 mM NaCl followed by destaining in 30% methanol and 100 mM NaCl. Sphingolipid content was quantified by densitometry using Image J software.

Statistical analysis

Statistical differences in cholesterol transbilayer distribution between different asymmetric LUVs were determined by one-way ANOVA. Post hoc comparisons were conducted relative to the mSM asymmetric sample with * indicating $P<0.05$, ** indicating $P<0.01$ and *** indicating $P<0.001$. For comparisons of erythrocyte number with and without cyclodextrin treatment, statistical differences were examined using an unpaired Student's *t*-test. Non-linear regressions were performed in Graphpad Prism 5.0 and fit using the equation: Y=Top*(1-exp(-K*X)). Error bars throughout represent standard error of the mean from 3 independent experiments.

Chapter 3 - Development and use of the cholesterol transbilayer distribution assay

3.1 - Introduction

The mammalian cell PM is strictly asymmetric with distinct phospholipid and protein composition in the inner (cytoplasmic) and outer leaflets. However, the cholesterol transbilayer distribution is still highly debated (Devaux and Morris, 2004; Devaux and Zachowski, 1994). The role of cholesterol in the PM is multifactorial. Classically, cholesterol is a structural molecule in the PM that modulates membrane fluidity and, because of a lack of a cell wall, also serves to control membrane permeability (Cooper, 1978). This view was later greatly expanded in recent years, as cholesterol was discovered to be involved in regulating protein-protein interactions and cell signalling events in the context of membrane microdomains, or lipid rafts (Eisenberg et al., 2006; Kabouridis et al., 2000). The lipid raft hypothesis proposes that cholesterol interacts with PM lipids, mainly sphingolipids, to form ordered membrane domains (Lingwood and Simons, 2010). The preferential hydrogen-bonding between cholesterol and the sphingolipid side chains is thought to enhance the cholesterol-sphingolipid interaction. Since sphingolipids are exclusively in the outer leaflet of the PM, cholesterol is assumed to also reside in the outer leaflet, although this has not yet been established.

Early attempts to characterize cholesterol partitioning in the PM generated conflicting results (Blau and Bittman, 1978; Fisher, 1976; Mondal et al., 2009). Using different techniques by independent research groups, cholesterol has been suggested to be primarily in the outer leaflet (Fisher, 1976), evenly distributed between leaflets (Blau and Bittman, 1978), and also highly enriched in the inner leaflet (Mondal et al., 2009; Schroeder et al., 1991). Furthermore, Leventis and Silvius *et al* used the rate of cholesterol efflux from model

membrane vesicles of different lipid compositions and found that cholesterol exhibits the highest affinity for saturated lipids over unsaturated lipids and a slight preference for sphingolipids compared to glycerophospholipids (Leventis and Silvius, 2001). Since the PM outer leaflet contains sphingolipids exclusively in the outer leaflet, these data suggested that cholesterol-lipid interactions may cause cholesterol to be localized in the outer leaflet as a result. Moreover, a high concentration of cholesterol in the outer leaflet could support the lipid raft hypothesis by increasing the propensity for cholesterol to interact with sphingolipids and outer leaflet PM proteins and, therefore, support protein-protein interactions in ordered membrane domains. Once again, however, this assumption has not been supported by direct experimental evidence. We, therefore, aimed to develop a novel strategy to define the cholesterol transbilayer distribution in live mammalian cells. The strategy developed here is to distinguish and quantify cholesterol in each leaflet of a bilayer without the transbilayer movement of cholesterol. Once flip-flop is stopped, cholesterol in the outer leaflet of a bilayer membrane can be quantitatively extracted or exchanged, using cholesterol chelating agents, such as cyclodextrin.

Cyclodextrins are polymers of glucose molecules (dextrin) that are arranged in a ring structure. There are three classes of cyclodextrins, α, β and γ that have 6, 7 or 8 glucose molecules in the ring, respectively (Zsadon et al., 1978). Although cyclodextrins are water soluble, the centre of the ring is non-polar and has been shown to bind hydrophobic compounds (Christian et al., 1999; Huang and London, 2013; Kilsdonk et al., 1995). As a result, each class of cyclodextrin has a uniquely sized pore that displays affinity for different molecules (Leventis and Silvius, 2001). The β-cyclodextrins (βCD) bind cholesterol with high affinity and specificity (Leventis and Silvius, 2001). Molecular dynamic simulations

have demonstrated that two molecules of βCD can surround one molecule of cholesterol to solubilize cholesterol in aqueous media by shielding the hydrophobic region (López et al., 2011). The α-cyclodextrins (αCD) on the other hand, have a smaller pore size, which does not accommodate cholesterol but has been shown to bind phospholipids (Lin and London, 2014). The γ-cyclodextrins (γCD) can also bind phospholipids and are particularly useful for binding lipids with long acyl chains (Raghupathy et al., 2015). Cyclodextrins can also be hydroxylated, methylated or hydroxypropylated around the ring, which alters their binding affinity for the target compounds. The experiments described in this work primarily utilized hydroxy-βCD, generally referred to simply as βCD, and methyl-βCD (MCD). Although both βCD and MCD bind cholesterol, they exhibit different binding affinities that can be exploited for specific applications. Since βCD binds cholesterol with lower affinity than MCD (Leventis and Silvius, 2001), βCD is preferable as a means to donate cholesterol to a membrane or to exchange cholesterol between adjacent membranes. MCD binds cholesterol with higher affinity and is more effective at sequestering cholesterol out of a membrane into the aqueous media with a reduced capacity to donate cholesterol back to the membrane. This distinction led us to develop a system to characterize the cholesterol transbilayer distribution using MCD. MCD is a membrane impermeable compound, which could enable selective outer leaflet cholesterol extraction from a bilayer. Additionally, cyclodextrins have been shown to be effective at extracting cholesterol at low temperature, which supports the plausibility of this approach (Ohvo and Slotte, 1996). By using MCD when cholesterol flip-flop is stopped, we could extract and quantify the amount of cholesterol in the outer leaflet relative to the total cholesterol to determine the percent of cholesterol in each leaflet.

Using MCD as a strategy to determine the cholesterol transbilayer distribution, however, initially presents a series of conceptual and technical challenges. Before directly attempting to selectively extract outer leaflet cholesterol from the mammalian cell PM, a series of control experiments and proof-of-concept experiments were performed to ensure that the system is reliable. Some of the foreseeable challenges include:

(**1**) Cholesterol rapidly flips spontaneously between the inner and outer leaflet, therefore, as cyclodextrin is extracting the outer leaflet cholesterol, the inner leaflet pool will migrate outwards and cause the extraction of cholesterol from both leaflets.

(**2**) Since cholesterol is approximately 30 % of the PM lipid, therefore, extracting a substantial percentage of the PM could compromise the PM integrity causing cell lysis.

(**3**) Although the majority of the mammalian cell cholesterol is in the PM, cholesterol is also present in other intracellular pools, which would need to be strictly distinguished from the PM pool.

We chose to address many of the technical challenges and the proof-of-concept experiments by first developing the protocol in a simplified model membrane system. Control experiments were initially carried out using artificial bilayer membrane vesicles, known as large unilamellar vesicles (LUV). These experiments involve generating vesicles, also referred to as liposomes, using commercially acquired pure lipids. We can then construct bilayer membranes with a defined size and composition and use these vesicles to determine if MCD can feasibly extract outer leaflet cholesterol. Since phospholipids in aqueous solution spontaneously form a bilayer, the LUVs that we used are symmetric membranes with the lipids distributed uniformly both laterally and transversely.

Furthermore, the curvature of LUVs that are100 nm, or greater in size, has previously been shown to be negligible (Nordlund et al., 1981). Under these conditions, the compositions of the two LUV leaflets should be identical. As such, 50% cholesterol will be present in each leaflet.

3.2 - Results

3.2.1 - Proof-of-concept experiments – producing 100 nm LUVs

A lipid mixture can be extruded repeatedly through filters with a defined pore size to form vesicles with single bilayer (unilamellar) that are uniform in size (MacDonald et al., 1991). When phospholipids are initially mixed in solution, various membrane structures of different sizes can form, mostly multilamellar vesicles. Dynamic light scattering (DLS), a cuvette-based technique, is particularly useful for determining LUV size because the vesicles are below conventional optical resolution (Egelhaaf et al., 1996). As described in the methods section, DLS showed that after freeze/thawing a lipid sample followed by extrusion of the vesicles through the mini-extruder system by Avanti Polar Lipids (MacDonald et al., 1991), LUVs were produced, which were uniform and 100 nm in size (**Figure 1A**).

To verify if LUVs produced above are unilamellar, we performed an assay to quantify the transbilayer distribution of aminophospholipids using TNBS, which was originally used to determine that PE and PS were localized to the inner leaflet of the mammalian cell PM (Bretscher, 1972a). TNBS reacts with the amino groups on the phospholipids to produce an orange colour that can be quantified by spectrophotometer. If the vesicles are unilamellar and at least 100 nm in size (i.e. negligible differences in surface area between the two leaflets), TNBS should react with 50% of the PE and PS. However, if the vesicles are multilamellar, there will be a portion of the lipid that is encapsulated within

A

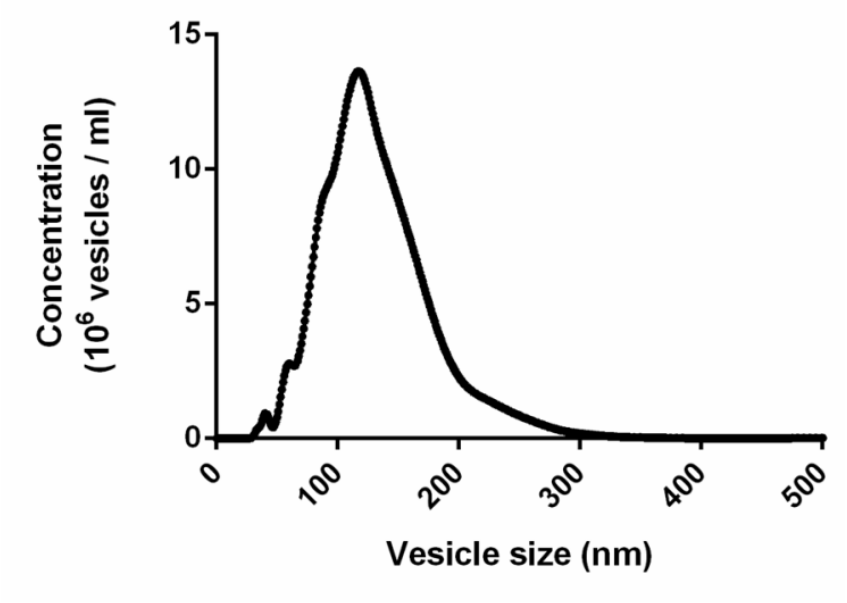
Concentration
(10^6 vesicles / ml)
15
10
5
0
0
100
200
300
400
500
Vesicle size (nm)

B

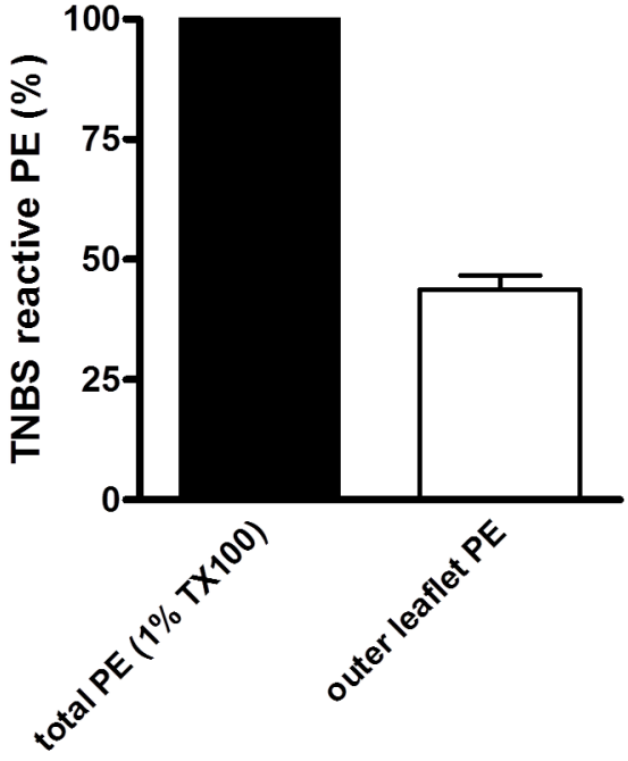
TNBS reactive PE (%)
100
75
50
25
0
total PE (1% TX100)
outer leaflet PE

Figure 1 – Extrusion of multilamellar vesicle samples through a membrane with 100 nm pores results in a uniform population of unilamellar vesicles. A) Size distribution of a vesicle population after extrusion through 100 nm membrane. Heterogeneous population of lipid vesicles were passed through a membrane containing 100 nm pores at least 15 times to produce a uniform size population. **B**) Extruded vesicles containing aminophospholipids PE and PS were incubated with membrane impermeable trinitrobenzene sulphonic acid (TNBS). Only outer leaflet PE and PS will react with TNBS to produce an orange colour. The amount of reactive lipid in intact vesicles was determined by reading absorbance at 410 nm compared with TNBS reactive lipid from TX-100 solubilized LUVs (100%). TNBS modified 50% of the vesicle aminophospholipids, demonstrating that PE and PS are equally distributed between leaflets and that the LUVs are unilamellar.

outermost surface vesicle that will not be accessible to react with TNBS. Therefore, a result of less than 50% PE and PS reacted would be indicative of multilamellar vesicles. The TNBS assay was performed on extruded vesicles composed of PC/PS/PE (1:1:1). The results showed that 50 % of the lipids reacted with TNBS, demonstrating the vesicles are unilamellar (**Figure 1B**).

We next aimed to determine if cyclodextrin treatment would compromise membrane integrity. The removal of lipid from a bilayer by MCD could rupture the vesicles or create pores in the membrane. To address this issue, we began with LUVs containing trace amount of cholesterol (0.0001 %). With the low cholesterol content, the LUVs could remain intact even if all the cholesterol extracted by MCD. To test this, LUVs with trace cholesterol were generated with encapsulated Cy3-tranferrin. If the LUVs remain intact, then the fluorescent transferrin should remain encapsulated and not be released into the supernatant. The LUVs were incubated with 5 mM MCD for 30 minutes and the amount of Cy3 present in the supernatant was monitored. We found no increase in fluorescence in the supernatant after the MCD treatment, compared to non-treated LUVs. As a positive control, 1 % TX-100 was added at the end, which lysed the vesicles and caused a dramatic increase in the supernatant fluorescence (**Figure 2**). Thus, for the concentration of MCD used in this study and when cholesterol is a minor component of the membrane, MCD does not compromise the membrane integrity.

3.2.2 - Temperature regulation of cholesterol flip-flop

The major foreseeable challenge in using MCD to extract and quantify the cholesterol transbilayer distribution comes from the rapid transverse movement of cholesterol across the bilayer (Lange et al., 1981). As described in **section 3.1**, our approach to address this issue

A

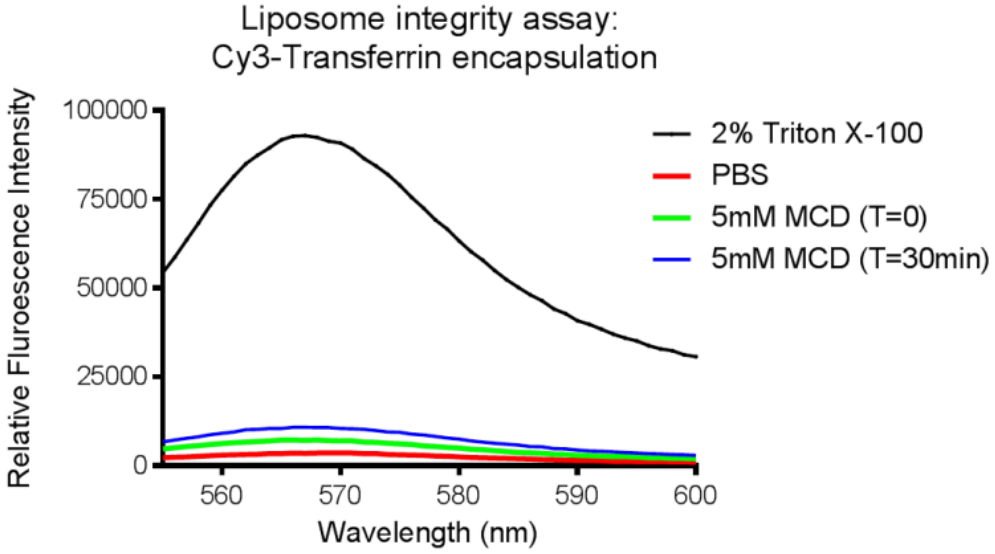
Liposome integrity assay:
Cy3-Transferrin encapsulation
Relative Fluroescence Intensity
100000
75000
50000
25000
0
560
570
580
590
600
Wavelength (nm)
2% Triton X-100
PBS
5mM MCD (T=0)
5mM MCD (T=30min)

B

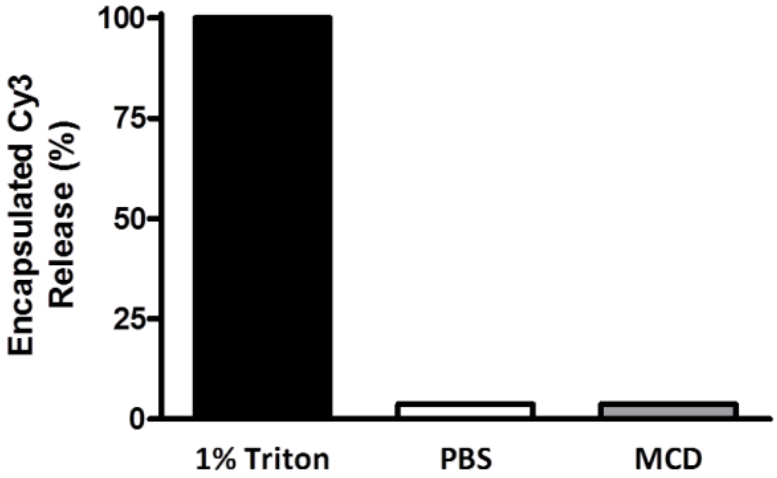
Encapsulated Cy3
Release (%)
100
75
50
25
0
1% Triton
PBS
MCD

Figure 2 – Large unilamellar vesicles remain intact during the cyclodextrin treatment. **A**) LUVs composed of POPE/POPS/POPC (1:1:1), plus 1 % biotinyl-PE were generated in the presence of Cy3-transferrin. The vesicles were then bound to streptavidin coated agarose beads and washed multiple times by brief centrifugation to remove un-encapsulated Cy3-transferrin. The Cy3-transferrin containing vesicles were then treated with PBS, MCD (5 mM) or dissolved with 1% TX-100. The amount of Cy3 released into the media after 30 minute treatment was quantified by fluorescence spectroscopy. MCD treatment did not cause Cy3 leakage and thus did not affect LUV structural integrity. **B**) Quantification of Cy3 release from unilamellar vesicles after PBS or MCD treatment relative to the triton X-100 sample. Values were determined by comparing the peak maximum of each curve.

was to prevent the transbilayer movement of cholesterol by lowering temperature. We proposed that if cholesterol flip-flop is prevented at low temperature, MCD would only have access to the cholesterol present in the outer leaflet. For the LUVs produced above, MCD would maximally extract 50 % of the cholesterol from the bilayer under this non-flip-flopping condition. However, at temperatures that allow flip-flopping, regardless of the steady state cholesterol partitioning, 100 % cholesterol should be accessible to MCD due to inner leaflet cholesterol flipping outward.

We began to test effect of temperature on cholesterol flip-flop using LUVs composed of PC/PS/PE (1:1:1) that contained only a trace amount of radiolabelled (^{3}H) cholesterol (100 pmol of ^{3}H-cholesterol per mM phospholipid). A detailed description of the cholesterol transbilayer distribution assay can be found in **Appendix 1**. Briefly, ^{3}H-cholesterol containing LUVs were generated with 1% biotinylated PE. This allows the vesicles to be attached to streptavidin coated agarose beads, which facilitates isolation of the vesicles from the aqueous supernatant by short low-speed centrifugation. LUVs are incubated with MCD over time and then separated from supernatant to quantify the percentage of cholesterol extracted by MCD, relative to total cholesterol (lysed LUVs).

Initially, the system did not appear to work. We were consistently extracting more than 50 %, but less than 100% cholesterol from the symmetric LUVs at 0 °C (**Figure 3A**). After trial and error, it was discovered that picking up the samples by hand to open the tubes was sufficient to warm the sample and temporarily activate flip-flop. To overcome this issue, the temperature was more stringently monitored and all sample manipulations were performed with pre-cooled utensils instead of by hand (**Figure 3B**). After optimizing the protocol, we found that in symmetric LUVs at 0 °C the cholesterol extraction consistently

A

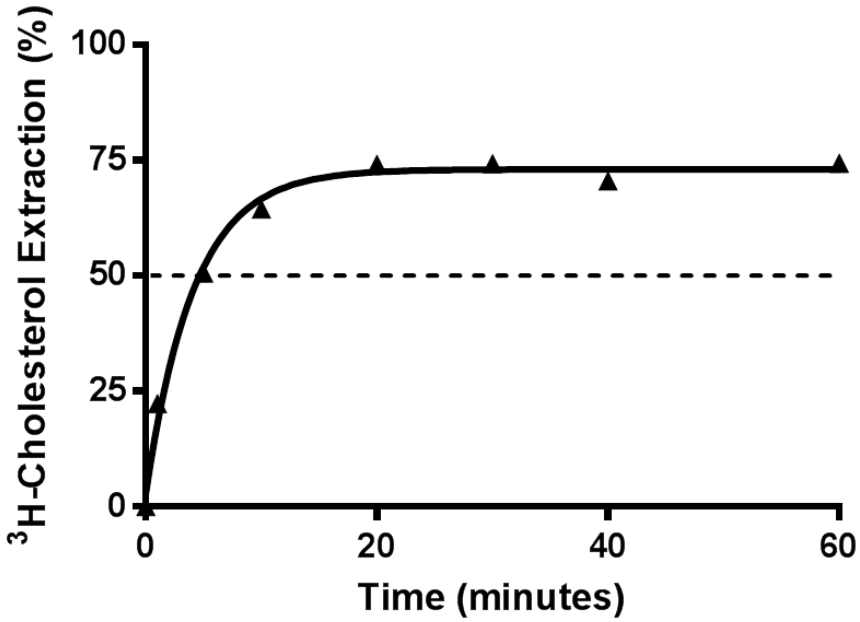
100
75
50
25
0
^{3}H-Cholesterol Extraction (%)
0
20
40
60
Time (minutes)

B

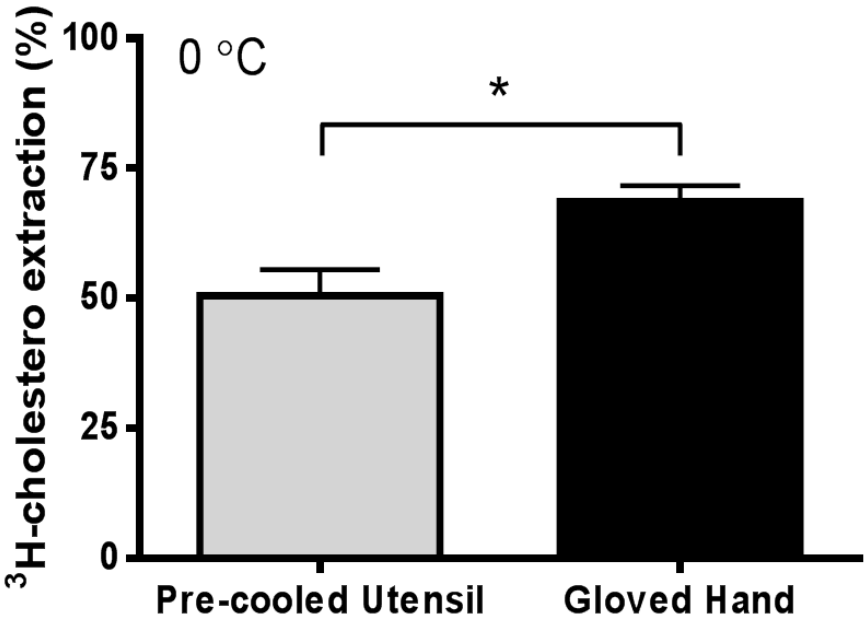
100
75
50
25
0
^{3}H-cholestero extraction (%)
0 °C
*
Pre-cooled Utensil
Gloved Hand

Figure 3 – The cholesterol extraction assay is sensitive to temperature. A) Cholesterol extraction from large unilamellar vesicles by MCD under sub-optimal experimental conditions. During optimization, cholesterol extraction from unilamellar vesicles on ice was consistently greater than 50 %, which suggested that cholesterol was still mobile in the membrane. **B)** Bar graph depicting the cholesterol extraction plateau value from a time course experiment. Further optimization determined that temperature must be very stringently controlled. Manipulation of samples by hand during the experiment causes an increase in cholesterol extraction (black bar) due to inadvertent warming of the sample and subsequent re-initiation of cholesterol flip-flop. If the experiment is performed with cooled utensils (grey bar), cholesterol flip-flop is prevented. Statistical significance was determined by T-test after 3 independent experiments.

reach a plateau at approximately 50 % (**Figure 4**). At 37 °C, when cholesterol is actively flip-flopping, the cholesterol extraction reached nearly 100 % (**Figure 4**). We also used other symmetric LUVs with different phospholipid compositions and consistently found that the cholesterol extraction reached a plateau at 50 % at 0 °C (**Figure 5**). Together, these results show that lowering temperature to 0 °C is sufficient to prevent cholesterol flip-flop.

3.2.3 - Cholesterol exchange from membranes with physiological cholesterol content

Knowing that lowering temperature to at 0 °C can prevent the transbilayer movement of cholesterol, we developed a similar protocol to assay cholesterol in LUVs with physiologically relevant cholesterol content (30 %). We anticipated that using MCD to directly extract outer leaflet cholesterol from a mammalian cell or a membrane with a high concentration of cholesterol could be problematic as a result of removing a substantial portion of the membrane lipids. To address this issue, a modified protocol was necessary to remove outer leaflet cholesterol without causing structural damage to the membrane. We developed an assay where ^{3}H-cholesterol can be removed from a membrane by exchange with unlabelled cholesterol (no net loss of cholesterol) (**Figure 6A**). Similar membrane exchange systems have been used previously in other contexts (Leventis and Silvius, 2001). However, to our knowledge, this is the first attempt to use this strategy to quantify the cholesterol partitioning. This assay involves incubating two populations of LUVs together: donor LUVs with ^{3}H-cholesterol and 100-fold excess acceptor LUVs with unlabelled cholesterol. Cholesterol is exchanged between the LUVs by using a low concentration of βCD as a shuttle. Since both populations of LUVs contain equal concentrations of cholesterol, there is no net loss of cholesterol. The outer leaflet ^{3}H-cholesterol from donor LUVs would exchange with non-radiolabelled cholesterol from the acceptor LUVs,

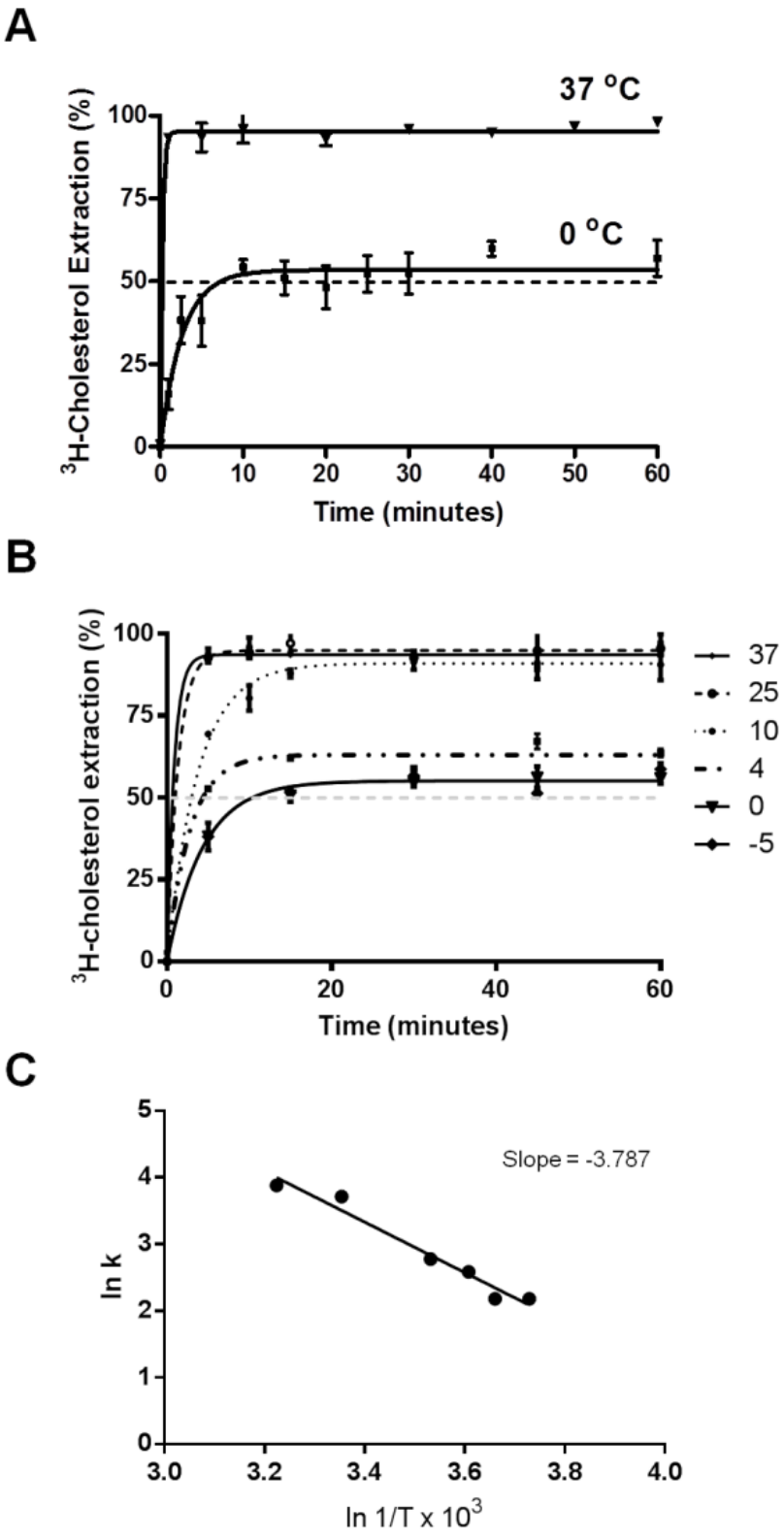
A
37 °C
0 °C
^{3}H-Cholesterol Extraction (%)
Time (minutes)
B
^{3}H-cholesterol extraction (%)
Time (minutes)
37
25
10
4
0
-5
C
Slope = -3.787
ln k
ln 1/T x 10^3

Figure 4 – Cholesterol is evenly distributed in symmetric large unilamellar vesicles. A) Symmetric POPC/POPS/POPE (1:1:1) LUVs containing trace cholesterol were incubated in 5 mM MCD over time. MCD was able to extract 100% cholesterol at 37 °C, but at 0 ^{o}C, only 50% cholesterol is removable. Error bars represent standard error of the mean from at least 3 independent experiments. **B**) Comparison of cholesterol extraction by 5 mM MCD from symmetric POPC/POPS/POPE (1:1:1) LUVs at various temperatures over time. **C**) Plot of the slopes (k) of the initial linear region of the cholesterol extraction curves from (**B**) as a function of temperature (kelvins). The slope of this curve was used to calculate the activation energy for cholesterol extraction from POPC/POPS/POPE (1:1:1) LUVs using the Arrhenius equation ($k=Ea/8.3145\ J\ K^{-1}mol^{-1}$). Activation energy was determined to be 31.485 KJ/mol (7.6 kcal/mol) for this system.

A

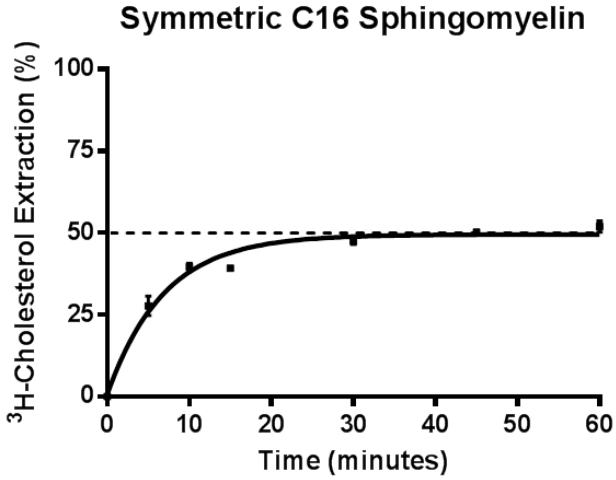
Symmetric C16 Sphingomyelin
^{3}H-Cholesterol Extraction (%)
100
75
50
25
0
0
10
20
30
40
50
60
Time (minutes)

B

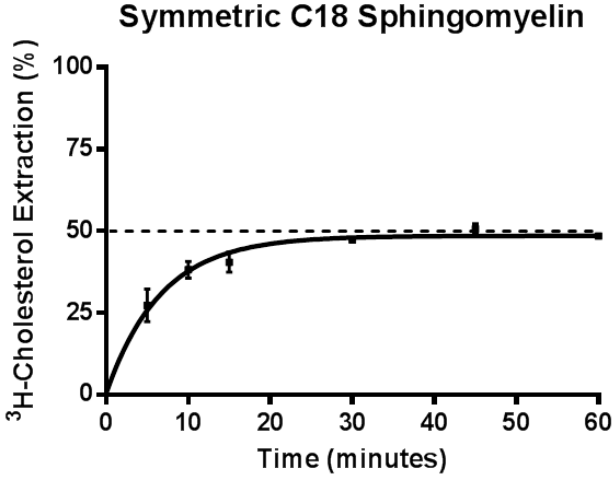
Symmetric C18 Sphingomyelin
^{3}H-Cholesterol Extraction (%)
100
75
50
25
0
0
10
20
30
40
50
60
Time (minutes)

C

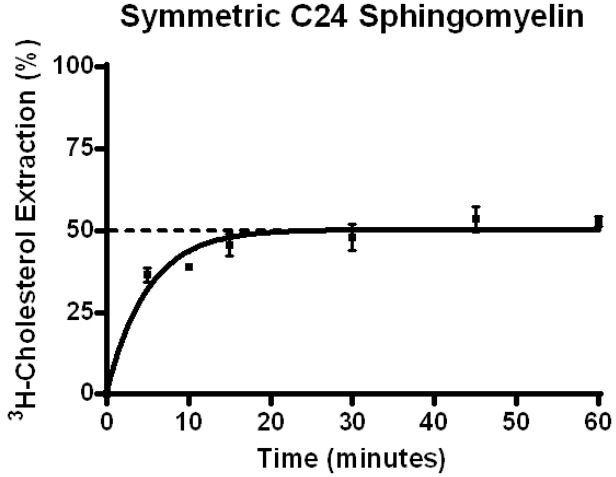
Symmetric C24 Sphingomyelin
^{3}H-Cholesterol Extraction (%)
100
75
50
25
0
0
10
20
30
40
50
60
Time (minutes)

Figure 5 – Cholesterol is evenly distributed between inner and outer leaflets of symmetric large unilamellar vesicles, regardless of phospholipid composition. Symmetric LUVs of 16:0 SM (**A**), 18:0 SM (**B**) and 24:0 SM (**C**) were treated with MCD (5 mM) at 0 °C overtime. MCD was only able to remove 50% cholesterol, which suggests cholesterol is evenly distributed between bilayer leaflets and the 50% cholesterol extraction plateau at 0 °C is independent of lipid composition. Error bars represent standard error of the mean from 3 independent experiments.

A

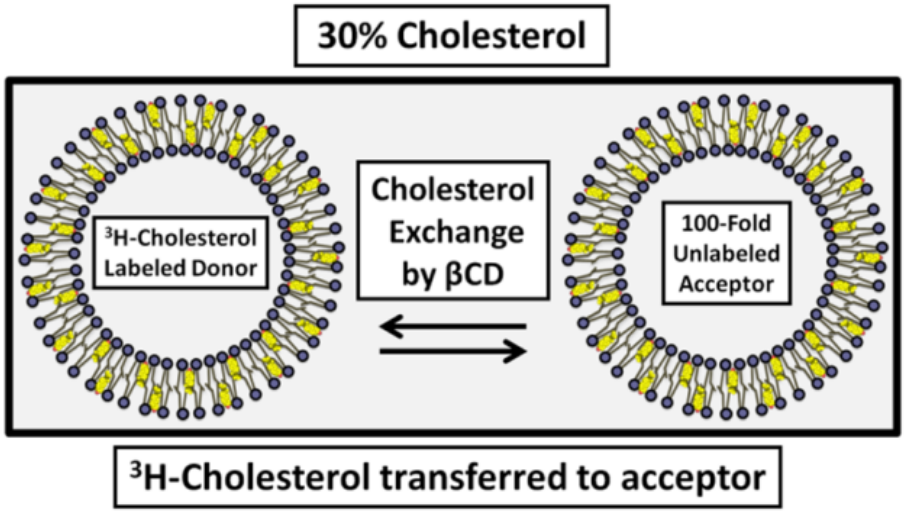
30% Cholesterol
³H-Cholesterol Labeled Donor
Cholesterol Exchange by βCD
100-Fold Unlabeled Acceptor
³H-Cholesterol transferred to acceptor

B

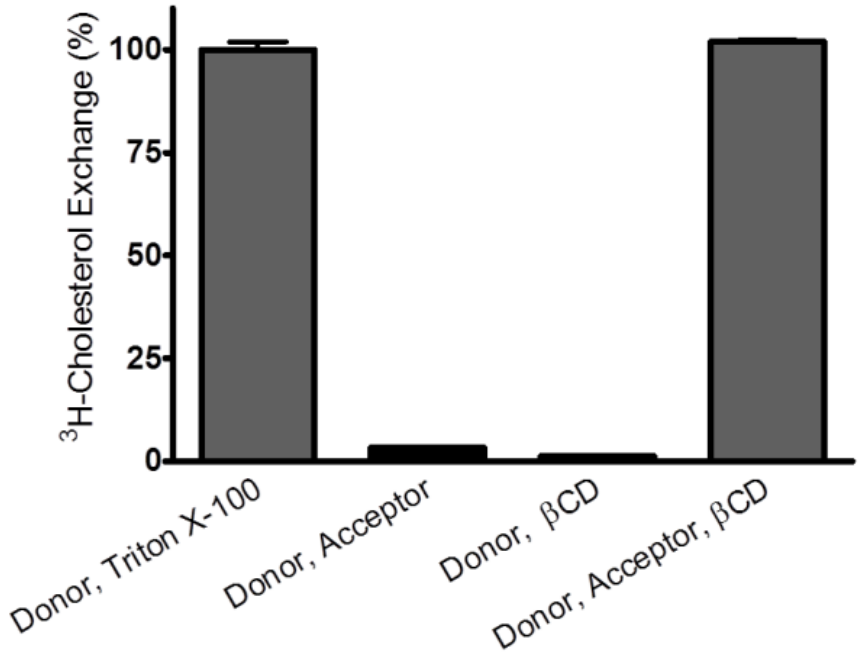
³H-Cholesterol Exchange (%)
100
75
50
25
0
Donor, Triton X-100
Donor, Acceptor
Donor, βCD
Donor, Acceptor, βCD

Figure 6 – Cholesterol extraction from membranes with a high concentration of cholesterol can be achieved by intermembrane exchange using β-cyclodextrin as a sterol shuttle. A) Pictogram of intermembrane cholesterol exchange, facilitated by βCD as shuttle, between donor and acceptor membrane with 30 % cholesterol. ^{3}H-Cholesterol is transferred from the donor membrane to acceptor membrane (100-fold excess) by βCD and replaced with unlabelled cholesterol. During exchange, the cholesterol content in the donor and acceptor membranes remains unchanged. **B**) ^{3}H-cholesterol labeled LUVs containing 30% cholesterol (donor) were attached to streptavidin coated agarose beads and incubated with 100-fold unlabeled but identical LUVs (acceptor), or βCD or acceptor plus βCD for 2 h at 37 °C. After the exchange, the bead-bound donor vesicles were pelleted by brief centrifugation and the ^{3}H-cholesterol in the medium was quantified. Some of the wells were directly lysed with 1% TX-100 (donor + TX100) as input control (100%). As shown above, neither acceptor nor βCD alone could significantly exchange cholesterol with donor LUVs. Only when both acceptor and βCD were present, could donor LUVs completely exchange ^{3}H-cholesterol (100%) at 37 °C.

which will eventually reach equilibrium. Given that the acceptor LUVs are 100-fold excess of the donor, 99 % of the ^{3}H-cholesterol from the donor should be transferred to the acceptors when cholesterol flip-flop is active. Once completed, the donor LUVs, attached to agarose beads, and the acceptor LUVs are separated by centrifugation and the amount of ^{3}H-cholesterol transferred to the acceptor LUVs (in supernatant) is quantified. This protocol was able to maintain membrane integrity and enables us to analyze LUVs with high cholesterol contents.

We first tested this exchange protocol using 100 nm symmetric LUVs that contained 30 % cholesterol. We used a range of donor/acceptor ratios in combination with different concentrations of βCD to establish the lowest possible concentration of βCD, capable of completely exchanging the ^{3}H-cholesterol within a reasonable timeframe. For example, as cholesterol is not soluble in the aqueous solution, βCD is necessary as a shuttle for inter-membrane cholesterol exchange. When considering the total available cholesterol (**Figure 6B,** *first bar*), we observed negligible exchange of cholesterol between populations in the absence of βCD (**Figure 6B**, *second bar*). Furthermore, in the absence of the lipid acceptor, βCD has limited capacity to retain cholesterol in the supernatant (**Figure 6B**, *third bar*). Thus, the complete system requires the donor, acceptor and βCD to shuttle cholesterol between membranes (**Figure 6B**, *fourth bar*). Also, 100-fold excess acceptor was necessary and sufficient to transfer essentially all the ^{3}H-cholesterol from the donor to the acceptor. Furthermore, we were able to conclude that 1 mM βCD was effective at exchanging the cholesterol between two LUV populations.

We next aimed to determine if low temperature can prevent cholesterol flip-flop in LUVs with high cholesterol content. The LUVs were composed of POPC/POPS/POPE

(1:1:1) with 30 % cholesterol. Again, the donor LUVs also received 100 pmol ^{3}H-cholesterol in addition to the 30 % unlabelled cholesterol. The 100-fold excess acceptor LUVs were identical to the donor, except without ^{3}H-cholesterol. To initiate the cholesterol exchange, the βCD was first mixed with the acceptor to pre-load the βCD with unlabelled cholesterol, followed by mixing the βCD/acceptor solution with the donor LUVs. A time course was then carried out by determining the percent of cholesterol exchanged from the donor to acceptor LUVs over time. Similar to **Figure 4**, the amount of ^{3}H-cholesterol exchanged was determined relative to total ^{3}H-cholesterol (parallel samples lysed by TX-100 to release all cholesterol into the supernatant). The results confirmed that βCD efficiently exchanges nearly all the ^{3}H-cholesterol from the donor to the acceptor at 37 °C (**Figure 7**). At 0 °C, however, the cholesterol exchange reached a plateau at 50 % (**Figure 7**). Thus, agreeing with our previous result (**Figure 4**) that cholesterol flip-flop is prevented at 0 °C and that the exchange protocol is a valid system to quantify the cholesterol in the outer leaflet of LUVs with 30% cholesterol.

3.2.4 - Cholesterol transbilayer distribution in mammalian cells

So far, we validated that lowering temperature to 0 °C can prevent cholesterol flip-flop, and enable the quantification of outer leaflet cholesterol from LUVs (**Figure 7**). We next applied this exchange protocol to quantify cholesterol partitioning in the mammalian cell PM. As stated above, most mammalian cells have intracellular membrane compartments that contain cholesterol, such as the ER, Golgi and endosomes (Iaea and Maxfield, 2015). This presents a challenge to distinguish the cholesterol specifically present in the PM, apart

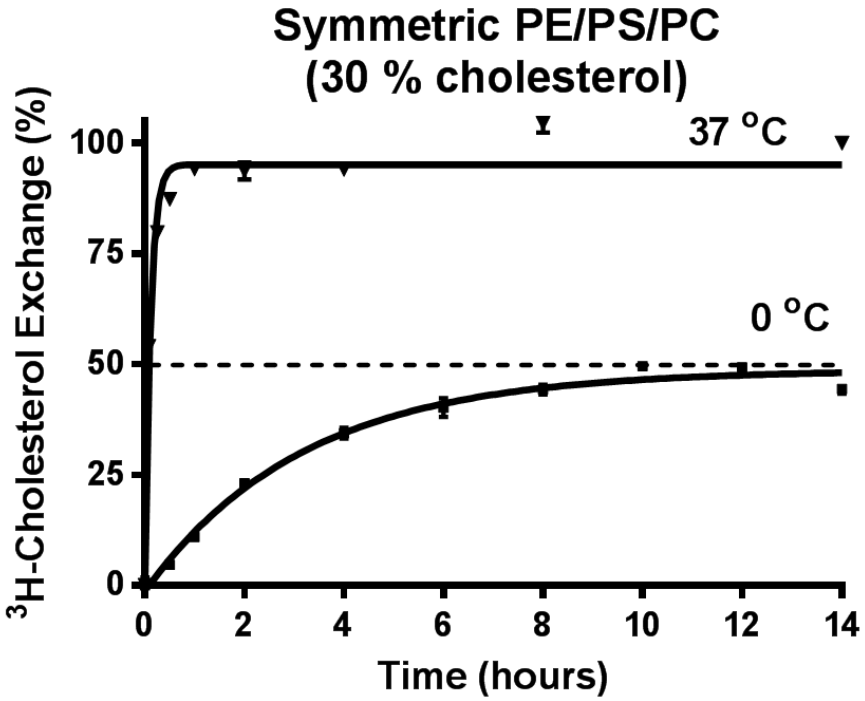
Symmetric PE/PS/PC
(30 % cholesterol)
37 °C
0 °C
^{3}H-Cholesterol Exchange (%)
100
75
50
25
0
0
2
4
6
8
10
12
14
Time (hours)

Figure 7 – Cholesterol is evenly distributed in symmetric large unilamellar vesicles with physiologically relevant cholesterol content. Cholesterol is exchanged between ^{3}H-cholesterol labelled donor vesicles and unlabelled, 100-fold excess acceptor vesicles at 0 °C and 37 °C by 1mM βCD. The amount of ^{3}H-cholesterol transferred to the acceptor vesicles was monitored overtime and quantified by scintillation counting. In symmetric POPE/POPS/POPC (1:1:1) LUVs containing 30% cholesterol, intermembrane exchange facilitates complete transfer of cholesterol from donor to acceptor membranes at 37 °C. At 0 °C, cholesterol flip-flop is prevented and only outer leaflet cholesterol is exchanged. Error bars represent the standard error of the mean from 3 independent experiments.

from the cholesterol from other internal organelles. The intracellular cholesterol pools are problematic for two reasons:

(**1**) Although the amount of cholesterol present in the outer leaflet of a mammalian cell could be quantified using the established protocol above, the intracellular cholesterol pools prevent us from accurately determining the total cholesterol in the PM.

(**2**) Although the protocol developed above could effectively control cholesterol flip-flop, it does not necessarily prevent diffusion or exchange of cholesterol between intracellular organelles including between PM and other intracellular membrane, which could act to re-supply the PM with intracellular cholesterol during cholesterol exchange at both 0 and 37 °C.

Historically, this issue was avoided simply by selecting a cell type that lacks internal membranous organelles. As such, much of the original work characterizing the mammalian cell PM came from studies of the human erythrocyte (Kahlenberg et al., 1974). Unlike most other cell types in mammals, mature erythrocytes are anucleate and do not have cholesterol containing intracellular organelles (Zhang et al., 2011). Erythrocytes are produced from hemocytoblast stem cells in the bone marrow that can differentiate into multiple cell types, such as monocytes, T-cells and B-cells. Prior to release into the circulatory system as an immature reticulocyte, the erythrocyte progenitor cells extrude the nucleus from the cell and release or degrade the intracellular organelles (Ji et al., 2008). The mature erythrocyte, therefore, becomes an ideal candidate cell type for characterizing the PM without the complications of other membrane compartments.

We thus chose to apply our exchange protocol to characterize cholesterol between leaflets in human erythrocytes. Erythrocytes were isolated from the whole blood of healthy

donors and used within one day of isolation. The method was analogous to the LUV cholesterol exchange protocol. Specifically, one population of erythrocytes are labelled with ^{3}H-cholesterol, biotinylated and attached to streptavidin coated dishes. The cells are then incubated with 100-fold excess unlabelled erythrocytes in the presence of βCD as a cholesterol shuttle. The cholesterol exchange proceeds until equilibrium when the exchange of cholesterol from the donor to the acceptor membrane reaches a plateau. We expected that 100% cholesterol could be exchangeable at 37 °C. However, when temperature is lowered to the non-flip-flopping condition, i.e. 0°C, we would expect maximally 50 % cholesterol exchanged, if cholesterol is evenly partitioned in each leaflet. Any diversion from 50% would indicate an asymmetry between leaflets.

The cholesterol exchange from human erythrocytes was first performed at 37 °C. We found that the transfer of ^{3}H cholesterol from donor to acceptor cells was approximately100 % (**Figure 8**). This supports the feasibility of the protocol and confirms that the 100-fold excess acceptor erythrocytes have sufficient capacity to exchange essentially all the ^{3}H-cholesterol from the donor cells within our experiment time frame. We then performed the identical assay at 0 °C. Remarkably, in contrast to the LUVs experiments at 0 °C (**Figure 7**), we found that the ^{3}H-cholesterol exchange reached a plateau at 20-25 % (**Figure 8**). This suggests that cholesterol flip-flop was prevented by lowering temperature. Furthermore, the cholesterol exchange plateau suggests that only 20-25 % of the cholesterol is in the outer leaflet and that the majority of cholesterol (75-80%) is present in the inner leaflet of the erythrocyte PM.

A

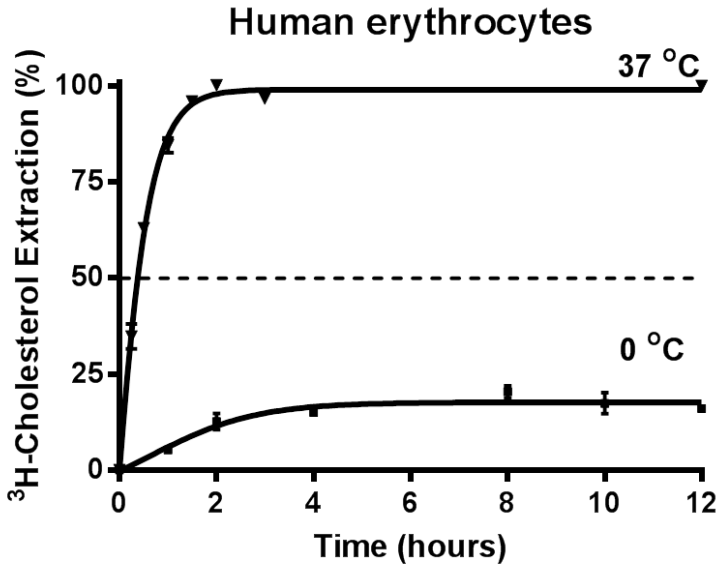
Human erythrocytes
37 °C
0 °C
^{3}H-Cholesterol Extraction (%)
100
75
50
25
0
0
2
4
6
8
10
12
Time (hours)

B

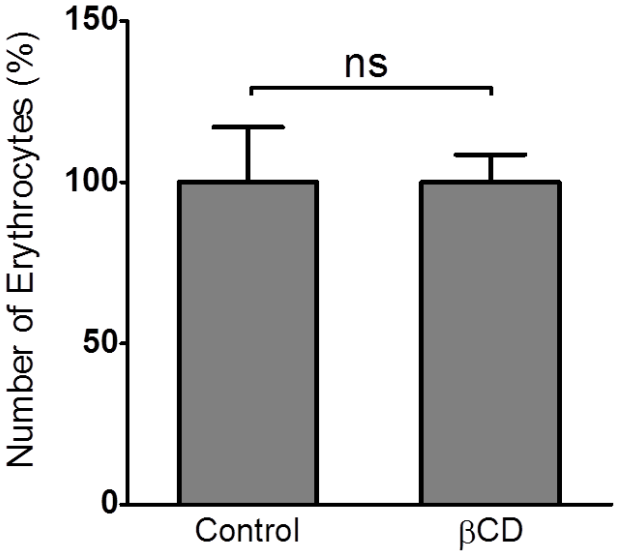
Number of Erythrocytes (%)
150
100
50
0
ns
Control
βCD

Figure 8 – Cholesterol is primarily in the inner leaflet of human erythrocyte plasma membrane. A) Cholesterol is exchanged between ^{3}H-cholesterol labelled erythrocytes and unlabelled, 100-fold excess erythrocytes at 0 °C and 37 °C by 1mM βCD. Labelled donor and unlabelled acceptor erythrocytes are combined with βCD and the amount of ^{3}H-cholesterol transferred to the acceptor cells was quantified by scintillation counting. Only approximately 20% ^{3}H-cholesterol was exchangeable from donor to acceptor cells at 0 °C, showing that cholesterol is primarily in the cytoplasmic leaflet. At 37 °C, 100% of the cholesterol is transferred from donor to acceptor cells. **B**) To confirm that cyclodextrin treatment did not cause significant cell lysis during membrane exchange, erythrocytes were treated with cyclodextrin or PBS overnight at 0 °C and the total number of cells was determined by haemocytometer.

3.3 - Conclusion

Here, we developed, validated and implemented a novel strategy to characterize the cholesterol distribution between bilayer leaflets of the mammalian cell PM. We provide the first evidence that the majority of the cholesterol (75-80%) is in the cytoplasmic leaflet of the PM. Previous attempts to determine the cholesterol distribution were either prone to artifact or indirect. Most recent studies, using fluorescent sterols that are structural analogues of native cholesterol, suggested that cholesterol is likely enriched in the cytoplasmic leaflet of the PM (Mondal et al., 2009; Schroeder et al., 1991). However, these results were not sufficiently convincing since fluorescent sterol analogues may not faithfully mimic the native cholesterol distribution. For example, the rate of cholesterol efflux is slower than dehydroergosterol (Ohvo and Slotte, 1996; Ohvo-Rekilä et al., 2000). Furthermore, minor modifications to the native cholesterol structure, such as the retention of a single extra double bond in the sterol ring structure, can have severe pathological consequences and cause Smith–Lemli–Opitz syndrome (Thurm et al., 2016). Our protocol quantified cholesterol directly, thereby avoiding uncertainties associated with fluorescent sterol analogues.

To our best knowledge, this is the first attempt to quantify native cholesterol partitioning by stopping the flip-flop of cholesterol between leaflets of a bilayer membrane. By preventing cholesterol flip-flop, we could analyze cholesterol in a leaflet specific fashion. We first confirmed that lowering temperature to 0 °C could prevent the transbilayer movement of cholesterol. When cholesterol flip-flop was inhibited, cyclodextrin is then capable of selectively extracting outer leaflet cholesterol, allowing the quantification of cholesterol in the outer leaflet, relative to the total membrane cholesterol. With the protocol further optimized to LUVs containing 30% cholesterol, we analyzed cholesterol in the

erythrocyte PM and found that cholesterol is primarily located in the cytoplasmic leaflet. To our knowledge, this is the first study to establish native cholesterol asymmetry in the mammalian PM.

Although erythrocytes are a common model cell for PM studies, it remains to be determined if a similar cholesterol transbilayer distribution is found in other or all mammalian cells. We exclusively tested erythrocytes as the mammalian cell model, due to technical limits mentioned above, yet it is possible that other cell types could generate different results. However, both Schroeder (1991) and Mondal (2009) independently observed the enrichment of fluorescent sterols into the inner leaflet of erythrocytes and epithelial cells, respectively. It is conceivable that the enrichment of native cholesterol into the inner leaflet may not be unique to erythrocytes. Further technical development would be required to ascertain if the erythrocyte results can be generalized to other cell types.

In addition, we believe that cholesterol asymmetry should be considered within the context of the lipid raft hypothesis. Typically, lipid rafts are considered to originate by interaction of lipids, particularly cholesterol and sphingolipid, in the outer leaflet. If cholesterol, one of the major components of a classical lipid raft, is primarily located in the inner leaflet, the lipid raft organization and assembly needs to be better elucidated. Our next objectives are to uncover and characterize how cholesterol asymmetry is maintained.

Chapter 4 - Asymmetric large unilamellar vesicles

4.1 - Introduction

The plasma membrane has long been known to have phospholipid asymmetry between bilayer leaflets (Bretsche, 1972b). Since we detected cholesterol asymmetry in the plasma membrane above (**Figure 8**), we wondered whether phospholipid asymmetry regulated cholesterol partitioning. We thus next focused on the development and characterization of LUVs with an asymmetric phospholipid distribution between the inner and outer leaflet to examine how this would influence cholesterol partitioning.

It is known that cholesterol has different affinity for different phospholipids including sphingomyelin (Leventis and Silvius, 2001). In mammalian cells, SM and PC are primarily in the outer leaflet, whereas PE and PS are localized to the cytoplasmic leaflet of the PM (Devaux and Morris, 2004). Since the PM phospholipids are asymmetrically distributed between leaflets and that cholesterol can flip rapidly between leaflets, it has previously been postulated that, at steady state, the distribution of cholesterol could be a consequence of chemical potential for each leaflet (Yesylevskyy and Demchenko, 2012). Conventionally, cholesterol is considered to have the highest affinity for lipids with long, saturated acyl chains compared to shorter and/or unsaturated chains. Of all the lipids, cholesterol is thought to prefer sphingolipids in the outer leaflet, due to the long and saturated acyl chains. Sphingolipids also have a nitrogen atom in the sphingoid backbone that can engage in hydrogen bonding with cholesterol (Ohvo-Rekila et al., 2002; Ramstedt and Slotte, 1999). Unfortunately, much of the evidence of cholesterol interaction with different lipids has come from symmetric membranes and also mostly with lipids that have 16 or 18 carbon acyl chains. In mammalian cells, sphingolipids have primarily very long acyl chains (24 carbons)

that are exclusively in the outer leaflet. Therefore, it remains to be determined if the biophysical principles generated by symmetric model membranes and also shorter acyl chain sphingolipids are relevant to asymmetric membranes with very long acyl chain sphingolipids that resembles the PM.

There have been both theoretical and experimental attempts to better understand how asymmetry influences membrane dynamics. A theoretical strategy to examine the cholesterol transbilayer distribution is to employ molecular dynamics (MD) simulations of asymmetric membranes. MD simulations have been used to characterize cholesterol flip-flop rates, as well as, principles of membrane domain assembly. It is only recently that MD simulations have begun to use asymmetric membranes to better understand cholesterol dynamics (Yesylevskyy and Demchenko, 2012). By simulating membranes with different lipid head groups and acyl chain lengths or degree of saturation between bilayer leaflets, the influence of the membrane lipid environment on cholesterol partitioning can be determined. Yesylevskyy et al addressed the question of how cholesterol is organized in an asymmetric membrane from a unique perspective. It was noted that in addition to differences in lipid head groups between bilayer leaflets, the presence of anionic PS and PI in the inner leaflet of the PM also generates a difference in charge. It was hypothesized that because of the charge, anionic lipids in the inner leaflet are mutually repulsive, which could create space in the membrane by altering the lipid packing density and allow cholesterol to intercalate more efficiently between the lipids. Coarse grain simulations of asymmetric membranes were carried out to examine factors that could shift the cholesterol distribution between bilayer leaflets. The results of these asymmetric membrane simulations found that, at equilibrium, cholesterol showed a preference for saturated lipids over unsaturated lipids, as previously

shown. Most interestingly, these studies found that cholesterol displayed a greater preference for anionic lipids over neutral lipids suggesting that charged lipids could act as a mechanism to enrich cholesterol in the inner leaflet (Yesylevskyy and Demchenko, 2012). This effect would otherwise be overlooked in a symmetric membrane system.

Another theoretical example of how lipid head group could favour cholesterol in the inner leaflet came from examining inner leaflet PE (Giang and Schick, 2014), a prominent inner leaflet lipid. When compared to the neutral phospho-choline containing lipids in the outer leaflet, the PE head group is small. From a structural perspective, a saturated PC has an even width between the head group and acyl chain (cylindrical) (**Figure 9A**) that will spontaneously assemble into a bilayer in aqueous solution (Dekruijff et al., 1980). PE on the other hand, is considered to have a head group that is smaller than the acyl chain, producing a cone-like structure (**Figure 9B**). Giang and Schick noted that a high concentration of cone-like PE in one leaflet of an asymmetric membrane would create a disparity in curvature (Giang and Schick, 2014). The small lipid head group gives PE spontaneous curvature that does not favour a bilayer and instead can result in an inverted micelle or a more complex inverted hexagonal arrangement (**Figure 9B**). Therefore, if one leaflet of a bilayer contains mostly cylindrical lipids and the other leaflet is primarily cone shaped lipids, the membrane could be unstable. It was proposed that an asymmetric cholesterol distribution could counterbalance the curvature problem by intercalating with the PE and flatten the membrane. This hypothesis seemed to support the enrichment of cholesterol into the inner leaflet of the PM.

In addition to the theoretical studies of asymmetric membranes, there have been some recent *in vitro* studies on asymmetric membrane bilayer. Serendipitously, London and

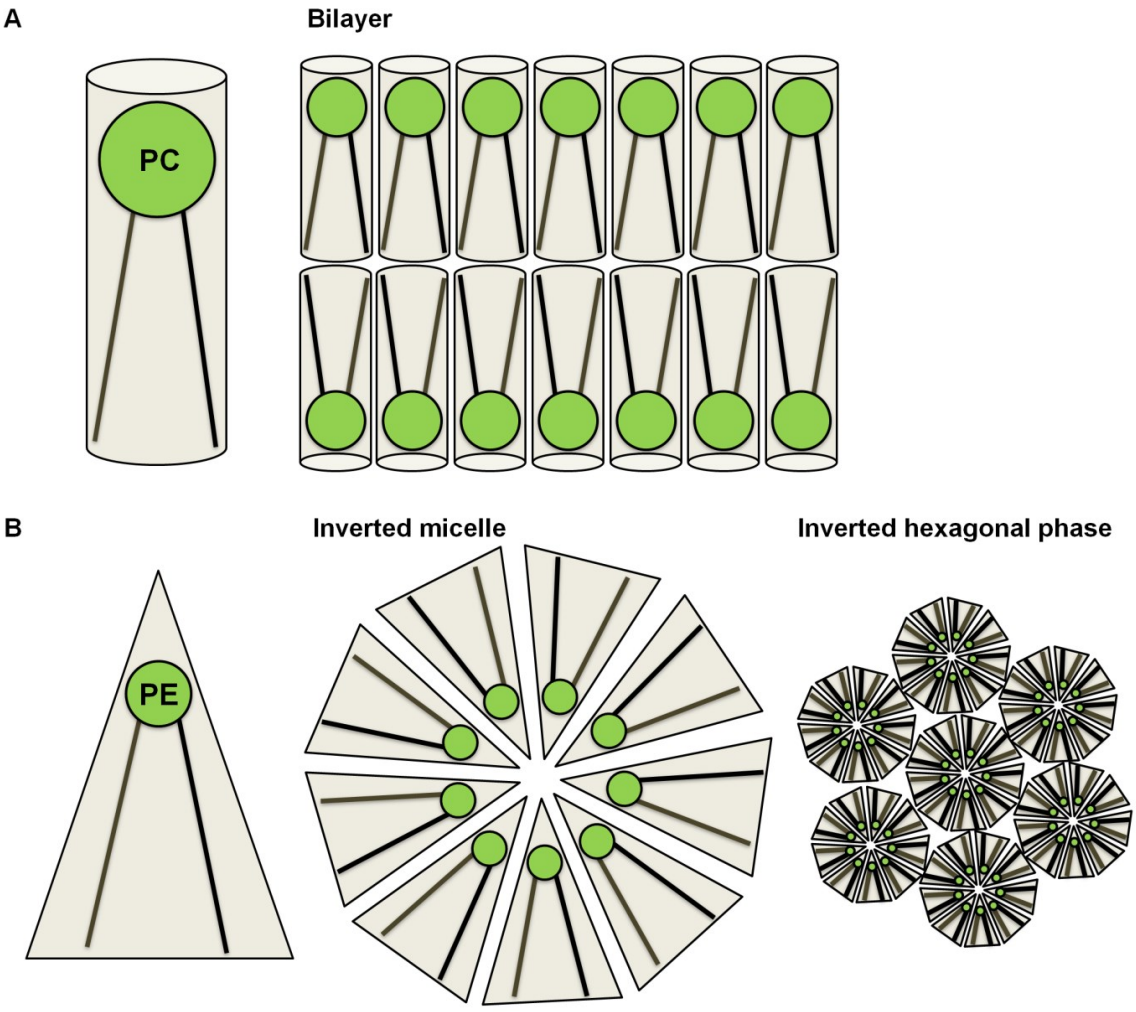
A
Bilayer
PC
B
Inverted micelle
Inverted hexagonal phase
PE

Figure 9 – Phospholipid structure determines how lipids pack together in a membrane. **A**) When a lipid, such as phosphatidylcholine (PC), has a head group with a similar width as the acyl chains, the lipid is considered cylindrical. Cylindrical lipids pack together laterally and spontaneously arrange into a bilayer by segregation of hydrophobic and hydrophilic components. **B**) Lipids with head groups that are smaller than the dimension of the acyl chain result in an overall conical structure. When arranging conical lipids together, the difference in size alters the curvature of the arrangement and inverted micelles are formed, which can also arrange into more complex hexagonal aggregations.

colleagues reported a method to generate LUVs with an asymmetric phospholipid distribution (Lin and London, 2014). This development enabled us to experimentally generate asymmetric LUVs with various phospholipid compositions to test how phospholipid asymmetry would influence cholesterol partitioning. Briefly, the protocol begins with generating two LUV populations of different compositions, followed by the exchange of the outer leaflet lipids between populations (Lin and London, 2014). The donor and acceptor LUVs were made with different concentrations of sucrose in the lumen, which enables the separation from each other by density centrifugation after outer leaflet exchange. As such, this newly published protocol allows us to generate asymmetric LUVs with defined inner and outer leaflet lipid compositions. Combined with our cholesterol extraction protocol discussed above, we can now characterize how lipid composition affects the cholesterol partition in an asymmetric membrane.

Another method of constructing asymmetric membranes, published around the same time, required specialized, custom built equipment that was inaccessible to us (Richmond et al., 2011). The London strategy, on the other hand, was a straightforward approach that could be performed using conventional laboratory equipment. Several articles were published by London and colleagues in quick succession, further improving the preparation and defining the biophysical properties of asymmetric membrane vesicles (Cheng and London, 2011; Cheng et al., 2009; Chiantia and London, 2012; Chiantia et al., 2011; Huang and London, 2013; Lin and London, 2014; Lin and London, 2015; Pathak and London, 2015; Son and London, 2013a, b; Son and London, 2011). We therefore used their approach to devise a model membrane system that can mimic the composition of the mammalian cell PM. We

hoped that this will allow us to answer questions in membrane biophysics that are relevant to mammalian cell membranes, for which symmetric membrane are not suitable.

To facilitate the exchange of the outer leaflet lipids, cyclodextrin was again used to convert symmetric vesicles into asymmetric vesicles. The first reports of attempting this strategy used MCD as the phospholipid carrier to exchange lipids between vesicles (Cheng and London, 2011; Cheng et al., 2009; Chiantia and London, 2012; Chiantia et al., 2011; Huang and London, 2013; Son and London, 2013a, b; Son and London, 2011). This was problematic because MCD binds cholesterol, so the asymmetric vesicles either lacked cholesterol or had to incorporate cholesterol in a second step after the asymmetry procedure. These earlier experiments focused primarily on the interactions between phospholipids and, for example, characterized factors that influence coupling of lipids across the asymmetric bilayer (Chiantia et al., 2012; Chiantia and London, 2012; Chiantia et al., 2011). It was later identified that HP-αCD was a more appropriate reagent to exchange the outer leaflet phospholipids, due to the specificity for phospholipids over cholesterol (Huang and London, 2013; Lin and London, 2014). Using HP-αCD instead of MCD allowed for the creation of asymmetric vesicles with high concentrations of cholesterol throughout the procedure. By experimenting with vesicles that contain cholesterol, this asymmetric membrane system was more versatile and capable of addressing questions pertaining to the formation of cholesterol dependent membrane domains. In addition, this asymmetry procedure has been used to construct small unilamellar vesicles (SUV), LUVs and GUVs (Cheng et al., 2009; Chiantia et al., 2011; Huang and London, 2013).

We modified the London protocol to generate asymmetric vesicles to particularly identify factors that could shift the cholesterol partitioning between leaflets. Primarily, we

incorporated SM into the outer leaflet of LUVs that contained PC/PS/PE on the inner leaflet. This allowed us to examine the role of SM asymmetry and its acyl chain length in regulating the cholesterol partitioning.

4.2 - Results

4.2.1 – Generation and characterization of asymmetric large unilamellar vesicles

The protocol to produce asymmetric vesicles, described above and in the Methods section, was robust and consistent with the literature (Lin and London, 2014). We first performed control experiments to confirm that after the lipid exchange procedure, the composition of LUVs was effectively altered as expected. Asymmetric LUVs were generated and lipids were subsequently harvested by a modified Bligh and Dyer lipid extraction method (Bligh and Dyer, 1959). The purified lipids were dried and resuspended in a chloroform/methanol solution (50:50) then loaded on a high performance thin layer chromatography (TLC) plate. Lipid standards were run on the TLC plate along with the donor and acceptor lipids before the outer leaflet exchange, as well as, the acceptor lipids after exchange. We found that, after the outer leaflet lipid exchange procedure, the acceptor LUVs showed an efficient incorporation of the donor lipid (**Figure 10A**). The asymmetric LUVs, along with the precursors, were also analyzed by mass spectrometry. These analyses confirmed that the donor lipid was being effectively incorporated into the acceptor vesicles (**Figure 10B**). The mass spectrometry analysis further differentiated acyl chain lengths of the phospholipids, such as PC or SM, which is important for the following sections.

We next confirmed the asymmetry, expected in these LUVs, and ensured that the phospholipids did not become scrambled before cholesterol characterization. For this, we

A

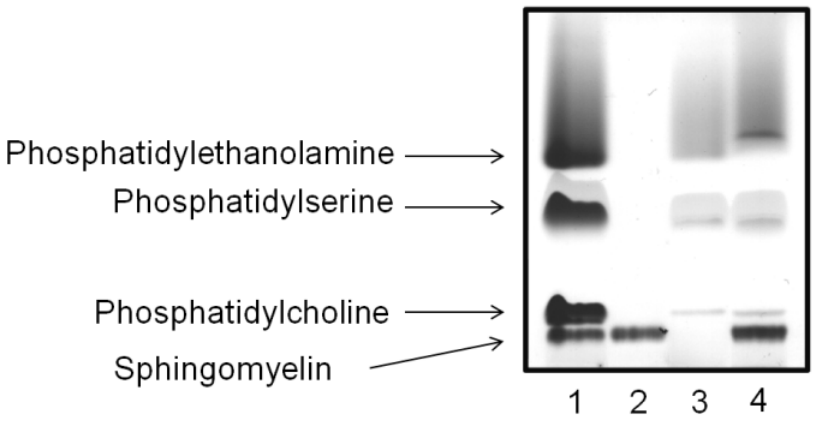

1 – Lipid standards
2 – Sphingomyelin liposome
3 – PE/ PS/ PC liposome
4 – Asymmetric vesicle liposome

B

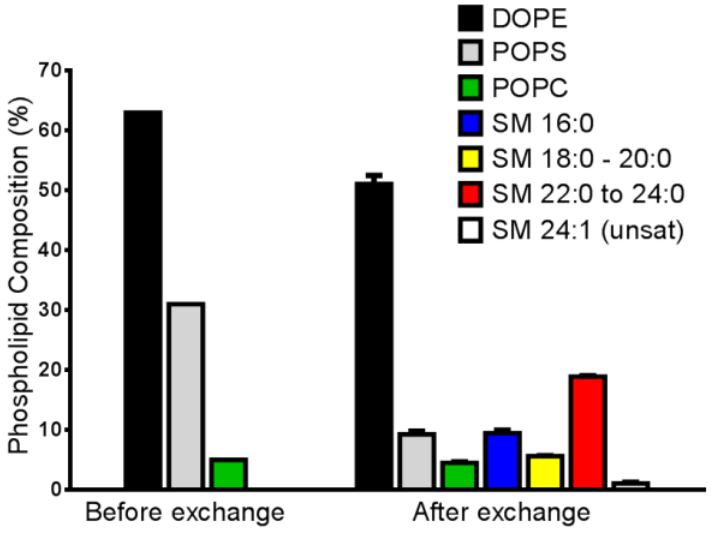

Figure 10 – Outer leaflet lipid exchange by cyclodextrin produces transversely asymmetric LUVs. A) Thin layer chromatography of lipids isolated from large unilamellar vesicle samples before and after the outer leaflet lipid exchange procedure. Prior to outer leaflet lipid exchange, the acceptor vesicles lack sphingomyelin (lane 3). After outer leaflet exchange of vesicles from lane 2 into vesicles of lane 3, sphingomyelin is found to be effectively incorporated into the lane 3 vesicles (Lane 4). **B)** Phospholipid composition in acceptor PE/PS/PC LUVs before and after outer leaflet exchange with milk sphingomyelin LUVs by mass spectrometry analysis.

analyzed the relative membrane fluidity of the vesicles using the fluorescent lipid probe, 1-(4-(trimethylamino)phenyl)-6-phenylhexa-1,3,5-triene (TMA-DPH). TMA-DPH is a derivative of the l,6-diphenyl-l,3,5-hexatriene (DPH) that can be used in fluorescence polarization studies to monitor the rotational mobility of the lipids and thus, membrane rigidity (Chazotte, 2011; Kuhry et al., 1983). Membrane rigidity is determined by exciting the probes with polarized light and then collecting the emitted light parallel and perpendicular to the excitation. If a membrane is rigid, the rotational mobility of the probes will be restricted and the emission in perpendicular planes will be limited. A fluid membrane, on the other hand, will allow the probe to rotate more freely and detect less of a difference in parallel and perpendicular emission. These differences in fluorescence emission of polarized light can be used to calculate the anisotropy (r) of the system using the equation: $r = \frac{I_{\parallel} - I_{\perp}}{I_{\parallel} + 2\,I_{\perp}}$ where $I_{\parallel}$ and $I_{\perp}$ refer to parallel and perpendicular fluorescence emission, respectively. With this equation, a higher anisotropy value is indicative of a more rigid membrane.

In contrast to DPH, which is lipophilic and diffuses rapidly throughout a membrane or cell, TMA-DPH is particularly useful for PM studies because of the addition of the trimethylammonium group. As an amphipathic molecule, TMA-DPH can be rapidly incorporated into a membrane. Particularly, it has the trimethylammonium group to restrict its transbilayer mobility (Kuhry et al., 1983), which is important for leaflet specific sensing. It has been shown, for example, that TMA-DPH will incorporate into the PM of cells within seconds and remain in the outer leaflet of the PM for up to 30 minutes (Kuhry et al., 1983).

We applied TMA-DPH to validate asymmetric vesicles produced by comparing the membrane fluidity of the donor (SM) and acceptor (PC/PS/PE) LUVs before and after the lipid exchange using a cuvette based fluorescence polarization detection system. As expected, since SM membranes are more rigid than PC/PS/PE membranes, the symmetric SM LUVs display a higher anisotropy than PC/PS/PE LUVs (**Figure 11**). The lipid exchange incorporated SM into PC/PS/PE LUVs, as seen by TLC and mass spectrometry analysis above, and preferably only in the outer leaflet of PC/PS/PE LUVs. At the same time, TMA-DPH from the outer leaflet of the PC/PS/PE LUVs was removed by exchange, leaving TMA-DPH in the inner leaflet. If SM did not become incorporated into inner leaflet during exchange, and since TMA-DPH is only in the inner leaflet, the anisotropy of the asymmetric LUVs should remain unchanged, similar to the symmetric PC/PS/PE vesicles. Indeed, this was the case (**Figure 11**), supporting that SM was restricted to the outer leaflet. However, if these LUVs were scrambled by lyophilizing the sample and reforming symmetric LUVs, TMA-DPH now senses the mixed membrane (PC/PS/PE/SM), which would display an intermediate anisotropy, as we observed here (**Figure 11**). We, therefore, conclude that the SM was successfully incorporated and is only in the outer leaflet of PC/PS/PE LUVs.

4.2.2 – Cholesterol partitioning in asymmetric unilamellar vesicles

Having produced LUVs with a defined inner and outer leaflet composition, we next proceeded to characterize how phospholipid asymmetry could influence cholesterol partitioning. Again, we began by generating symmetric PC/PS/PE LUVs and then incorporated different lipids into the outer leaflet using HP-αCD as a phospholipid shuttle. We also incorporated a trace amount of ^{3}H-cholesterol into the asymmetric LUVs, which allowed us to perform the cholesterol extraction protocol with MCD as described earlier

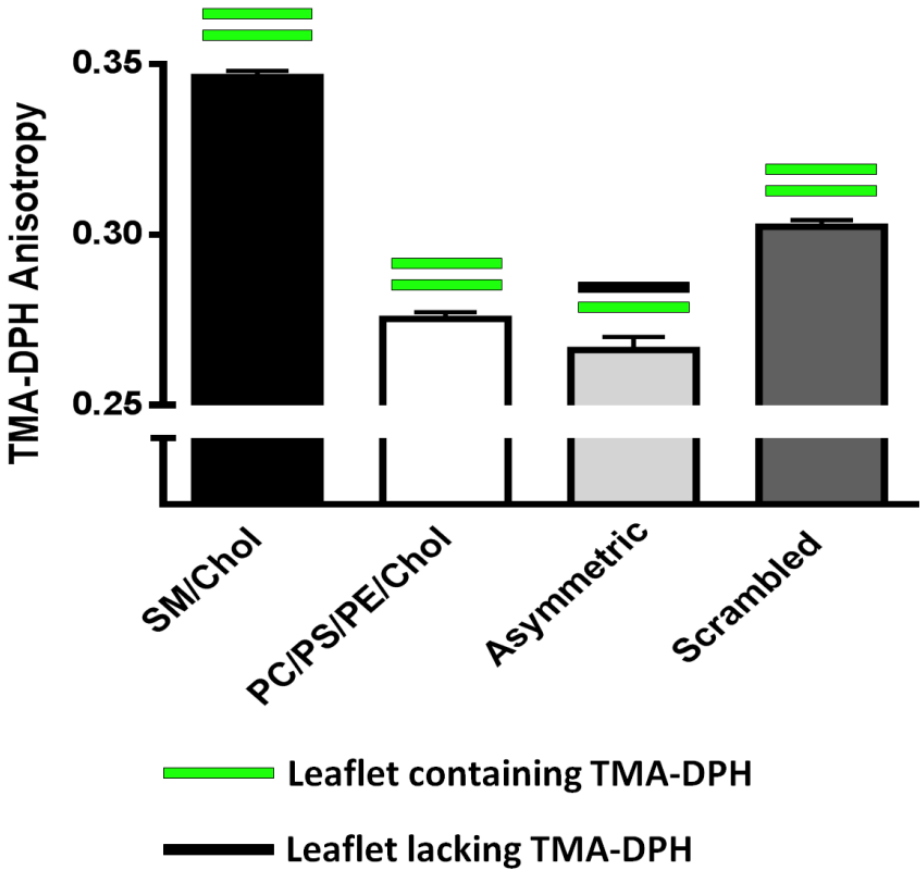
TMA-DPH Anisotropy
0.35
0.30
0.25
SM/Chol
PC/PS/PE/Chol
Asymmetric
Scrambled
Leaflet containing TMA-DPH
Leaflet lacking TMA-DPH

Figure 11 – The outer leaflet lipid exchange protocol introduces lipids selectively into the outer leaflet of the acceptor vesicles. LUVs were made with 1% TMA-DPH and anisotropy was determined using a cuvette based fluorometer system. As expected, SM/cholesterol LUVs (black bar) had higher anisotropy value than POPC/POPS/POPE/cholesterol LUVs (white bar). Asymmetric vesicles were then generated with 24:0 SM/cholesterol LUVs without TMA-DPH as the donor lipid and POPC/POPS/POPE/cholesterol LUVs with TMA-DPH as acceptor. Resulting asymmetric LUVs maintained the acceptor's anisotropy, since only the inner leaflet was labelled with TMA-DPH after the outer leaflet exchange with SM (asymmetric, light gray bar). However, if the same LUVs were dissolved and remade into symmetric LUVs (scrambled, dark gray bar), anisotropy took an intermediate value between donor and acceptor. As TMA-DPH is now in both leaflets again, this indicated the successful introduction of SM into the outer leaflet of the acceptor LUVs.

(**Figure 4**). If phospholipids in an asymmetric membrane influence cholesterol partitioning, we postulated that cholesterol would shift to partition into the leaflet that contained the preferred lipid. We found that replacing PC/PS/PE in the outer leaflet with egg SM (eSM), brain SM (bSM) or POPC did not have a significant effect on the cholesterol partitioning, which remained at 50% extraction at 0 C and 100% at 37 C (**Figure 12A**). The outer leaflet lipids, eSM, bSM and POPC have primarily 16:0, 18:0 and 16:0/18:1 acyl chains, respectively. We did, however, notice a subtle trend for cholesterol to prefer the eSM leaflet, which could potentially be a consequence of hydrogen bonding in the outer leaflet. This trend, however, was not significant under our experimental conditions. Interestingly, when we incorporated milk SM (mSM), primarily 24:0, into the outer leaflet of PC/PS/PE LUVs, we observed a significant shift in the cholesterol partitioning towards the inner leaflet. Cholesterol extraction by MCD reached a plateau at 20-25 %, which indicates that 75-80 % of the cholesterol was located in the inner leaflet (**Figure 12B**). Moreover, if the asymmetric 24:0 SM LUVs were scrambled by lyophilization and reformed into symmetric SM/PC/PS/PE LUVs, the cholesterol returned to an even partitioning with 50 % of the cholesterol present in each leaflet (**Figure 12B, *inset***). These results are the first experimental demonstration that phospholipid asymmetry can govern the cholesterol partitioning between leaflets.

Curiously, cholesterol has long been believed to associate strongly with SM through hydrogen bonding between the cholesterol hydroxyl group and the SM sphingoid backbone. This concept was reinforced by the fact that cholesterol interacts identically with 16:0 18:0 and 24:0 SM in symmetric bilayers (Ramstedt and Slotte, 1999). Nevertheless, our results showed that 24:0 SM is fundamentally distinct from 16:0 and 18:0 SM in asymmetric

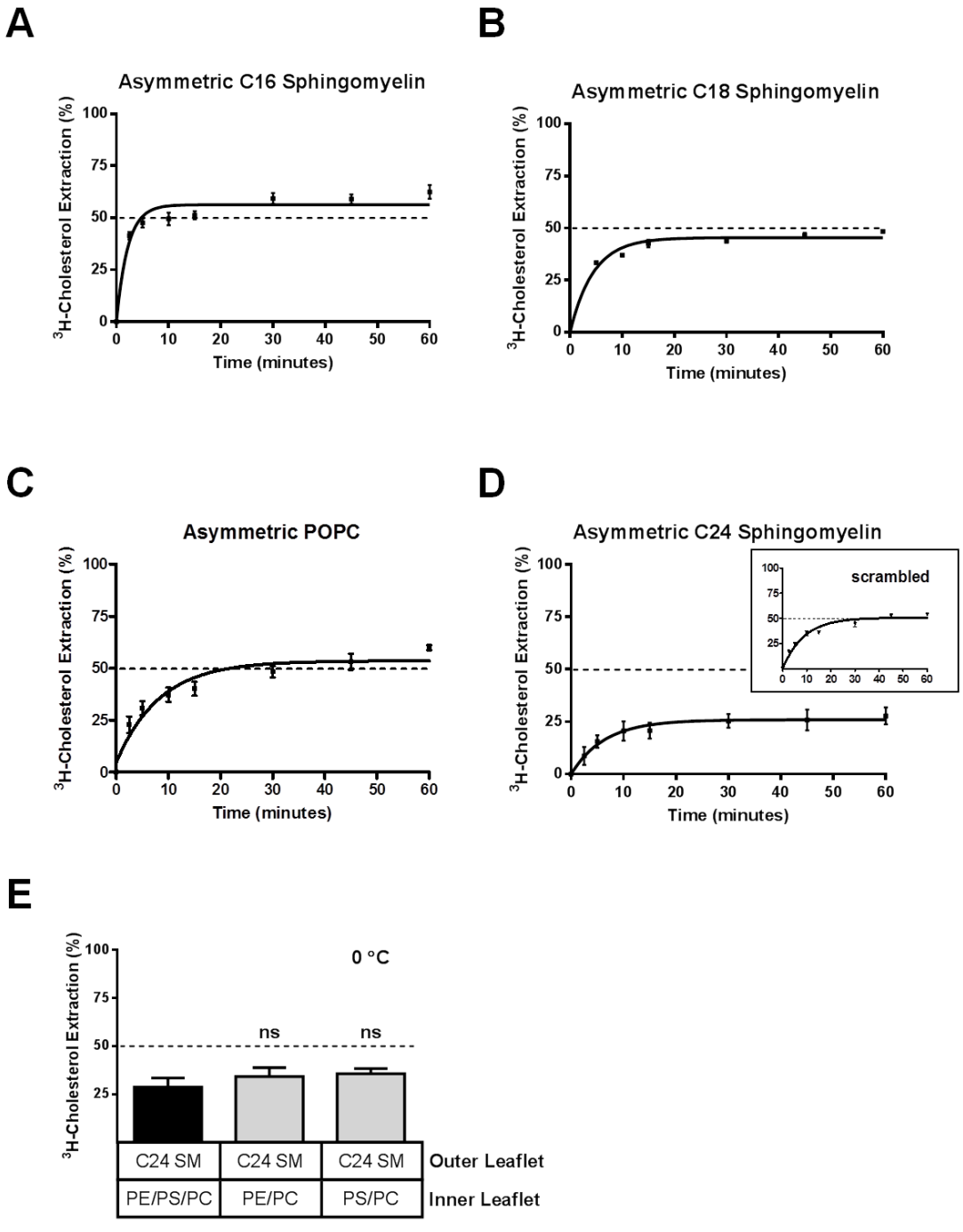
A
Asymmetric C16 Sphingomyelin
^{3}H-Cholesterol Extraction (%)
Time (minutes)
B
Asymmetric C18 Sphingomyelin
^{3}H-Cholesterol Extraction (%)
Time (minutes)
C
Asymmetric POPC
^{3}H-Cholesterol Extraction (%)
Time (minutes)
D
Asymmetric C24 Sphingomyelin
scrambled
^{3}H-Cholesterol Extraction (%)
Time (minutes)
E
0 °C
ns
ns
^{3}H-Cholesterol Extraction (%)
C24 SM
C24 SM
C24 SM
Outer Leaflet
PE/PS/PC
PE/PC
PS/PC
Inner Leaflet

Figure 12 – Outer leaflet very long acyl chain sphingomyelin causes the enrichment of cholesterol into the inner bilayer leaflet. PE/PS/PC vesicles were converted into asymmetric membranes by incorporation of 16:0 SM, C18 SM, 24:0 SM or POPC into the outer leaflet. Outer leaflet lipids were exchanged between donor and acceptor vesicles by α-CD and the two populations of vesicles were isolated by centrifugation. The distribution of cholesterol between bilayer leaflets was then quantified in the asymmetric vesicles, similar to **Figure 4**. Cholesterol is evenly distributed in asymmetric vesicles with 16:0 SM (**A**), C18 SM (**B**) or POPC (**C**) in the outer leaflet. When introducing 24:0 SM into the outer leaflet (**D**), only 25 % cholesterol was accessible for extraction, suggesting the majority of the cholesterol is in the inner leaflet. Scrambling the 24:0 SM asymmetric vesicles into symmetric vesicles similarly returns the cholesterol to a symmetric distribution (**D**, *inset*). **E)** Removing PE or PS from the inner leaflet of the 24:0 SM asymmetric vesicles continued to shift cholesterol to the inner leaflet. All results are presented as standard error of the mean from at least 3 independent experiments.

membranes, in terms their interactions with cholesterol. Most importantly, this result should be directly relevant to real mammalian cells, as 24:0 SM is the predominant sphingolipid species and exclusively in the outer leaflet of the PM. Indeed, we had observed earlier that 80% cholesterol is in cytoplasmic leaflet of erythrocytes (**Figure 8**) where 24:0 SM is most abundant and in the outer leaflet (Verkleij et al., 1973).

Until this point, the asymmetric LUVs that were characterized had kept the inner leaflet composition constant, while altering the outer leaflet composition. We found that outer leaflet 24:0 SM shifted cholesterol inward. It was, however, unknown if the composition of the inner leaflet also played a role in the redistribution of cholesterol. As previously mentioned, inner leaflet PS and PE have each been hypothesized to be involved or facilitate inner leaflet enrichment of cholesterol (Giang and Schick, 2014; Yesylevskyy and Demchenko, 2012). With this in mind, we next investigated if the outer leaflet 24:0 SM shifted cholesterol inward because of PS and/or PE in the inner leaflet. To address this, 24:0 SM asymmetric LUVs were generated as above, except lacking PS or PE in the inner leaflet. We found that removing either PS or PE from the inner leaflet of asymmetric 24:0 SM LUVs had little effect on the preferred partitioning of cholesterol into the inner leaflet (**Figure 12C**). This suggests that the presence of 24:0 SM exclusively in the outer leaflet is likely the major factor that shifted cholesterol partitioning.

The mammalian cell PM is composed of a high concentration of cholesterol (Van Meer et al., 2008). Yet, the characterizations of cholesterol partitioning in asymmetric LUVs above contained only a trace amount of cholesterol. To examine if the 24:0 SM results would translate into a membrane system with physiological cholesterol content, asymmetric 24:0 SM LUVs were constructed with 30 % cholesterol. This was achieved by a similar outer

leaflet phospholipid exchange protocol (**Figures 10-12**) used above except both donor and acceptor contain 30% cholesterol. We then analyzed cholesterol partitioning as in the symmetric LUV experiments (**Figure 7**). Specifically, to assess the percentage of cholesterol present in the outer leaflet of the LUVs, the asymmetric donor LUVs were labelled with ^{3}H-cholesterol and the amount of cholesterol transferred to the unlabeled acceptor LUVs (100-fold in excess, which match the composition of the donor outer leaflet) was monitored over time. Once again, the cholesterol exchange was performed at 0 °C under non-flip-flop conditions and at 37 °C. The latter condition was to confirm that the acceptor LUVs have sufficient capacity to remove all the ^{3}H-cholesterol from the donor when cholesterol flip-flop is permitted. We found that, at 37 °C, the ^{3}H-cholesterol is effectively transferred (about 100%) from the donor to the acceptor LUVs (**Figure 13**). However, when the temperature was lowered to 0 °C, the cholesterol exchange plateaued at 20 %, again indicating that 80 % of the cholesterol was in the inner leaflet of the asymmetric 24:0 SM LUVs with 30% cholesterol (**Figure 13**). These results are consistent with asymmetric LUVs containing a trace amount of cholesterol (**Figure 12**) and further confirm that 24:0 SM is involved in redistributing cholesterol away from the SM containing leaflet.

4.3 – Conclusion

The inner and outer leaflets of the mammalian cell PM are composed of distinct lipids (van Meer, 2011). Although the PM is transversely asymmetric, methods to characterize the effects of this asymmetry on cholesterol had previously been lacking. Due to this technical limitation, much of the published literature pertaining to lipid interactions in model membranes has used symmetric membrane systems and also shorter acyl chain SM (16:0 or 18:0). Although fruitful, it is conceivable that some of the principles identified in

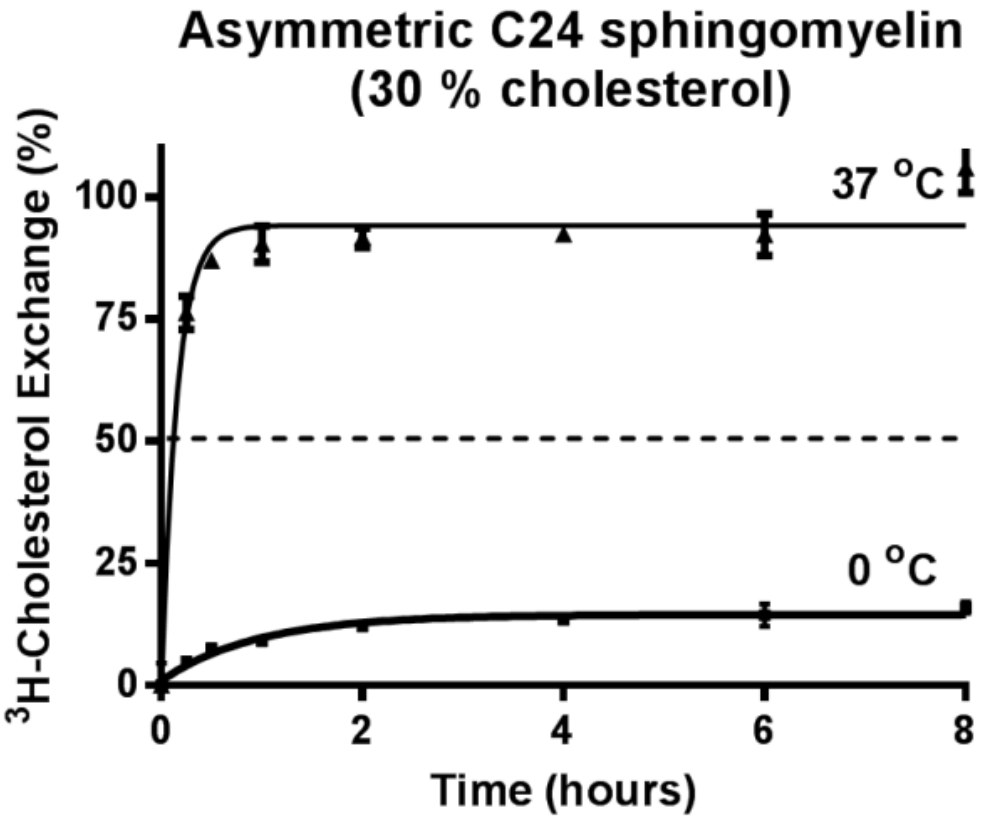
Asymmetric C24 sphingomyelin
(30 % cholesterol)
^{3}H-Cholesterol Exchange (%)
100
75
50
25
0
37 °C
0 °C
0
2
4
6
8
Time (hours)

Figure 13– Cholesterol is primarily in the inner leaflet of asymmetric LUVs with 30 % cholesterol. Symmetric PC/PS/PE (1:1:1) vesicles with 30 % cholesterol were converted into asymmetric vesicles by outer leaflet lipid exchange, as described for **Figure 12.** Cholesterol exchange between donor and acceptor vesicles was then performed, analogously to **Figure 7**. When selectively extracting cholesterol from the outer leaflet of 24:0 SM asymmetric LUVs with 30 % cholesterol, only 20 % of the total cholesterol is accessible to βCD at 0 °C. 24:0 SM in the outer leaflet redistributes cholesterol and results in 80 % of the cholesterol in the inner bilayer leaflet. At 37 °C, cholesterol flip-flop is active and all of the cholesterol is accessible to βCD. The results are presented as standard error of the mean from at least 3 independent experiments.

symmetric membranes may not necessarily translate well into an asymmetric membrane such as the PM. For example, critical phospholipid-cholesterol interactions in transversely asymmetric membranes could be overlooked in symmetric membranes. Therefore, we aimed to understand how lipid transbilayer asymmetry influenced the partitioning of cholesterol between bilayer leaflets.

Since the mammalian cell PM is composed of SM and PC in the outer leaflet and PE and PS on the inner leaflet, we generated asymmetric LUVs that mimicked this composition and asymmetric distribution. We successfully generated asymmetric LUVs that mimic the PM, as described in the literature (Lin and London, 2014), which provided us the platform to address how lipid asymmetry regulates the cholesterol partitioning. Using a combination of TLC, mass spectrometry and fluorescence anisotropy, we verified that the protocol efficiently incorporated the donor lipids into the acceptor vesicles and, importantly, the donated lipids indeed specifically incorporated into the outer leaflet of the LUVs. This created asymmetric LUVs. The literature would suggest that cholesterol has the highest affinity for SM, due to favourable side-by-side hydrogen bonding, over other lipids (Ohvo-Rekila et al., 2002; Ramstedt and Slotte, 1999). However, these conclusions could have limited application to the plasma membrane of live cells, since they were generated using symmetric membranes (Mombelli et al., 2003). Indeed, we found that, when 24:0 is in the outer leaflet, cholesterol prefers the inner leaflet (**Figure 12D & Figure 13**).

To our best knowledge, this is the first evidence that cholesterol prefers to partition into the leaflet opposite to SM. Lateral hydrogen bonding between SM and cholesterol has been thought as the strongest association between phospholipid and cholesterol (Mombelli et al., 2003). We show here, however, 24:0 SM is functionally distinct from 16:0 and 18:0 SM,

when in an asymmetric membrane. Asymmetric 16:0 and 18:0 SM did not have any effect on the cholesterol partitioning (**Figure 12A & B**). Furthermore, this conclusion holds true for LUVs with a trace amount or physiological cholesterol levels (30%) (**Figure 12 & Figure 13**). We speculate that the VLAC of SM, as in 24:0 SM, could penetrate from the outer leaflet into the inner leaflet to interact with cholesterol in a tail-to-tail interdigitation manner. At this moment, however, we do not have sufficient evidence to prove such a quantitative relationship. Moreover, the number of cholesterol molecules exceeds the number of SM in the PM, which suggests that a 1:1 interdigitated interaction between cholesterol and VLAC SM is unlikely. We have established collaboration with a molecular dynamics simulation research group to investigate how asymmetric 24:0 SM would influence cholesterol partitioning between leaflets. The simulation results were in agreement with our experimental data and found that cholesterol displayed an energetic preference to partition into the inner leaflet with 24:0 SM in the outer leaflet (**Appendix 3**). Although a conclusive mechanism was lacking from the simulations, they found that VLAC interdigitation could influence cholesterol partitioning by modifying the organization of the bilayer. For example, it was concluded that the sphingolipid VLAC in the outer leaflet can penetrate into the inner leaflet, which could alter the lateral packing density of the inner leaflet lipids. Furthermore, they concluded that cholesterol displays a reduced hydrogen bonding capacity with 24:0 SM compared to 16:0 SM, which could reduce the affinity of cholesterol for the outer leaflet. Much more detailed analysis is required to fully illustrate the mechanisms, which is beyond the scope of my thesis research. Nevertheless, the major factor that we identified, which can alter the partitioning of cholesterol between bilayer leaflets, was VLAC SM in an asymmetric membrane. We suspect that enrichment of cholesterol in the inner leaflet of mammalian cells, as found in human erythrocytes (**Figure 8**), is, at least partially, attributed

to the presence of VLAC sphingolipids in the PM. With that, we asked next examined how an asymmetric cholesterol distribution would impact on membrane microdomain formation.

Chapter 5 - Membrane microdomain formation in asymmetric giant unilamellar vesicles

5.1 - Introduction

We have established above that asymmetric membranes with 24:0 SM in the outer leaflet causes preferential partitioning of cholesterol into the opposing inner leaflet. We hypothesized that this would effectively remove cholesterol from canonical lateral side-by-side interactions with SM. Interestingly, this lateral interaction between SM and cholesterol is thought to be reason for microdomain formation (Pralle et al., 2000). We thus next investigated whether an asymmetric cholesterol distribution would influence the formation of membrane microdomains. In this section, we will describe the development of a giant unilamellar vesicle (GUV) model system to characterize microdomain formation in symmetric and asymmetric membranes. This will allow us to test how transbilayer asymmetry, particularly SM with different acyl chain lengths, influences membrane domains in GUVs.

Live mammalian cells are hypothesized to compartmentalize protein-protein interactions in membrane microdomains (Simons and Ikonen, 1997). One of the most commonly employed model membranes to test domain formation, or membrane phase separation, are the GUVs (Juhasz et al., 2010; Veatch and Keller, 2003). Model membranes have provided many critical principles how phospholipids interact with each other and with cholesterol. Model membranes, such as GUV, have also been used to visualize microdomain formation. Particularly, GUVs directly derived from plasma membrane (GPMVs) were also shown capable of forming micron-sized microdomains, similar to model membrane GUVs (Baumgart et al., 2007a; Veatch and Keller, 2003, 2005). However, phase separation, either micron or submicron sized, has not been directly observed in the PM of the live cells, which

has long puzzled the scientific community (Munro, 2003). Nevertheless, we noted that none of above mentioned studies considered the effect of bilayer asymmetry. Particularly, little attention has paid to the acyl chain length of sphingolipids regarding microdomain formation. We, therefore, systematically characterized asymmetric GUVs to understand how outer leaflet SM acyl chain length, which governed cholesterol partitioning, influences membrane microdomains.

Initially, GUVs were produced passively simply by drying lipids on glass or teflon sheets, followed by hydrating the lipids and allowing the vesicles to form spontaneously in aqueous solution (Needham and Evans, 1988). Although this procedure does generate GUVs, the process is not well controlled and results in a heterogeneous population of vesicles. Furthermore, as a result of the random nature of the vesiculation, this method also produces multilamellar vesicles and other irregular structures, such as tubules. Another early GUV strategy was to hydrate the dried lipids in detergent, followed by dialysis. Once the lipids are resuspended in solution, the detergent helps to shield the lipid acyl chains from the aqueous media and allows the lipids to be dissolved as monomers. As the detergent is slowly removed during dialysis, the lipids self-assemble into bilayers that form GUVs (Marassi et al., 1993). Unfortunately, similar to the passive teflon method, this procedure is also not well controlled and generates a population of vesicles that has limited experimental applicability as GUVs.

The production of GUVs was substantially improved when vesiculation from a lipid film into an overlaid aqueous solution is carried out in the presence of an electric field. Angelova and Dimitrov (1986) were the first to describe a procedure for generating GUVs, termed liposome electroformation (Angelova and Dimitrov, 1986). Unlike the previous GUV strategies, electroformation resulted in a high yield of unilamellar vesicles with a

homogeneous size distribution of approximately 30 μm. It was observed by microscopy that small vesicles begin to form from the lipid film and, as the density of the vesicles increases, the small vesicles coalesce making larger vesicles suitable for experimentation. This method originally used a direct current (DC) electric field to stimulate swelling of a lipid film from platinum electrodes. There, temperature, voltage and the thickness of the lipid film influenced the efficiency of vesiculation. In particular, the vesiculation should be carried out above the transition temperature of the sample, the voltage should be below 3 V and using a thin lipid film to produce the GUVs. Furthermore, it was found that the platinum cathode was more efficient at stimulating vesiculation compared to the anode (Angelova and Dimitrov, 1986). A more detailed examination of the effect of an electric field on vesiculation was published two years later, which included both DC and alternating current (AC) electric fields (Dimitrov and Angelova, 1988). As it turned out, the AC electric field caused the lipids to vibrate in the same frequency as the applied electric field. This causes mechanical stress and destabilizes the lipid film to promote lipid swelling (Angelova et al., 1992). This method has since been widely used to generate GUVs to understand the interactions and dynamics of lipids (Bagatolli and Gratton, 1999; Dietrich et al., 2001; Mathivet et al., 1996; Montes et al., 2007; Pott et al., 2008; Veatch and Keller, 2003). Furthermore, due to their size, GUVs has been particularly useful for observing phase separation of membrane bilayer and instrumental in supporting the lipid raft hypothesis (Juhasz et al., 2010; Veatch and Keller, 2003).

Until recently, GUV studies were restricted to symmetric membrane bilayers. Although useful, these symmetric GUVs are not ideal models for the transversely asymmetric PM. To address this issue, a procedure was developed that again uses

cyclodextrin to exchange the outer leaflet phospholipids between two vesicle populations (Chiantia et al., 2011) . This produces GUVs with distinct outer and inner leaflet phospholipid compositions that more closely mimics the PM. We hope to use the asymmetric GUVs to complement our studies using asymmetric LUV and, particularly, to directly visualize how cholesterol partitioning influences the formation of lateral membrane microdomains.

5.2 - Results

5.2.1 - Symmetric giant unilamellar vesicles

We began by optimizing the procedure for producing symmetric GUVs. As described in the Materials and Methods section, as well as, the detailed protocol in **Appendix 2**, we generated GUVs according to the original Angelova protocol (Angelova and Dimitrov, 1986; Angelova et al., 1992; Dimitrov and Angelova, 1988). Specifically, lipids were dried on two parallel platinum electrodes, vesiculation was performed in glass tubes at 70 °C and the sample was then transferred to a glass bottom microscope dish for visualization. In accordance with Juhasz et al (2010), we first selected several ordered and disordered domain labelling fluorescent probes to establish the optimal probe pair for our applications. Some of the most commonly used lipid probes have a 1,2-dipalmitoyl-*sn*-glycero-3-phosphoethanolamine (DPPE) or 1,2-dioleoyl-*sn*-glycero-3-phosphoethanolamine (DOPE) backbone with a fluorophore conjugated to the amine group on the ethanolamine. We primarily used rhodamine-DPPE (Rho-DPPE), rhodamine-DOPE (Rho-DOPE), nitrobenzoxadiazole-DPPE (NBD-DPPE), as well as, the non-phospholipid probe napthopyrene. Interestingly, although NBD-DPPE and Rho-DPPE both have the same lipid anchor, these two probes preferentially associate in opposing ordered and disordered

domains, respectively (Juhasz et al., 2010). Most of the GUV work of this thesis used Rho-DPPE and NBD-DPPE as the probe pair, due to the highly polarized nature of the combination.

As reported elsewhere, the addition of cholesterol into GUVs with saturated and unsaturated lipids, such as DPPC and DOPC, can cause phase separation of lateral ordered and disordered domains (Veatch and Keller, 2003) (**Figure 14A**). The ratio of the lipids used, as well as, the temperature of the sample determines if domains can be visualized (Veatch and Keller, 2003). Although we performed experiments with a range of cholesterol concentrations (**Figure 14B**), we largely focused on GUVs containing 30 % cholesterol. For these GUVs, room temperature is generally suitable for visualizing phase separated microdomains since saturated lipids, such as DPPC, have a high Tm (41 °C) and unsaturated lipids, such as DOPC, have a low Tm (-17 °C). DPPC is rigid and DOPC is fluid at room temperature, which results in the phase separation. If the temperature of the sample is increased to above 41 °C, however, the DPPC will become fluid and the two phospholipids will become miscible. The process is considered reversible since lowering the temperature of the sample back below 41 °C will again cause lipid immiscibility and the membrane domains will re-appear (Veatch and Keller, 2003, 2005). We used DOPC as the unsaturated lipid. When experimenting with different saturated phospholipids, we found that DPPC, 16:0 SM and 24:0 SM function equally to produce the phase separation in symmetric GUVs containing DOPC and 30 % cholesterol at room temperature (**Figure 14C**).

5.2.2 – Asymmetric giant unilamellar vesicles

Once the symmetric GUV system was reproducible, we proceeded to optimize the protocol for generating asymmetric GUVs. The asymmetric GUVs typically started as

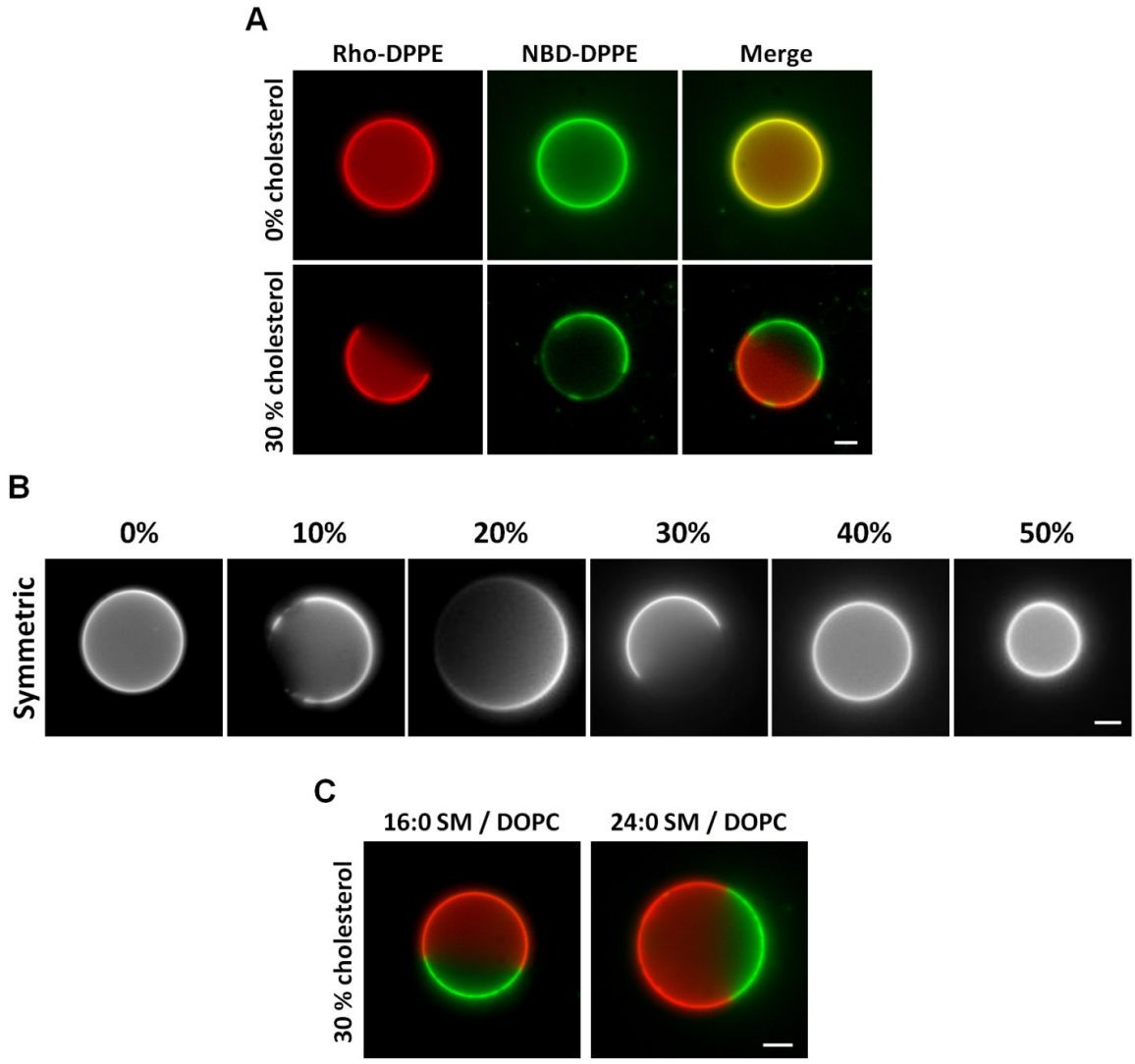
A
Rho-DPPE
NBD-DPPE
Merge
0% cholesterol
30 % cholesterol
B
0%
10%
20%
30%
40%
50%
Symmetric
C
16:0 SM / DOPC
24:0 SM / DOPC
30 % cholesterol

Figure 14 – Cholesterol induces phase separation of saturated and unsaturated lipids in giant unilamellar vesicles. A) GUVs were generated with DOPC/DPPC (1:1) with or without 30 % cholesterol. Without cholesterol, no phase separation is observed. Introduction of cholesterol into GUVs containing saturated DPPC and unsaturated DOPC phospholipids causes lipid immiscibility. NBD-DPPE (green) and Rho-DPPE (red) segregate to the liquid ordered (L_o) and liquid disordered (L_d) regions, respectively. **B**) Symmetric GUVs form membrane domains when the cholesterol concentration is less than 40%. GUVs are composed of 24:0 SM/DOPC (1:1) with various cholesterol concentrations. Vesicles were visualized by incorporation of 0.05% rhodamine-DPPE. **C**) Symmetric giant unilamellar vesicles with saturated lipids 16:0 SM and 24:0 SM form domains with DOPC and 30 % cholesterol. Vesicles were visualized by incorporation of 0.05% rhodamine-DPPE and NBD-DPPE. Scale bars represent 5μm.

symmetric DPPC/DOPC/cholesterol (35:35:30) GUVs that were then converted to asymmetric GUVs by exchanging outer leaflet phospholipids with HP-αCD and an excess amount of LUVs as a phospholipid donor (See Methods section for details). To confirm that efficient lipid exchange occurred, the starting DPPC/DOPC/cholesterol GUVs (acceptor) contained only Rho-DPPE as the fluorescent probe, whereas, the donor LUVs were labelled with only NBD-DPPE. After exchange, the resulting GUVs lost DPPC, DOPC and Rho-DPPE from the outer leaflet and gained phospholipids from the LUVs, including NBD-DPPE. Therefore, after exchange, the GUVs contained both fluorescent lipid probes, which was used to indirectly monitor the exchange efficiency (**Figure 15**). The amount of NBD-DPPE incorporated and the amount of Rho-DPPE removed could be used to estimate exchange efficiency. For example, if the exchange was suboptimal, the NBD-DPPE signal in resultant GUVs would be very low, suggesting the incubation period should be longer or the cyclodextrin concentration should be increased. Conversely, if the lipid exchange was too harsh, it would result in a near complete depletion of the Rho-DPPE, likely representing phospholipid scrambling, a sign for compromised integrity of the GUVs.

The previous results from LUVs indicated that 24:0 SM redistributes cholesterol to the inner leaflet (**Figure 12**), while 16:0 SM does not. It is also well established that cholesterol is essential for microdomain formation in symmetric GUVs (Veatch and Keller, 2003), We, therefore, aimed to corroborate the LUV data by generating asymmetric GUVs with either 16:0 or 24:0 SM exclusively in the outer leaflet. As expected, prior to lipid exchange, the symmetric acceptor GUVs lacked a signal in the green fluorescent (NBD-DPPE) channel and displayed distinct membrane microdomains (**Figure 15**). When

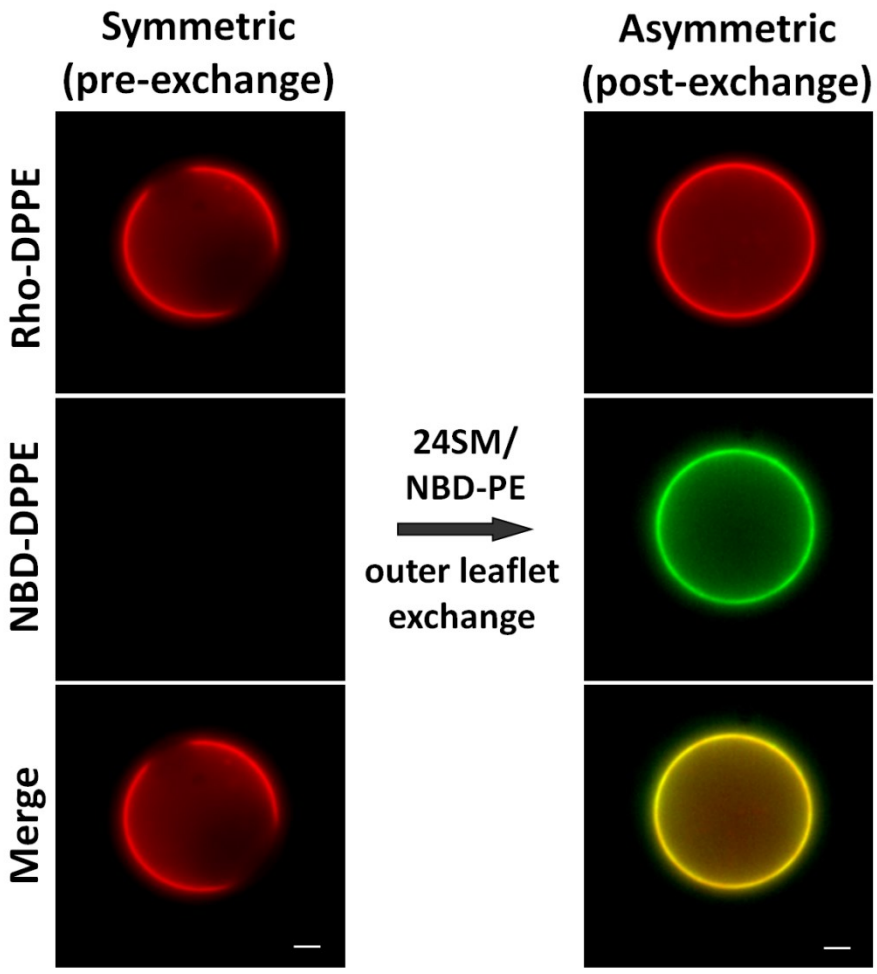
Symmetric
(pre-exchange)
Asymmetric
(post-exchange)
Rho-DPPE
NBD-DPPE
Merge
24SM/
NBD-PE
outer leaflet
exchange

Figure 15 – Outer leaflet lipid exchange effectively transfers the desired lipids from donor to acceptor membranes to create asymmetric giant unilamellar vesicles. Symmetric GUVs are converted to asymmetric GUVs by outer leaflet lipid exchange with donor LUVs by α-CD. Prior to outer leaflet lipid exchange, the symmetric acceptor vesicles are composed of DPPC/DOPC (1:1) with 30 % cholesterol. The acceptor vesicles also contain 0.05% rhodamine-DPPE for visualization. The acceptor vesicles consistently display segregation of ordered and disordered lipids. The donor LUV vesicles, such as 24 SM, contain NBD-DPPE, which becomes incorporated into the acceptor membranes during outer leaflet lipid exchange. The exchange of lipids results in an asymmetric GUV with both rhodamine-DPPE and NBD-DPPE.

introducing 16:0 SM into the outer leaflet, the exchange was evident by the incorporation of NBD-DPPE from the donor LUVs into the acceptor GUVs. This had no effect on the membrane microdomains. Thus, with 16:0 SM exclusively in the outer leaflet, the asymmetric GUVs continued to form microdomains (**Figure 16A, *b***). However, when 24:0 SM was similarly introduced into the outer leaflet of the acceptor GUVs, the visible membrane microdomains were completely abolished (**Figure 16A, *a***). Furthermore, milk SM (mainly 24:0 SM) or synthetic pure 24:0 SM functioned identically in asymmetric GUVs and abolished membrane microdomains (**Figure 16B**). Interestingly, if GUV are generated with the identical composition as the asymmetric 24:0 SM GUV (**Figure 16A, *a***) but symmetric, the membrane domains return (**Figure 16A, *c***). Over all, these data suggest asymmetrically placed 24:0 SM suppresses microdomain formation. We also examined the potential influence of temperature and cholesterol concentration in asymmetric 24:0 SM GUVs. In all cases, asymmetric 24:0 SM was sufficient to prevent the formation of microdomains (**Figure 16C & Figure 16D**). Therefore, similar to the asymmetric LUV experiments (**Figure 12 & Figure 13**), 24:0 SM in asymmetric membranes displays a unique function, completely distinct from that of 16:0, which is to suppress the formation of membrane microdomains. Given that this is the precise condition where LUVs concentrate cholesterol in the inner leaflet, we suggest that 24:0 SM, when exclusively placed in the outer leaflet of the membrane, prevents microdomain formation by partitioning cholesterol into the inner leaflet.

5.3 - Conclusion

Many PM protein-protein interactions are known to be influenced by the surrounding membrane environment (Eisenberg et al., 2006; LaRocca et al., 2013; Lasserre et al., 2008; Lingwood et al., 2008; Popik et al., 2002; Takeda et al., 2003; Zhu et al., 2010). Cholesterol

A

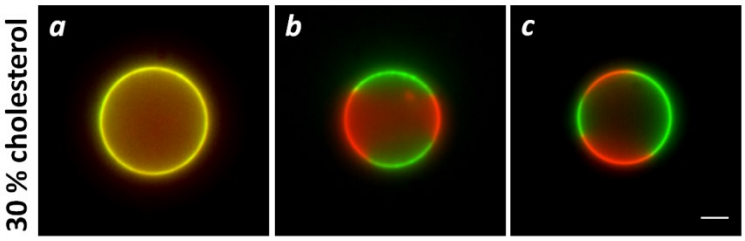

Inner	DPPC/DOPC	DPPC/DOPC	24SM/DPPC/DOPC
Outer	24SM/DOPC	16SM/DOPC	24SM/DPPC/DOPC

B

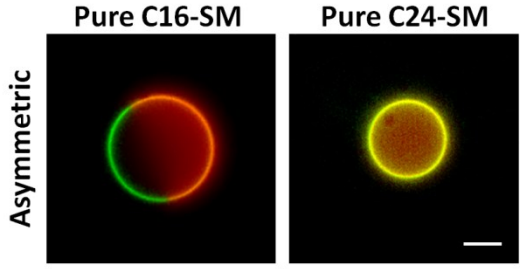

C

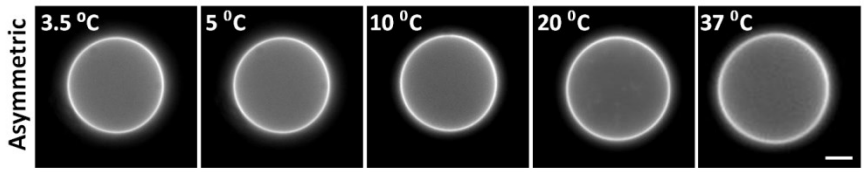

D

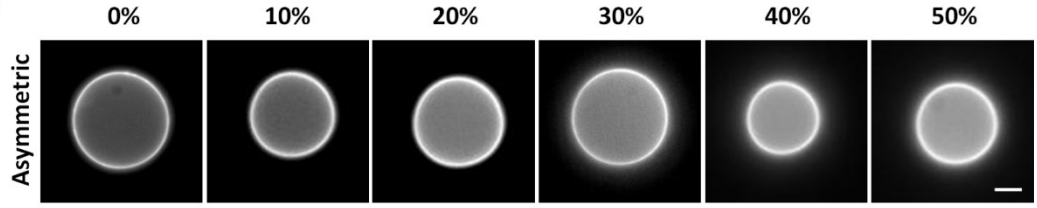

Figure 16 – The presence of very long acyl chain sphingomyelin exclusively in the outer leaflet of giant unilamellar vesicles prevents membrane domain formation. Symmetric GUVs are converted to asymmetric GUVs by outer leaflet lipid exchange with donor LUVs by α-CD. **A)** 24:0 SM in the outer leaflet of giant unilamellar vesicles abolished membrane domains (***a)***. Having 16:0 SM only in the outer leaflet (***b)*** or 24:0 SM in both leaflets (**c**) continues to form domains. **B)** Pure synthetic sphingolipids introduced into the outer leaflet of giant unilamellar vesicles produces similar results as natural sphingolipids. **C)** Introduction of very long acyl chain SM into the outer leaflet of DOPC/DPPC/cholesterol GUVs prevents microdomain formation in a wide range of temperatures. **D)** Asymmetric 24:0 SM GUVs prevent microdomain formation at all cholesterol concentrations. Vesicles were visualized by incorporation of 0.05% rhodamine-DPPE and NBD-DPPE.

is essential for many interactions and is believed to associate with saturated acyl chains of phospholipids to promote the phase separation. However, the direct visualization of membrane microdomains in live cells has been elusive. The existence of lipid-mediated membrane microdomains in the PM has been predicted by model membrane systems, which have been a useful to tool to understand the dynamics of membranes (Levental et al., 2016; Sezgin et al., 2012; Veatch and Keller, 2003, 2005). By reconstituting pure lipids into membrane bilayers with a defined composition, GUVs are used to infer about fundamental processes that may similarly occur in the PM of live cells. Indeed, membrane microdomains can be directly visualized in GUVs by fluorescence microscopy. However, GUV studies are almost entirely conducted with symmetric membranes. Since the mammalian cell PM has distinct lipids on each bilayer leaflet, symmetric GUVs intrinsically fail to take into consideration how the asymmetry influences the dynamics of the membrane, particularly microdomains. Here, we developed a procedure to successfully convert symmetric GUVs into asymmetric GUVs. These asymmetric GUVs can now be used to address more complex questions in membrane biophysics that are more relevant to the PM of live cells.

We took the advantage that an asymmetric GUV procedure was published at approximately the same time as this thesis project began (Chiantia et al., 2011). Since our data suggested that cholesterol is asymmetrically partitioned in the PM of erythrocytes (**Figure 8**), we were keen to understand the factors that regulate cholesterol transbilayer asymmetry and also the consequence of asymmetry on the dynamics of membrane microdomains. The LUV experiments in **Chapter 4** uncovered a unique function of 24:0 SM in redistributing cholesterol into the inner leaflet. Furthermore, we found that cholesterol similarly favoured the cytoplasmic leaflet of the human erythrocyte PM (**Figure 8**). Human

A

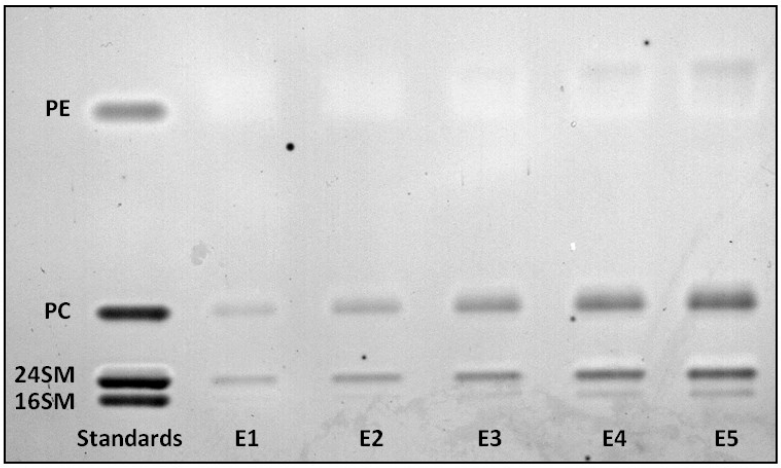
PE
PC
24SM
16SM
Standards
E1
E2
E3
E4
E5

B

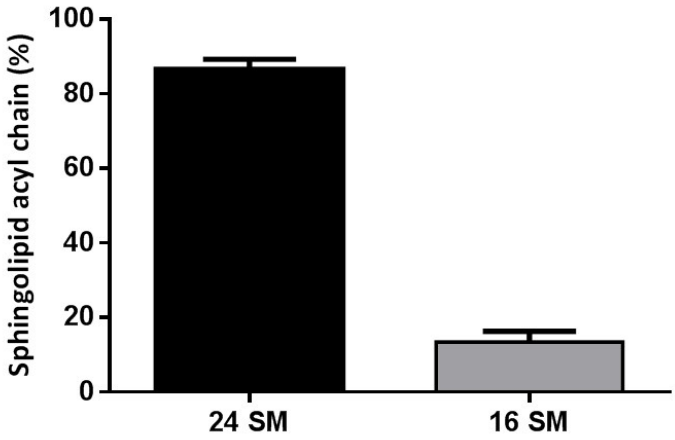
Sphingolipid acyl chain (%)
100
80
60
40
20
0
24 SM
16 SM

Figure 17 – Very long acyl chain sphingomyelin is the most abundant sphingolipid in human erythrocytes. A) Representative thin layer chromatography showing the relative quantities of lipids isolated from human erythrocytes. Lane 1 shows the reference location for SM, PC and PE lipids using pure lipid standards. Lanes 2-6 show increasing quantities (E1-60 μL, E2-90 μL, E3-130 μL, E4-170 μL, E5-200 μL) of lipids isolated from human erythrocytes. Lipids were resolved on the chromatography plate using a chloroform/methanol (50:50) solvent system and visualized by coomassie blue G staining. **B)** Replicated quantification of the relative abundance of 16:0 and 24:0 sphingolipid acyl chains isolated from human erythrocytes.

erythrocytes contain high levels of 24:0 sphingolipids in the outer leaflet (**Figure 17**). We, therefore, generated asymmetric GUVs with 24:0 SM exclusively in the outer leaflet to visualize the relationship between cholesterol asymmetry and membrane microdomain formation.

Our symmetric GUV data supports previous reports that combining saturated and unsaturated phospholipids with 30 % cholesterol causes phase separation in a membrane bilayer. Particularly, membrane domains readily form in symmetric GUVs with 24:0 SM in both leaflets (**Figure 14C & Figure 16A, *c***). However, if 24:0 SM is present exclusively in the outer leaflet, membrane microdomains are abolished (**Figure 16A, *a***). GUVs with 16:0 SM in the outer leaflet continued to form microdomains that are indistinguishable from symmetric 16:0 SM GUVs (**Figure 16, *b***). Together, our data demonstrate that the abolition of membrane domains in GUVs is specific to asymmetric 24:0 SM.

The precise mechanism for the 24:0 SM effect of altering cholesterol partitioning between leaflets and suppressing microdomains is not known. It is possible that transbilayer interdigitation of 24:0 SM could be responsible, by altering cholesterol partitioning and thus removing cholesterol from lateral hydrogen bonding with SM. Compared to 16:0 SM, the 24:0 SM acyl chain extends beyond the SM sphingosine backbone (**Figure 18**) and has been shown to protrude through from the outer leaflet to the inner leaflet (Niemelä et al., 2006). The MD simulation work of our collaborators supports this conclusion (**Appendix 3**). It is not clear, at this point, if cholesterol interacts uniquely with VLAC sphingolipids due to the length discrepancy between the acyl chain and the sphingosine chain. It is equally plausible that the very long acyl chain is sufficient to generate the unique effect, regardless of the length discrepancy with the sphingosine backbone. For example, PC with two saturated

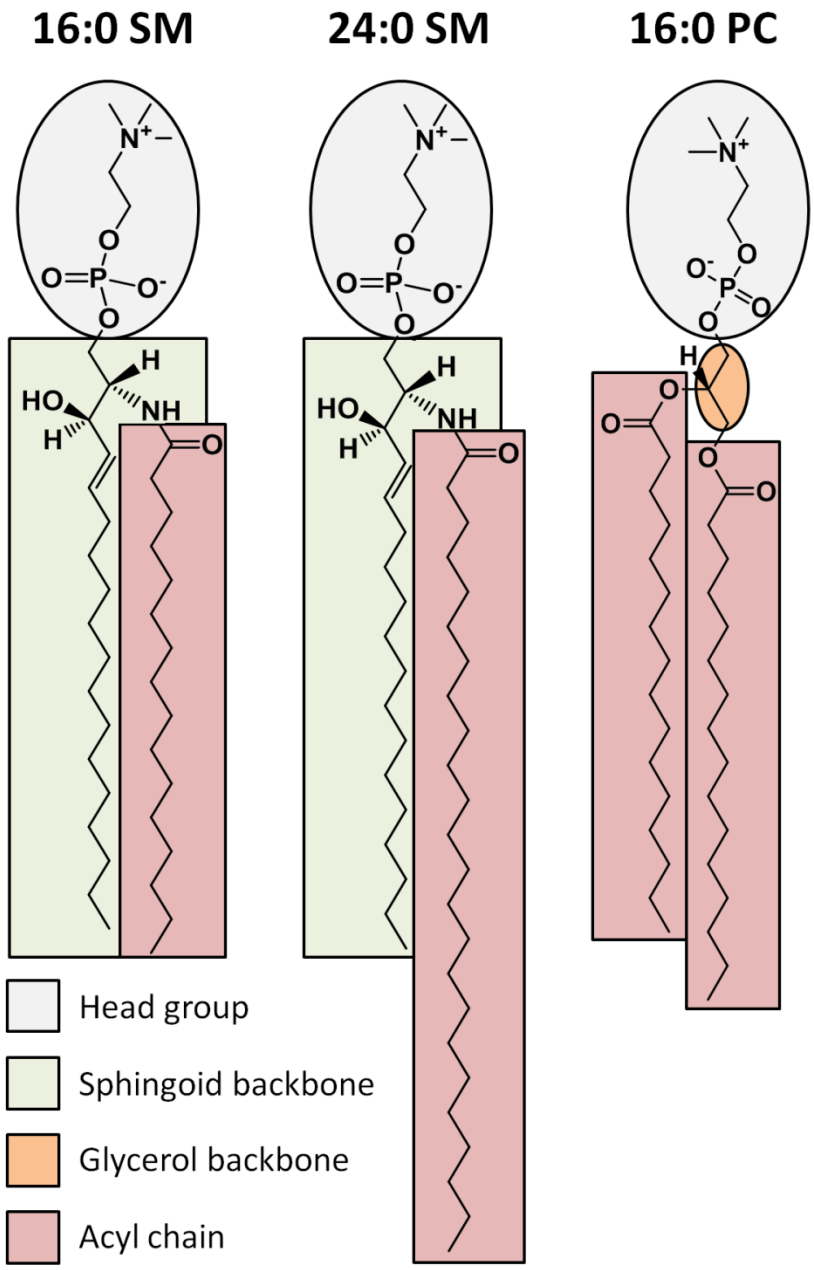
16:0 SM
24:0 SM
16:0 PC
Head group
Sphingoid backbone
Glycerol backbone
Acyl chain

Figure 18 – Comparison of sphingolipid and glycerophospholipid structure. The critical precursor molecule of a sphingolipid is the sphingoid base backbone. The precursor molecule can be further modified by the addition of a head group or acyl chain. By contrast, the glycerophospholipids have a glycerol molecule as the basic building block. The glycerol can be modified by the addition of two acyl chains and a head group.

VLACs may display the same results as 24:0 SM. Importantly, if VLAC sphingolipids are symmetrically distributed between bilayer leaflets, cholesterol is also evenly distributed and, therefore, the unique cholesterol/sphingolipid interaction that we uncovered is masked. This, in our hands, produces microdomains (**Figure 16A, *c***), whereas, asymmetric 24:0 SM does not (**Figure 16A, *a***). This also highlights the importance of continued experimentation with asymmetric model membranes, rather than conventional symmetric membrane systems. With the generation of a feasible procedure to create asymmetric model membranes, asymmetric GUVs should now be able to address increasingly more complex and physiologically relevant questions to help better understand PM function.

Chapter 6 - The role of very long acyl chain sphingolipids on microdomains in live mammalian cells

6.1 - Introduction

Sphingolipids are predominantly located in the outer leaflet of the mammalian cell PM and are associated with the formation of cholesterol-dependent membrane domains (Slotte, 2013; Verkleij et al., 1973). Although this association between cholesterol and sphingolipids has been extensively investigated, recent reports highlight the need to distinguish between sphingolipid species, such as SM, by acyl chain length rather than solely subdividing sphingolipids by head group (Hartmann et al., 2012; Ohno et al., 2010). In line with this view, our work, presented in earlier chapters, has identified that the most abundant sphingolipid in the mammalian cell PM, 24:0 SM, interacts with cholesterol differently than 16:0 SM in an asymmetric membrane. However, in a symmetric membrane, the differences between 16:0 and 24:0 SM are no longer visible (**Figure 5 & Figure 18**) (Ramstedt and Slotte, 1999). Our studies suggest that the conical cholesterol/sphingolipid interaction hypothesis may be limited to shorter chained sphingolipids, such as 16:0 and 18:0 SM, the most widely used SM in model membrane studies. However, the results above from asymmetric LUVs and GUVs indicate that 24:0 SM interacts with cholesterol uniquely. To determine the relevance of this newly discovered biophysical principle, we aimed next to understand how 24:0 SM affects the microdomains in the PM in live mammalian cells. For this, we manipulated the acyl chain length of sphingolipids in live cells and characterized PM domains by FRAP and FRET.

The sphingolipids are differentiated from the glycerophospholipids by having a sphingoid base as the central building block (**Figure 18**), rather than glycerol (Breslow,

2013). The sphingolipid precursor can be modified by acylation to form ceramide, which structurally resembles a saturated diacylglycerol. Ceramide can then be further modified by the addition of a head group moiety, such as phospho-choline to form sphingomyelin or a polysaccharide to form a ganglioside (Gault et al., 2010). De novo sphingolipid synthesis is initiated in the cytoplasmic ER membrane by the enzyme serine palmitoyl transferase that catalyzes the condensation of palmitoyl-CoA and a serine molecule to form 3-keto-sphinganine (Pewzner-Jung et al., 2006). The 3-keto-sphinganine is then reduced by 3-keto-sphinganine reductase to form sphinganine followed by acylation mediated by 1 of 6 ceramide synthase proteins to form dihydroceramide. The final ER-resident reaction in sphingolipid synthesis is desaturation by ceramide desaturase to catalyze the addition of a trans double bond in the 4th carbon of the acyl chain to form ceramide. Ceramide can then be transported from the ER to the Golgi apparatus by vesicular trafficking or by ceramide transfer protein (CERT) for further modification (Hanada et al., 2003). While at the Golgi, ceramide can be converted to sphingomyelin, a cerebroside or a ganglioside (Gault et al., 2010) and trafficked to the PM.

The most abundant sphingolipid in the mammalian cell PM is sphingomyelin, which constitutes up to 40-50 % of the outer leaflet phospholipids (Van Meer et al., 2008; Warnock et al., 1993). In addition to various head group modifications, sphingolipids also display a wide distribution of acyl chain lengths that are conjugated to sphinganine molecule by an amide bond (Breslow, 2013). There are two major factors that determine the sphingolipid acyl chain length in the PM: (1) fatty acid elongation to produce various fatty acid substrates and (2) the subsequent selection of specific fatty acid substrates for the addition of a fatty acid to the sphinganine precursor (Sassa and Kihara, 2014). Prior to sphinganine acylation,

fatty acid elongation is carried out by 7 different elongase enzymes that belong to the elongation of very long chain fatty acids (ELOVL) family (Jakobsson et al., 2006; Naganuma et al., 2011). Each of the 7 elongases demonstrates substrate specificity and is responsible for creating different fatty acid lengths that can be used for acylation during membrane lipid synthesis. Although some crossover does exist, ELOVL1 generates VLAC fatty acids (≥ 22 carbons long), ELOVL2 produces polyunsaturated fatty acids with 20 carbons, ELOVL3 produces 20 and 22 carbon fatty acids, ELOVL4 produces ultra-long acyl chain fatty acids (≥ 28 carbons), ELOVL5 and ELOVL7 produce polyunsaturated 18 carbon fatty acids and ELOVL6 produces 16 carbon fatty acids (Naganuma et al., 2011; Ohno et al., 2010; Sassa and Kihara, 2014). Since each ELOVL protein produces specific fatty acid lengths, the ELOVL protein expression profile determines the relative quantity of each fatty acid length. ELOVL protein expression has been shown to be correlated with the fatty acid composition among different tissues (Ohno et al., 2010). ELOVL therefore, can regulate sphingolipid acyl chain length by controlling fatty acid substrate availability.

Once the ELOVL family of proteins produce the various fatty acid substrates, the sphingolipid precursor, sphinganine, is then acylated by the action of a ceramide synthase (CerS). Mammalian cells have six known CerS proteins in the ER that, like ELOVL, display specificity for the length of acyl chain. CerS1 is primarily for 18:0 sphingolipids, CerS2 for 22:0 and primarily 24:0 sphingolipids, CerS3 for ≥ 26:0 sphingolipids, CerS4 for 18:0 and 20:0 sphingolipids and both CerS5 and CerS6 for 14:0 and 16:0 sphingolipids (Park and Park, 2015). The relative expression profile of the CerS proteins regulates the quantity of mature sphingolipids with each acyl chain length. For example, CerS2 is highly expressed in many tissues and results in 24:0 SM being the most abundant sphingolipid. Furthermore,

knockdown of CerS2 depletes 24:0 sphingolipids and results in the subsequent increase in 16:0 sphingolipids (Sassa et al., 2012). By manipulating individual CerS levels, the effects of altering sphingolipid acyl chain length can be investigated.

Increasingly, human health and disease has been shown to be influenced by sphingolipid acyl chain length. The balance between 24:0 and 16:0 sphingolipids, mediated by CerS2 and CerS6, in particular, is tightly regulated to maintain homeostasis (Raichur et al., 2014; Turpin et al., 2014). CerS2 is significantly reduced in the brain tissue of Alzheimer's patients (Couttas et al., 2016) and the accumulation of VLAC fatty acids leads to the induction of neuroinflammation (Singh et al., 2009). Haploinsufficiency of CerS2 has also been shown to increase susceptibility to insulin resistance (Raichur et al., 2014; Sassa et al., 2012). The levels of VLAC sphingolipids are also associated with cancer; curiously however, conflicting results have been published and a consensus has not been established in the context of cancer since VLAC sphingolipids have been shown to promote and inhibit cell proliferation (Fan et al., 2013; Fan et al., 2015; Hartmann et al., 2012; Mei et al., 2015; Sassa et al., 2012). Interestingly, hepatitis C viral infection, which is known to manipulate the host cell to promote membrane domain formation (Sakamoto et al., 2005), depletes the cell of 24:0 sphingolipids in patients with chronic infection (Grammatikos et al., 2016). Based on our discovery above, reducing 24:0 sphingolipids in patient cells could help or enhance viral infectivity by promoting the formation of membrane microdomains.

Although there are a few studies that examined the role of 24:0 sphingolipids on the physical properties of membranes, conflicting conclusions have been reported (Bjorkqvist et al., 2009; Iwabuchi et al., 2010; Park et al., 2013; Silva et al., 2012). Bjorkqvist et al (2009). 24:0 SM showed a high acyl chain packing density that excluded and altered the lateral

packing density of cholesterol. Alternatively, genetic knockout of CerS2 in mice, which replaced 24:0 SM with 16:0 SM, was reported to cause hepatic insulin resistance by inhibiting recruitment of the insulin receptor into caveolar membrane domains (Park et al., 2013). This conclusion, however, is confounded by Kabayama et al (2007), which found that accumulation of ganglioside sphingolipids into caveolae similarly excluded the insulin receptor from the domains (Kabayama et al., 2007). Therefore, since 24:0 sphingolipid depletion results in the increase of 16:0 sphingolipids (Park et al., 2013), our model membrane data would suggest that the CerS2 knockout effect of inhibiting recruitment into caveolae would likely be caused by increasing 16:0 gangliosides in the caveolae, rather than by the depletion of 24:0 gangliosides. It was also reported that CerS2 knockout altered the biophysical properties of membranes (Silva et al., 2012). However, this study was performed on microsomal lipids and, therefore, may have limited applicability to the PM.

With the exception of characterizing cholesterol partitioning in human erythrocytes (**Figure 8**), the majority of the data in earlier chapters examined the dynamics of a membrane bilayer using a series of model membrane systems. The work thus far suggested that outer leaflet VLAC sphingolipids have a unique effect on the lateral organization of membranes. We, therefore, next investigated if the principles generated from asymmetric model membranes are applicable to the live mammalian cell PM.

6.2 - Results

To characterize the role of VLAC sphingolipids in the formation of membrane domains in the PM of live cells, we used two approaches to manipulate the sphingolipid levels:

(**1**) *Using shRNA to deplete CerS2 from mammalian cells.* We expect to reduce the levels of 24:0 SM in the PM. The diffusional properties of PM proteins that are known to localize within membrane microdomains were analyzed using FRAP.

(**2**) *Generating live cells with either 24:0 SM or 16:0 SM in the PM and characterize microdomains by density-dependent FRET of GPI-anchored proteins.* We depleted sphingolipids from the cells pharmacologically and then resupplied the cells with either 16:0 or 24:0 SM. We then analyzed FRET between CFP- and YFP-GPI-anchored proteins.

6.2.1 - Fluorescence recovery after photobleaching

We hypothesized that since CerS2 depletion significantly reduces 24:0 SM, which could decrease cholesterol inner leaflet partition, outer leaflet cholesterol content could be increased in CerS2 knockdown cells. Under this scenario, we also postulated that reducing 24:0 sphingolipids would enhance membrane microdomains in the PM of live cells and thus reduce the lateral mobility of proteins known to be associated with microdomains. In order to reduce VLAC SM levels in the PM, we expressed a short hairpin RNA (shRNA) in HeLa cells that targeted CerS2 (shCerS2) or a scrambled shRNA (shScramble). We found that shCerS2 effectively reduced the levels of CerS2 protein and that the knockdown of CerS2 reduced 24:0 sphingolipid levels (**Figure 19**).

We then proceeded to determine if cholesterol was increased in the outer leaflet of the PM of shCerS2 cells. For this, shCerS2 and shScramble cells were trace labelled with ^{3}H-cholesterol and allowed to equilibrate overnight. The cells were then washed and placed at 0 ^{o}C to prevent cholesterol flip-flop, as well as, to prevent endocytic membrane trafficking to and from the PM. Analogously to the strategy used to determine the cholesterol distribution in our model membrane studies and human erythrocytes (**Figure 4 & Figure 8**), MCD was

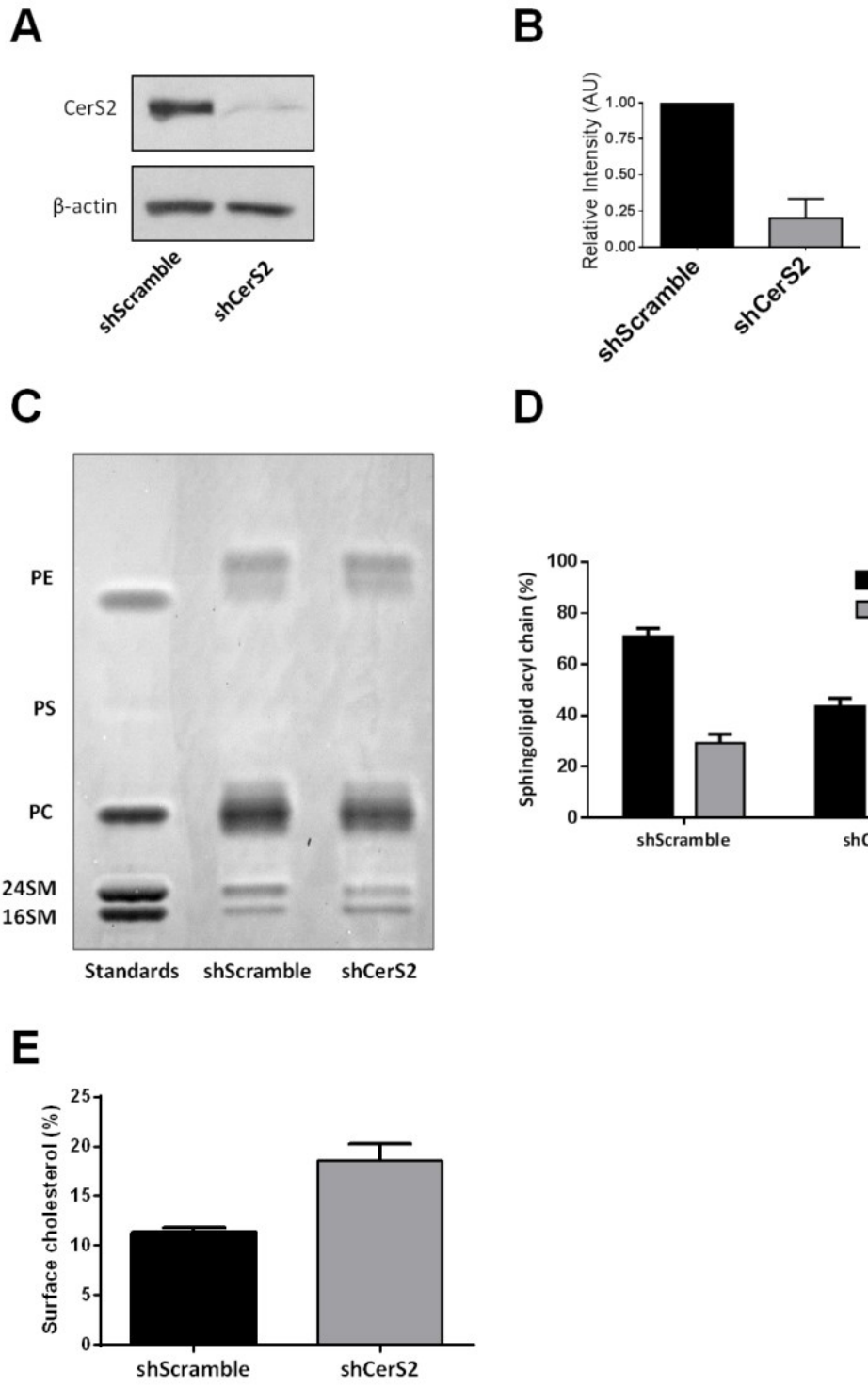
A
CerS2
β-actin
shScramble
shCerS2
B
Relative Intensity (AU)
1.00
0.75
0.50
0.25
0.00
shScramble
shCerS2
C
PE
PS
PC
24SM
16SM
Standards
shScramble
shCerS2
D
Sphingolipid acyl chain (%)
100
80
60
40
20
0
C24 SM
C16 SM
shScramble
shCerS2
E
Surface cholesterol (%)
25
20
15
10
5
0
shScramble
shCerS2

Figure 19 –Knockdown of ceramide synthase 2 increases the 16:0/24:0 SM radio and increases outer leaflet cholesterol content. A) Representative western blot of ceramide synthase 2 protein levels after shRNA knock down treatment for 3 days. **B)** Quantification of ceramide synthase 2 protein levels after the knock down from three independent experiments. **C)** Representative thin layer chromatography to examine changes in 24:0 SM levels after ceramide synthase 2 knock down. Lane 1 shows the pure lipid standards with the scrambled shRNA control and the specific ceramide synthase 2 shRNA in lanes 2 and 3, respectively. **D)** Thin layer chromatography quantification of sphingomyelin levels with and without ceramide synthase 2 knock down from three independent experiments. **E)** Outer leaflet cholesterol content in live HeLa cells with and without ceramide synthase 2 knock down. HeLa cells were trace labelled with ^{3}H-cholesterol overnight, washed and then incubated at 0 °C to prevent cholesterol movement. Cholesterol was extracted from the outer leaflet of the plasma membrane by 10 mM MCD for 30 minutes and quantified relative to whole cell cholesterol content by scintillation counting.

then used to extract outer leaflet cholesterol from shCerS2 and shScramble cells over time under non-flip-flopping conditions. The results show that knockdown of CerS2 in live mammalian cells causes a significant increase in outer leaflet cholesterol content, relative to total cellular cholesterol (**Figure 19**).

Knowing that 24:0 SM depletion caused a redistribution of cholesterol to the outer leaflet, we performed FRAP analysis on live shCerS2 and shScramble transfected cells. FRAP has been widely used to probe restricted mobility of fluorescently tagged proteins associated with membrane domains (Kenworthy, 2007; Kenworthy et al., 2004). In particular, FRAP is advantageous in this context since single cell microscopy allows for the specific selection of transfected cells. We expressed the membrane microdomain associated GPI-anchored proteins, GFP-Lck or mCherry-CD59 (Lipp et al., 2014) into the HeLa cells, along with either shCerS2 or shScramble and measured the FRAP. Indeed, for the membrane domain associated proteins, GFP-Lck and mCherry-CD59, the fluorescence recovery was significantly slower when CerS2 was silenced (**Figure 20A, Figure 20B & Table 2**), consistent with enforced microdomains (Kenworthy, 2007). At the same time, shCerS2 had no effect on the fluorescence recovery of the non-membrane domain associated protein GFP-VSVG (Kenworthy et al., 2004), compared to the shScramble control (**Figure 20C**). Furthermore, diffusion coefficients were determined for each domain and non-domain associated protein using a program described by Siggia *et al*. (Siggia et al., 2000). The results further confirmed that the lateral diffusion coefficient of membrane domain associated proteins was significantly slower in shCerS2 cells, while the non-domain associated protein was unchanged (**Table 2**). Thus, replacing VLAC sphingolipids with shorter acyl chain sphingolipid, by silencing CerS2, restricted the lateral diffusion of proteins

A

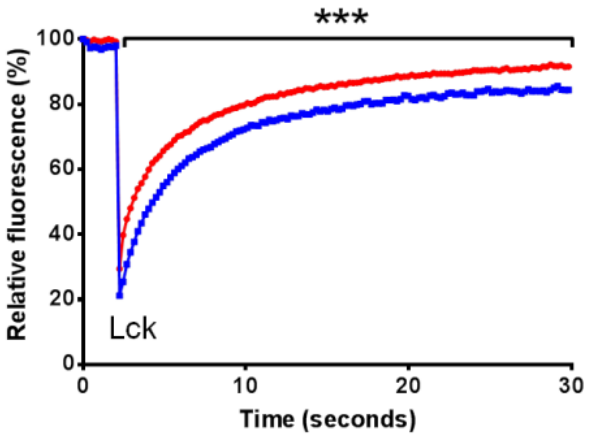
***
Relative fluorescence (%)
100
80
60
40
20
0
Lck
0
10
20
30
Time (seconds)

B

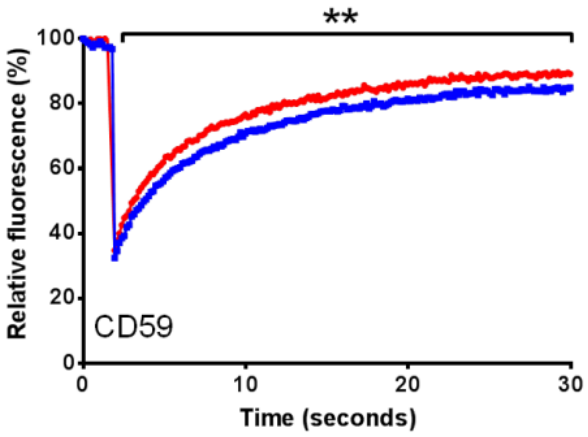
**
Relative fluorescence (%)
100
80
60
40
20
0
CD59
0
10
20
30
Time (seconds)

C

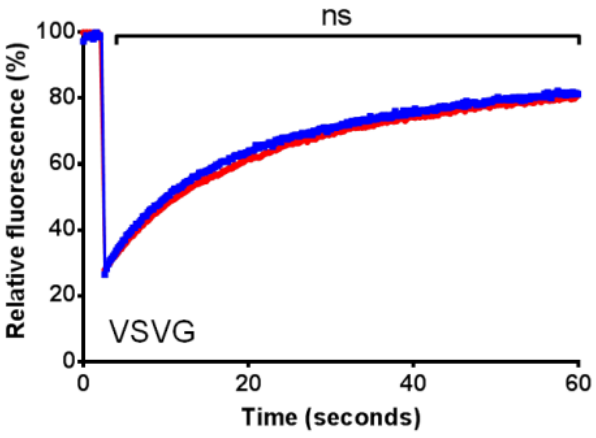
ns
Relative fluorescence (%)
100
80
60
40
20
0
VSVG
0
20
40
60
Time (seconds)

Figure 20 – Depletion of very long acyl chain sphingolipids from live cell plasma membrane causes an increase in outer leaflet cholesterol and subsequently slows the fluorescence recovery of lipid raft associated proteins. Fluorescence recovery after photobleaching was performed to examine membrane diffusion after depletion of very long acyl chain sphingolipids from live HeLa cells. Knockdown of CerS2 by shRNA significantly attenuated the lateral mobility of lipid raft associated proteins, Lck (**A**) and CD-59 (**B**). **C)** Fluorescence recovery was unaltered for VSVG (see **Table 2** for corresponding diffusion coefficients). Fluorescence recovery figures represent the mean recovery from 15 cells per treatment and each experiment was repeated at least 3 times.

Membrane Protein	Treatment	Diffusion coefficient	p value
GFP-Lck	shScramble	0.826 (± 0.237)	**0.039**
	shCERS2	0.623 (± 0.232)	
mCherry-CD59	shScramble	0.286 (± 0.054)	**0.004**
	shCERS2	0.207 (± 0.074)	
GFP-VSVG	shScramble	0.129 (± 0.062)	**0.101**
	shCERS2	0.176 (± 0.092)	

Table 2 – Fluorescent recovery after photobleaching of proteins in the plasma membrane of live HeLa cells. Depleting very long acyl chain sphingolipids from the plasma membrane of live cells by shRNA knockdown of CerS2 slows the lateral diffusion of membrane domain associated proteins. Lateral diffusion of non-domain protein, VSVG, is unchanged by CerS2 knockdown. Data acquired by following Siggia *et al* (2000) and represents the mean recovery from 15 cells per treatment and each experiment was repeated at least 3 times.

known to associate with membrane microdomains, consistent with enforcing membrane microdomain in these cells.

6.2.2 - Förster resonance energy transfer

To further validate the role of 24:0 sphingomyelin on membrane microdomains, as implied by the live cell FRAP experiments above, we proceeded to examine the role of sphingolipid acyl chain length using FRET between GPI-anchored proteins in the live cell PM. Specifically, this set of experiments used fumonisin b1 as a pan-inhibitor of CerS proteins and myriocin to prevent *de novo* sphingolipid synthesis. After thorough depletion of endogenous sphingolipids, we then re-supplied the cells with either 16:0 or 24:0 SM and compared FRET between GPI-anchored proteins.

GPI-anchored proteins are well-documented to prefer ordered membrane domains, or lipid rafts (Brown and Rose, 1992; Varma and Mayor, 1998). FRET has been used to analyze interactions between GPI-anchored proteins in live cells (Rao and Mayor, 2005). There are two major methods for FRET: (**1**) homo-FRET, which uses polarized excitation to monitor the energy transfer between same fluorophore, such as GFP and (**2**) heteroFRET, which measures energy transfer between different donor and acceptor fluorophores, such as YFP emission by CFP. Homo-FRET has been used to demonstrate nanodomains in the PM of live cells, where GPI-anchored proteins clustering in cholesterol dependent fashion (Raghupathy et al., 2015; Rao and Mayor, 2005). Hetero-FRET, however, does not detect specific interactions between GPI-anchored proteins. Nevertheless, these proteins were capable of producing density-dependent FRET when expressed in high levels (Kenworthy and Edidin, 1998). We reasoned that, if cholesterol-dependent microdomains form on the PM, GPI-anchored proteins would be recruited into these domains and therefore enhance

density-dependent FRET, compared with a random distribution (**Figure 21**). Indeed, we found that hetero-FRET between CFP- and YFP-GPI-anchored proteins increases linearly with increasing density of fluorescent proteins (**Figure 22**). This is consistent with the theoretical simulation for random CFP and YFP FRET (**Figure 23**). If, at steady state, the PM contains cholesterol-dependent membrane microdomains that sequester GPI-anchored proteins, the apparent density dependence of FRET would have a steeper slope than the FRET from randomly distributed proteins (**Figure 21 & Figure 22**). Furthermore, the enhanced FRET should be reduced by cholesterol depletion, as GPI-anchored proteins would be dispersed back to a random distribution (**Figure 21 & Figure 22**). Therefore, by this approach, the slope of FRET and protein density (FRET/YFP) can be used to monitor the recruitment of GPI-anchored proteins into microdomains (**Figure 21**).

Cells were first treated with myriocin and fumonisin b1 (M+FB1) to deplete all sphingolipids (Lasserre et al., 2008; Merrill et al., 1993). A subset of the M+FB1 cells were then resupplied with 16:0 or 24:0 SM by incubating the cells with a SM/cyclodextrin complex. This proved to be a highly effective strategy for altering SM composition, as shown by thin layer chromatography, which confirmed a thorough depletion of sphingolipids by the M+FB1 treatment, as well as, the efficient donation of 16:0 and 24:0 SM into the PM (**Figure 24**).

FRET was then measured on the live cells at approximately 12 °C, using 3-cube system on a wide-field fluorescence microscope (see method section for detail). Each treatment (control, M+FB1, 16SM and 24SM) was also accompanied by an additional sample that was treated with saponin for 30 minutes to deplete cholesterol. We found that

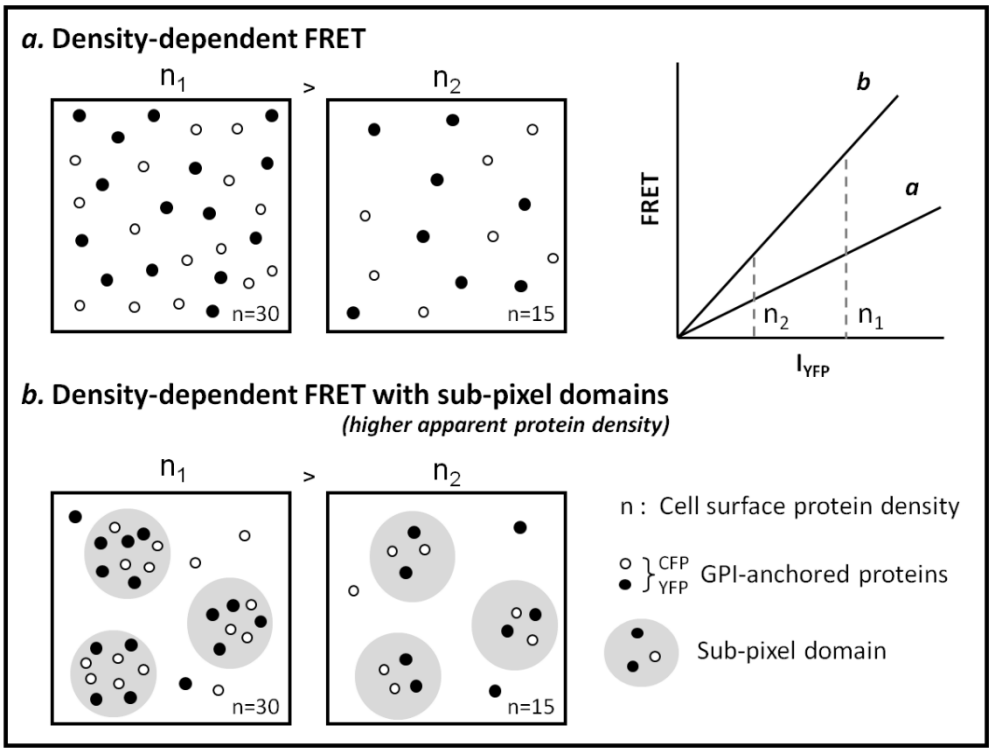
a. Density-dependent FRET
n1
>
n2
n=30
n=15
FRET
b
a
n2
n1
IYFP
b. Density-dependent FRET with sub-pixel domains
(higher apparent protein density)
n1
>
n2
n=30
n=15
n : Cell surface protein density
CFP
YFP
GPI-anchored proteins
Sub-pixel domain

Figure 21 – Model of density-dependent FRET between GPI-anchored proteins in membranes with and without microdomains. Pictogram depicting how the presence of membrane domains would affect density-dependent FRET between mCFP and mYFP GPI-APs. In the absence of membrane domains (***a***), FRET between GPI-anchored proteins is random and concentration dependent. In the presence of ordered membrane domains (***b***), CFP and YFP GPI-anchored proteins are recruited to the domains and the relative molecular density is locally increased, which causes an increase in FRET.

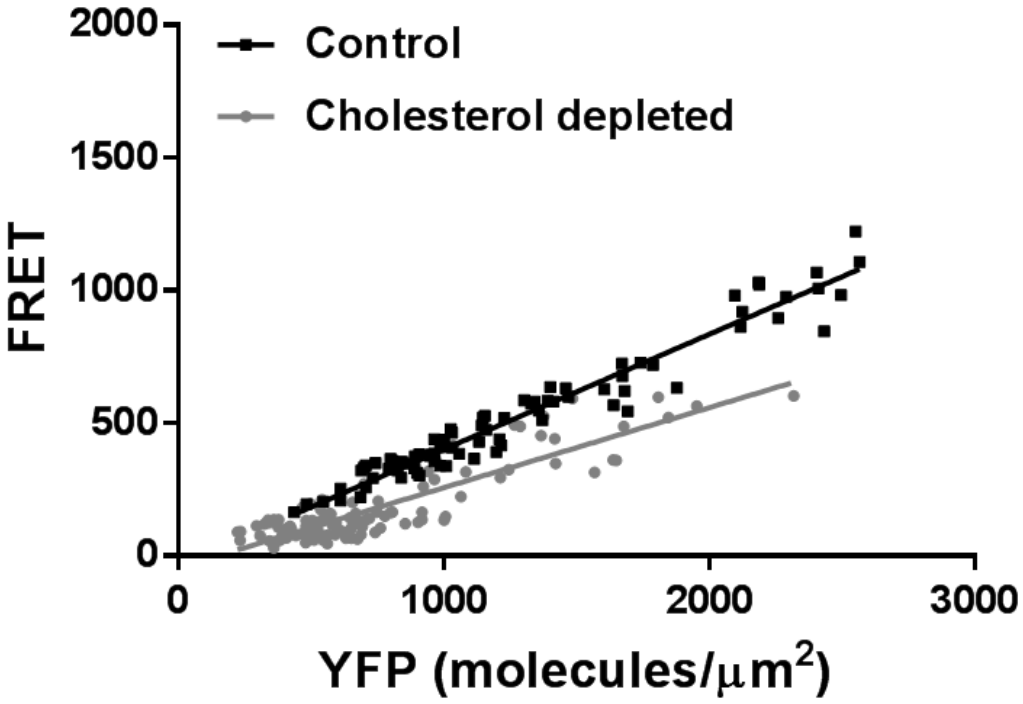
Control
Cholesterol depleted
FRET
2000
1500
1000
500
0
0
1000
2000
3000
YFP (molecules/μm²)

Figure 22 – Förster resonance energy transfer between CFP and YFP GPI-anchored proteins increase linearly with the concentration of fluorescent protein. As the molecular density of YFP increases in the plasma membrane of live cells, FRET between CFP and YFP increases linearly (black line). Depleting cholesterol from the cells disperses GPI-anchored proteins from ordered domains to a random distribution, which reduces density-dependent FRET (grey line).

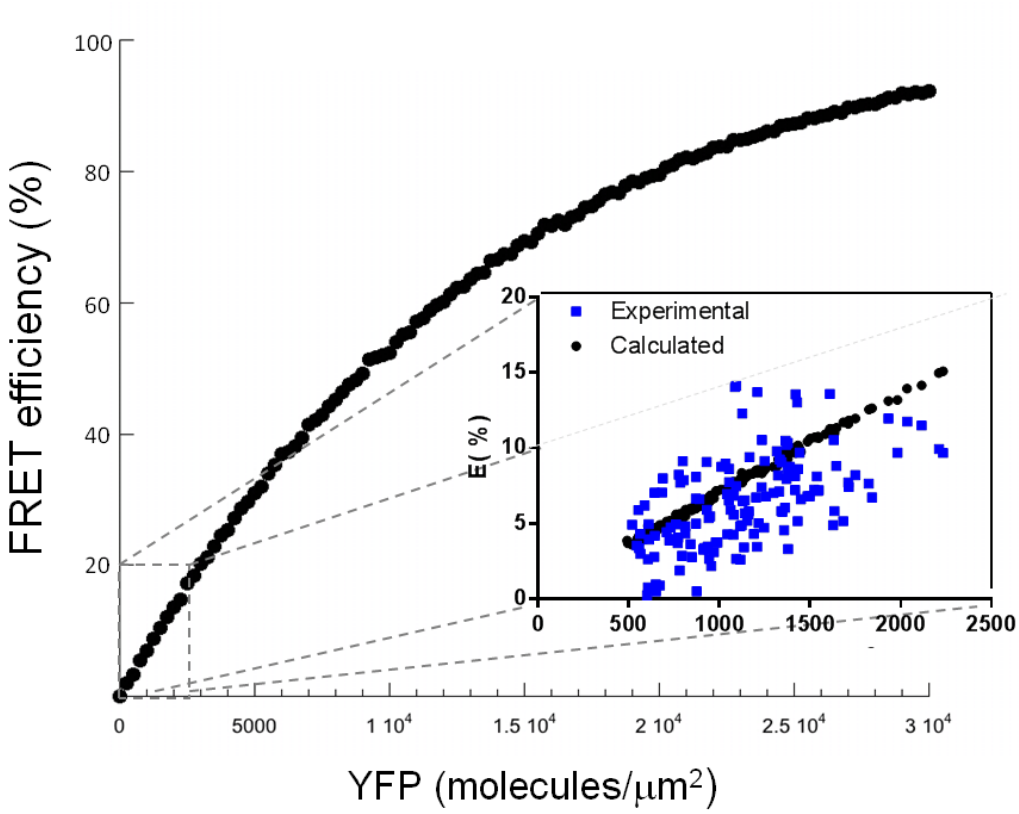
FRET efficiency (%)
100
80
60
40
20
0
5000
1 10^4
1.5 10^4
2 10^4
2.5 10^4
3 10^4
YFP (molecules/μm²)
Experimental
Calculated
E(%)
20
15
10
5
0
0
500
1000
1500
2000
2500

Figure 23 – Simulation of FRET efficiency as a function of YFP molecular density. Density-dependent FRET efficiency simulation: the solid points represent simulated density-dependent FRET predicted from density of YFP protein. Blue dots represent experimentally obtained FRET efficiencies from the cells treated with saponin. Notice that the stimulated line is linear within the range of the true experimental YFP density.

A

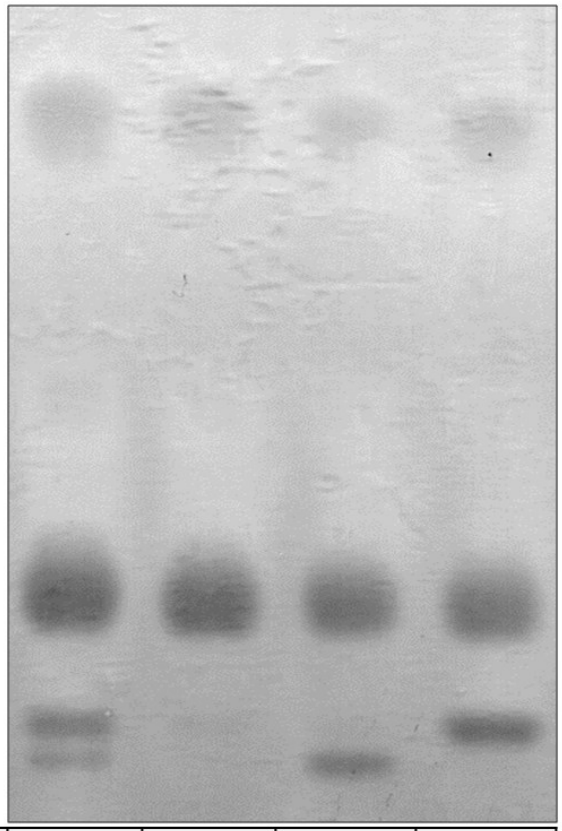

DMSO	+	+	+	+
M + FB1	-	+	+	+
16:0 SM	-	-	+	-
24:0 SM	-	-	-	+

B

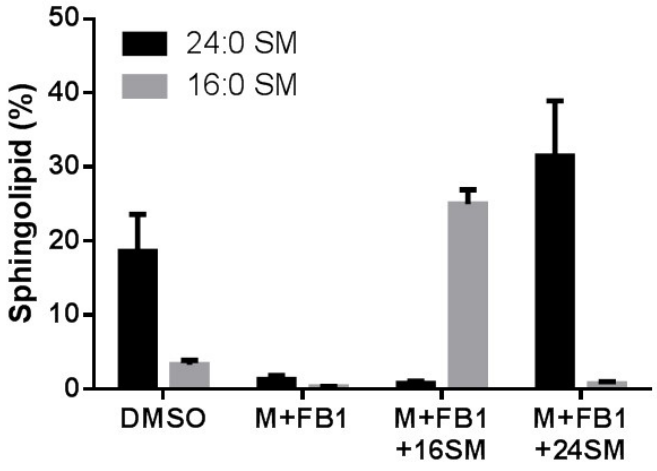

Figure 24– Thin layer chromatography of whole cell lipids after depletion of sphingolipids and subsequent supplementation with 16:0 or 24:0 sphingomyelin. HeLa cells were treated with DMSO or myriocin and fumonisin b1 (50 μM) for 3 days. To incorporate the desired sphingolipids, the cells were incubated with a sphingomyelin/γ-cyclodextrin complex containing 6.7 μM sphingomyelin for 1 hour at 37 °C. The cells were then lipid extracted, purified and run on a thin layer chromatography plate. **A**) Representative image of isolated lipids that were resolved by thin layer chromatography using a chloroform/acetone/methanol/acetic acid/water (6:8:2:2:1) solvent system and visualized with coomassie blue G stain. Lane 1 shows the control cells have 24:0 sphingolipids as the predominant species. Myriocin and fumonisin b1 treatment effectively depleted the cells of endogenous sphingolipids (lane 2). Treatment of the 16:0 or 24:0 SM/cyclodextrin complex returns the sphingolipid content to the control level. **B**) Quantification of sphingolipid species after depletion and supplementation of exogenous 16:0 and 24:0 sphingomyelin. Error bars represent standard error of the mean from 3 independent experiments.

sphingolipid depletion by M+FB1 caused a significant increase in FRET (**Figure 25A, *green line***), in comparison with untreated (control) cells (**Figure 25A, *black line***), consistent with enhanced recruitment of GPI-anchored proteins into membrane microdomains. This result is initially counter intuitive since sphingolipids are thought to support the formation of membrane domains. However, since the majority of sphingolipids in mammalian cells have VLACs (Boegheim Jr et al., 1983), we reasoned that global sphingolipid depletion in cells would be similar to GUVs without SM, which forms microdomains (**Figure 14A**), perhaps reflecting an increase in outer leaflet cholesterol (**Figure 12**). Consistent with this notion, cholesterol depletion by saponin greatly diminished FRET in these cells (**Figure 25B, *grey lines***). Interestingly, we found that if the M+FB1 cells are resupplied with pure 16:0 SM, the increase in FRET persisted (**Figure 25A, *blue line***), which is also cholesterol sensitive, supporting the notion that 16:0 SM promotes membrane domains (**Figure 16**). When resupplying the cells with 24:0 SM, however, the density-dependent FRET was returned to the level of the control cells (**Figure 25A, *red line***).

Importantly, cholesterol depletion by saponin reduced FRET down to the same level in all 4 treatments (**Figure 25B, *grey lines***), consistent with its role in dispersing microdomains (**Figure 21 &Figure 22**). The effects of saponin were much more dramatic in M+FB1 and 16:0 SM supplemented cells, supporting existence of microdomains in these cells. Also, the effects of saponin were minimal in 24:0 SM supplemented or control cells, suggesting limited microdomain formation in cells with very long acyl chain sphingolipids. Thus, VLAC sphingolipids exhibit an inhibitory effect on the formation of membrane domains in live cells, just as in asymmetric GUVs (**Figure 16**).

A

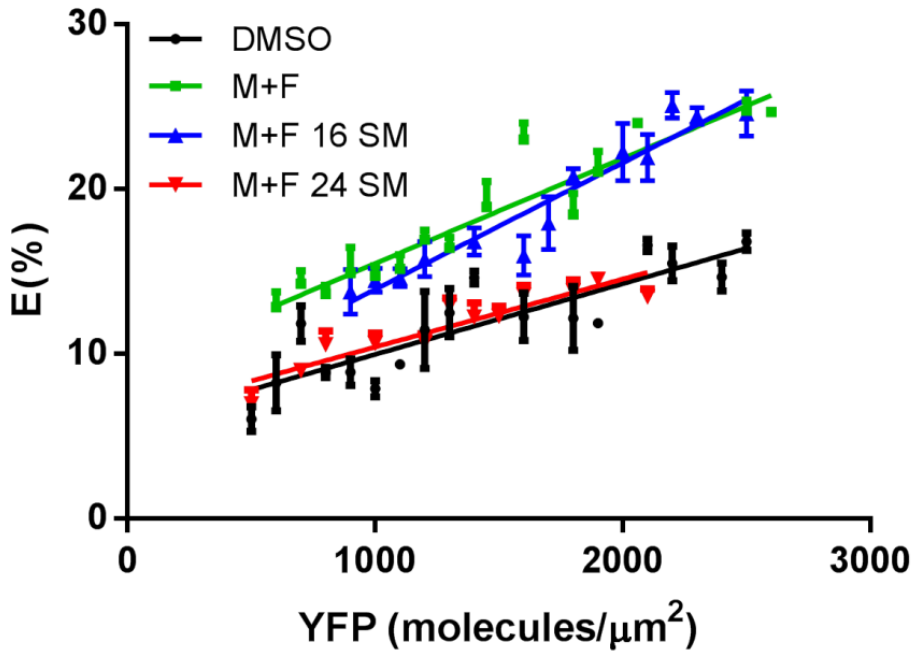
DMSO
M+F
M+F 16 SM
M+F 24 SM
E(%)
YFP (molecules/μm²)

B

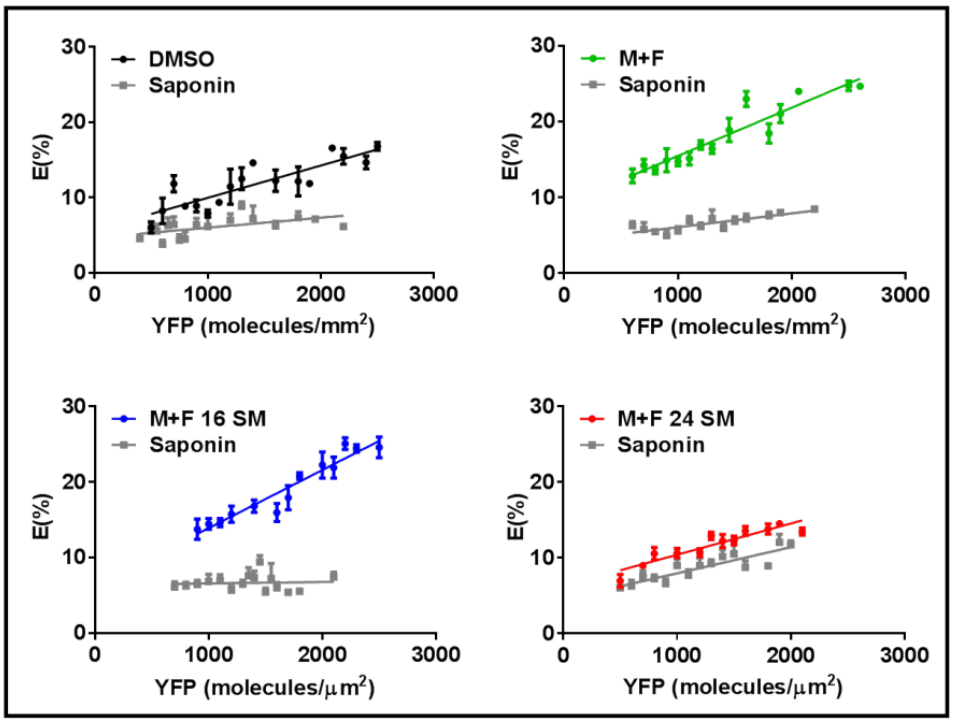
DMSO
Saponin
M+F
Saponin
M+F 16 SM
Saponin
M+F 24 SM
Saponin
E(%)
YFP (molecules/mm²)
YFP (molecules/μm²)

Figure 25 – Outer leaflet 24:0 sphingomyelin suppresses membrane domains in the live cell plasma membrane. HeLa cells were treated with DMSO or myriocin and fumonisin b1 (50 μM) for 3 days. To incorporate the desired sphingolipids, the cells were incubated with a sphingomyelin/γ-cyclodextrin complex containing 6.7 μM sphingomyelin for 1 hour at 37 °C. FRET was then determined by live cell microscopy. **A)** FRET between mCFP and mYFP GPI-anchored proteins in live HeLa cells with sphingolipid depletion (M+F) and subsequent supplementation with 16:0 or 24:0 SM. **B)** Comparison of FRET between mCFP and mYFP GPI-anchored proteins in live HeLa cells from all treatments with and without cholesterol depletion by saponin.

6.3 - Conclusion

In this chapter, we attempt to translate the conclusions drawn from our model membrane studies into live cells. Using simplified model membrane systems, described in previous chapters, we identified that transbilayer SM asymmetry is an important factor in regulating cholesterol partitioning and microdomains in a membrane bilayer. The results here demonstrate that these principles, derived from asymmetric model membranes, are applicable to live cells. We found the sphingolipid acyl chain length in the mammalian cell PM regulates lateral membrane microdomain formation.

We found that both strategies selectively reduce VLAC sphingolipids, i.e. shRNA and sphingolipid depletion/supplementation, was able to alter microdomain formation in the PM of live cells (**Figure 20 & Figure 25**). Admittedly, using the shRNA to reduce CerS2 levels was only partially effective, likely due to incomplete knockdown and variability of transfection efficiency. We observed that the VLAC sphingolipid level was not as dramatically affected, even when CerS2 was knocked down to a very low level (**Figure 19**). This result is not surprising, considering other studies that utilized primary cells isolated from a CerS2 knockout mouse also had residual VLAC sphingolipids (Pewzner-Jung et al., 2010a; Pewzner-Jung et al., 2010b). In our study, the residual 20 percent of the CerS2 protein, after knockdown, could continue to generate VLAC sphingolipids and prevent the complete depletion of 24:0 SM. Furthermore, ceramidase enzymes have been shown to catalyze both hydrolysis and synthesis of sphingolipids (Okino et al., 2003) and could facilitate a compensatory mechanism for the lack of CerS2 in the presence of a functional ELOVL1 enzyme. Nevertheless, FRAP analysis on single cells has the advantage of selecting only transfected cells, which may explain why we saw differences in FRAP

(**Figure 20**) without complete depletion of VLAC from all cells shown by TLC (**Figure 19**). In the future, generating a stable and inducible shCerS2 system would be advantageous to create a more robust and homogeneous effect.

We also estimated the cholesterol transbilayer distribution in the shCerS2 expressing cells using a protocol similar to the one used with human erythrocytes (**Figure 8**). In principle, shCerS2 could alter the cholesterol partitioning between leaflets of the PM. We did observe significantly more cholesterol in the outer leaflet of the mammalian cells when CerS2 was silenced (**Figure 19**). Although increase in outer leaflet cholesterol was consistently observed, shCerS2 transfection could potentially alter the total cell cholesterol content or the relative amount of cholesterol present in the PM. With these other possibilities in mind, the conclusions drawn from the outer leaflet cholesterol content assay remains equivocal.

FRAP was performed on fluorescent GPI-anchored proteins in HeLa cells expressing shCerS2 or shScramble. We hypothesized that shCerS2 would promote membrane microdomains and sequester GPI-anchored proteins into these to these domains, resulting in slower diffusion. Indeed, the GPI-anchored proteins displayed a slower fluorescence recovery in these cells, whereas the non-domain associated protein, VSVG, was unaffected (**Figure 20**). Taken together, the results here are consistent with the notion that reducing VLAC sphingolipids increases cholesterol in the outer leaflet and enhances membrane microdomains.

We used second and more direct strategy to examine the effect of sphingolipid acyl chain length on microdomain formation. It has long been known that molecular density

determines the FRET efficiency, even if there is no specific interaction (Fung and Stryer, 1978; Snyder and Freire, 1982). As molecular density increases, FRET efficiency also increases (Fung and Stryer, 1978). Furthermore, clustered, or non-randomly distributed fluorescent molecules exhibit distinct FRET efficiencies from randomly distributed fluorophores (Snyder and Freire, 1982). We, therefore, hypothesized that clustering of GPI-anchored proteins into membrane microdomains, even at sub-micron scale, could be detected by changes in FRET. We characterized density-dependent FRET between CFP and YFP GPI-anchored proteins in live cells, treated with M+FB1 to deplete all sphingolipids, and then resupplied with 16:0 or 24:0 SM. TLC analysis showed a clean alteration of sphingolipids by this strategy (**Figure 24**), rather than an incomplete depletion of VLACs by shCerS2 (**Figure 19D**). We found that the FRET between CFP- and YFP-GPI-anchored proteins increased linearly with acceptor (YFP) concentration (**Figure 22**). Moreover, this protein density dependent FRET was validated by theoretical simulations (**Figure 23**).

Based on the model presented in **Figure 21**, we used the slope of FRET/YFP, to monitor the relative recruitment of GPI-anchored proteins into membrane domains. In cells with 16:0 SM supplementation, density dependent FRET, or FRET/YFP, is enhanced relative to control cells, indicating GPI-anchored protein recruitment into domains. Similar enhancement is seen in M+FB1 treated cells. However, 24:0 SM supplementation returned FRET/YFP to the level of control cells. This difference in 16:0 and 24:0 SM supplementation is significant at two aspects. First, the data support the notion that very long acyl chain sphingolipids play a major role in lateral organization or microdomain formation in the plasma membrane. Second, cholesterol depletion by saponin in both control and 24:0 SM supplemented cells has limited effect in FRET/YFP, compared to 16:0 SM supplemented

cells. This implies that control and 24:0 SM supplemented cells have rather limited microdomains, if at all. FRET/YFP in 16:0 SM supplemented and M+FB1 treated cells, however, is highly sensitive to cholesterol depletion, supporting the existence of microdomains in these cells.

Thus, by two independent strategies, we discovered a critical and central role played by the acyl chain length of PM sphingolipids in live cells. In the absence of VLAC sphingolipids, membrane microdomains are enhanced. Conversely, VLAC SM limited membrane microdomain formation, presumably due to the redistribution of cholesterol away from the SM containing outer leaflet. Given that VLAC sphingolipids are the predominant sphingolipids in most mammalian cell types (Park and Park, 2015), our results demonstrate that, at steady state, membrane microdomains are limited in the PM of mammalian cells. We postulate that cholesterol asymmetry, generated by VLAC sphingolipids in the outer leaflet of the PM, is the key to the suppression of membrane microdomains. Thus, dynamic and localized loss of sphingolipid asymmetry, as it may occur under various metabolic conditions, can redistribute cholesterol to the outer leaflet and promote membrane microdomains. This could dynamically regulate protein-protein interactions.

Chapter 7 - Summary and conclusions

7.1 – Thesis overview

Mammalian cells are surrounded by a bilayer lipid membrane that insolates the internal cellular components from the external environment. In addition to providing a physical barrier, the PM is also actively involved in many cellular processes (Van Meer et al., 2008). Initially, the PM was considered to be homogeneous (Singer and Nicolson, 1972); however, it is now widely agreed that the organization of both the proteins and lipids of the PM are non-uniform (Lingwood and Simons, 2010). In addition, it is well established that the inner and outer leaflets of the PM have distinct protein and lipid compositions. It is thought that, this compositional complexity allows the PM to be organized into regions or microdomains with specialized functions. For example, membranes can be organized into ordered and disordered domains, which recruit specific proteins to facilitate protein-protein interaction (Simons and Ikonen, 1997). In particular, the PM contains saturated and unsaturated lipids. Saturated lipids are hypothesized to preferentially associate with cholesterol in the membrane and form order microdomains separating from the more fluid membranes rich in unsaturated lipids (Armstrong et al., 2012). If a subset of PM proteins displayed a preference to partition into, for example, the ordered lipid domain, microdomains would provide a platform to locally enrich these proteins and increase the propensity for protein-protein interactions.

The current model for PM lateral organization has not considered the potential influence of phospholipid asymmetry, intrinsic to live cells. In particular, although cholesterol is believed to be integral to the formation of membrane domains, the partitioning

of cholesterol between bilayer leaflets is largely overlooked. A recent report, using fluorescent cholesterol analogues, suggested that cholesterol could be mainly in the cytoplasmic leaflet of PM (Mondal et al., 2009). This scenario, however, is in conflict with our current concept of the PM lateral organization, as cholesterol is thought to preferentially associate laterally with sphingolipids in the outer leaflet of the PM (Brown and London, 2000) to promote microdomains. This potential discrepancy, sphingolipids in the outer leaflet and cholesterol in the inner leaflet, was the primary motivation for the work presented in this thesis.

Another intrinsic feature of the mammalian cell PM is the composition of sphingolipids in the outer leaflet. These sphingolipids have primarily very long acyl chains (>C22-24) (**Figure 17**). Interestingly, most our knowledge of microdomains has come from 16:0 and 18:0 SM containing model membranes and the majority of the model membranes are transversely symmetric (Leventis and Silvius, 2001; Veatch and Keller, 2003). We, therefore, aimed to determine if native cholesterol is enriched in the cytoplasmic leaflet of the PM and whether asymmetric 24:0 sphingolipids are functionally unique, compared to 16:0 and 18:0 sphingolipids.

We first developed a protocol to characterize how cholesterol partitions between the leaflets of a bilayer. We then aimed to uncover factors that can alter cholesterol partitioning and identify how these factors would affect PM microdomains. By comparing differences in sphingolipid acyl chain length, we find that membrane asymmetry is critical for the regulating how cholesterol partitions in membrane bilayer.

7.2 – Development of protocols to determine the cholesterol transbilayer distribution

Prior to this thesis, there were not any reliable methods to determine cholesterol in the individual leaflets of a bilayer membrane. Determining the asymmetry of PM phospholipids was, in comparison, quite feasible since flip-flop of phospholipids happens slowly ($T_{1/2}$= hours or days), due to the large hydrophilic head groups (Kornberg and McConnell, 1971). Without significant flip-flop, there are many membrane impermeable probes or catalytic enzymes with high specificity for each major class of phospholipids that can be applied to unilamellar vesicles or live cells (Bretsche, 1972b; Verkleij et al., 1973) to determine the outer leaflet contents. The contents in the inner leaflet can then be deduced from total amounts of dissolved vesicles or erythrocytes. Similar cholesterol analysis, however, is not feasible due to the rapid transbilayer flip-flopping ($T_{1/2}$~ seconds) (Leventis and Silvius, 2001). In principle, if the movement of cholesterol between bilayer leaflets could be prevented, a similar strategy can also be applied. With this in mind, we were looking for conditions where cholesterol flip-flop could be stopped. Considering the action of flip-flop is driven by thermal energy, we hypothesized that lowering the temperature could potentially prevent cholesterol movement between leaflets. As described in Chapter 3, we indeed found that MCD could efficiently extract 50% cholesterol from symmetric LUVs at 0 °C (**Figure 4**), indicating that cholesterol flip-flop was effectively prevented. We then modified the protocol to quantify membranes containing 30 % cholesterol, similar to physiological concentration found in the PM. This modified protocol utilized an exchange strategy, i.e. exchanging ^{3}H-cholesterol from donor LUVs to 100-fold unlabeled acceptor LUVs. This allowed ^{3}H-cholesterol to be completely removed and quantified with no net change of cholesterol (**Figure 6**) to preserve LUV structural integrity. Symmetric LUVs

were indeed only able to exchange 50% cholesterol at 0 °C and 100% at 37 °C when cholesterol flip-flop was active. With this modified protocol, we then quantified cholesterol in each leaflet of human erythrocytes (**Figure 8**). We observed that only 20 % of the PM cholesterol was exchangeable at 0 °C, but 100% at 37 °C (**Figure 8**). This demonstrated that, similar to the study with fluorescent analogues (Mondal et al., 2009), 75-80 % of the cholesterol is in the inner leaflet of the PM in mammalian cells. This represents the first direct evidence that native cholesterol is highly enriched in the cytoplasmic leaflet of the PM.

7.3 – Transversely asymmetric model membranes

To understand why cholesterol is enriched in the cytoplasmic leaflet of the PM, we characterized asymmetric model membranes. Recently, a novel protocol was published to generate asymmetric LUVs (Cheng and London, 2011). For our purposes, the ability to create asymmetric membranes was ideal to explore if phospholipid asymmetry, as seen in native PM, could dictate how cholesterol partitions in a bilayer. By introducing a series of different lipids exclusively into the outer leaflet of asymmetric LUVs, we identified that only 24:0 SM specifically altered the cholesterol partitioning in our experimental system (**Figure 12**). In particular, 24:0 SM, which was exclusively in the outer leaflet of the LUVs, concentrated cholesterol (80 %) in the inner leaflet. The unique effect of 24:0 SM in LUVs was observed with both low and high cholesterol content (**Figure 12 & Figure 14**). 16:0 or 18:0 SM, however, did not affect the cholesterol partitioning in asymmetric LUVs (**Figure 12A & Figure 12B**). This was our first evidence that 24:0 SM is distinct from 16:0 or 18:0 SM in asymmetric membranes. These results are intriguing for at least two reasons: (**1**) Cholesterol is thought so associate laterally, i.e. side-by-side, with sphingolipids; however, 24:0 SM and cholesterol primarily reside in opposing leaflets and (**2**) the fact that 24:0

sphingolipids are the most abundant sphingolipid in mammalian cells (**Figure 17**) suggests the current microdomain concept may not be applicable to mammalian PM. Together, the results highlight major limitations of current model membrane approaches, which widely employ shorter acyl chain (16:0 or 18:0) SM and symmetric membranes. As we show here for the first time, cholesterol-sphingolipid interactions are more complex than previously reported and, importantly, there is a critical functional difference between 24:0 and 16:0 SM in asymmetric membranes. Although additional factors are surely involved in regulating the PM lateral organization, our data should incite greater research activities in understanding phospholipid sub-classes, including acyl chain length and particularly in asymmetric membranes.

7.4 – Very long acyl chain sphingolipids in asymmetric giant unilamellar vesicles and the plasma membrane of live cells

With the knowledge that 80 % of the PM cholesterol is in the inner leaflet (**Figure 8A**) and that sphingolipid acyl chain length can alter cholesterol partitioning (**Figure 12**), we next focussed on how sphingolipid acyl chain length influences microdomains, particularly in asymmetric membranes. Using a similar protocol for asymmetric LUVs, we first generated asymmetric GUVs with either 24:0 or 16:0 SM in the outer leaflet and examined microdomain formation. Here, we again identified a unique effect of 24:0 SM: when introducing 24:0 SM selectively into the outer leaflet of GUVs, the pre-existing membrane domains disappeared (**Figure 15 and Figure 16**). Similarly placed 16:0 SM, however, did not alter the microdomains (**Figure 16A, *a***). Importantly, the abolition of microdomains caused by asymmetric 24:0 SM persisted across a wide range of temperatures (**Figure 16C**) and cholesterol concentrations (**Figure 16D**). Furthermore, if 24:0 SM was present in both

leaflets of the GUVs (symmetric), then microdomains would again form (**Figure 16A, *c***), highlighting the importance of membrane asymmetry. Given that only asymmetric 24:0 SM was able to shift the partitioning of cholesterol into the inner leaflet (**Figure 12**), we believe the disappearance of membrane domains in GUVs is the consequence of cholesterol transbilayer asymmetry.

We next examined if the effect of asymmetric 24:0 SM can be replicated in the PM of live cells. First, we used a shRNA to selectively reduce CerS2 and altered the 16:0/ 24:0 sphingolipid ratio (**Figure 19C and Figure 19D**). Although the 16:0/ 24:0 sphingolipid ratio was only moderately increased, FRAP between control and shCerS2 cells showed significant differences. Expressing shCerS2 slowed the lateral diffusion of known microdomain-associated proteins (**Figure 20 & Table 2**), consistent with enhanced microdomains. We also took a second approach to deplete all sphingolipids from the cells and then resupplied the cells with either 24:0 or 16:0 SM (**Figure 24**) to mimic the asymmetric GUV experiments (**Figure 16**) using live cell PM. We then measured density-dependent FRET between GPI-anchored proteins. GPI-anchored proteins are well established to prefer rigid or L_o domains (Brown and Rose, 1992; Mayor and Riezman, 2004; Zurzolo and Simons, 2016). If the PM contains membrane domains, GPI-anchored proteins would be recruited to these domains and cause an increase in FRET. We indeed found that 16:0 SM increased FRET between CFP- and YFP-GPI-anchored proteins relative to control cells, indicative enhanced membrane microdomains. Cells with 24:0 SM, however, displayed similar FRET as untreated control cells (**Figure 25A**). In addition, cholesterol depletion by saponin returned the density-dependent FRET back to the same level in all treatments, consistent with the dispersal of microdomains (**Figure 25B**) (Raghupathy et al., 2015). Thus, altering SM acyl

chain length in asymmetric unilamellar vesicles and in the PM of live cells produced the similar results. We established that 24:0 sphingolipids are functionally distinct from shorter acyl chain lipids, such as 16:0 or 18:0 sphingolipids in an asymmetric membrane.

7.5 – Domain size in model membranes and the live cell plasma membrane

An unresolved question in PM studies is that visible microdomains are conspicuously absent from the PM of live cells. PM domains are only detected in live cells by advanced microscopy techniques such as FRET, fluorescence correlation spectroscopy or super resolution microscopy (Eggeling, 2015; Lasserre et al., 2008; Rao and Mayor, 2005). However, model membranes such as GUVs and GPMVs readily form visible microdomains (Juhasz et al., 2010; Levental et al., 2009). This discrepancy between the detection of sub-optical nanodomains in the PM and visible microdomains in model membranes is not well understood. Although model membranes can closely mimic the PM, several factors could prevent the enlargement of small, dynamic assemblies into large-scale domains. For example, domains were recently shown to be suppressed in model membranes by interactions with an artificial cytoskeleton (Arumugam et al., 2015). Although GPMVs are derived from live cell PM, which have similar lipid/protein compositions as the unperturbed PM, these vesicles are devoid of actin. The presence of an intact PM cytoskeleton could interfere and generate barriers for large-scale domains.

Another important distinction between the PM and model membranes is that live cells are metabolically active and maintained in a state of disequilibrium. Isolating GPMVs from cells or producing GUVs, however, allows the membrane to equilibrate and settle into the lowest energy state, which could potentially be necessary for large-scale domains.

Importantly, it has been shown that GPMVs lose phospholipid transbilayer asymmetry after isolation (Keller et al., 2009). Therefore, our data would suggest that a disruption in the PM asymmetry would promote sub-micron membrane domains by altering cholesterol asymmetry in the GPMVs. Although other factors are likely involved, we speculate that PM asymmetry, particularly the enrichment of cholesterol in the cytoplasmic leaflet and 24:0 sphingolipids in the outer leaflet, is a major factor governing the formation membrane domains.

7.6 – Membrane domain theory revisited

Two major aspects of the work presented in this thesis challenge the status quo definition of microdomains in live cells. First, we find that cholesterol is primarily in the inner leaflet of the PM. Second, since sphingolipids reside in the outer leaflet, PM cholesterol does not interact laterally with the majority of sphingolipids (24:0 SM) in mammalian cells. How this inner leaflet enrichment of cholesterol fits within the current lipid raft hypothesis has yet to be established. Our data show that when cholesterol is concentrated into the inner leaflet, membrane domains are supressed. It is currently unknown if this domain inhibition is indeed a result of too much cholesterol in the inner leaflet, too little cholesterol in the outer leaflet, or perhaps, a combination of both. The GUV results show that, in symmetric membranes, a low concentration (< 10 %) of cholesterol is sufficient to form microdomains; however, cholesterol content above 40 % prevents large-scale domains (**Figure 14B**). If the data generated from symmetric GUVs are translatable to the PM, this implies that cholesterol asymmetry may inhibit domains due to elevated inner leaflet cholesterol, rather than depletion of outer leaflet cholesterol. It is possible that concentrating cholesterol into the inner leaflet makes this leaflet excessively rigid to the

point where membrane domains are not supported (> 40 % cholesterol), similar to GUVs (**Figure 14B**). Concentrating cholesterol in the inner leaflet could keep membrane microdomains suppressed and allow for more fine-tuned and dynamic microdomain assembly.

The second major discovery is the that primary sphingolipid species in most cell types, 24:0 SM, (Park and Park, 2015) concentrates cholesterol in the opposing inner leaflet, rather than interacting laterally in the outer leaflet. This conclusion could have significant implications for general lipid raft hypothesis. Our results show that in symmetric membranes, or asymmetric membranes lacking VLAC SM, cholesterol is evenly distributed; however, the presence VLAC SM in the outer leaflet caused cholesterol asymmetry (**Figure 5 & Figure 12).** Under the current definition of membrane domains, cholesterol is thought to interact with sphingolipids to create ordered regions in the membrane. Although cholesterol has been shown to have high affinity for sphingomyelin, these data were generated with symmetric membranes, which may not be relevant to more complex asymmetric membranes (Leventis and Silvius, 2001; Ramstedt and Slotte, 1999). The affinity of cholesterol to different species of sphingolipids in an asymmetric membrane has yet to be determined. The results of this thesis emphasize that sphingolipids should not be generalized into classes based solely on the head group constituent. When combining all sphingolipids indiscriminately into one group, potentially important findings could be overlooked.

7.7 – Implications for health and disease

As described in chapter 6, aberrant changes in the distribution of sphingolipid acyl chain lengths have shown to have pathological consequences (Couttas et al., 2016; Fan et al.,

2013; Fan et al., 2015). The sphingolipid acyl chain lengths are primarily determined by the relative expression of the different ELOVL and CerS proteins. If ELOVL protein expression is altered, acyl chain substrate availability will similarly be altered and CerS proteins would not function normally. Likewise, if the balance of different CerS proteins expressed becomes disrupted, then regardless of the fatty acid chains that are produced by the different ELOVL proteins, the distribution of sphingolipids would also be perturbed. Although this was not tested directly, our data suggests that pathologies associated with an altered ratio of 16:0/ 24:0 sphingolipid could be, at least partially, attributed to changes in the partitioning of cholesterol or microdomains in the PM.

In addition, the balance between 16:0 and 24:0 sphingolipids is also implicated in several, seemingly unrelated diseases (Park and Park, 2015). Studies *in vitro* and *in vivo* have found that reduced CerS2 expression levels lower VLAC sphingolipids, which leads to insulin resistance, cancer and neurodegeneration (Couttas et al., 2016; Fan et al., 2013; Raichur et al., 2014). In humans, changes in the CerS protein expression profile have been identified to be associated with susceptibility to obesity, as well as, axon demyelination, leading to the development of Alzheimer's disease. Most commonly, VLAC sphingolipids show a trend for having protective effect against disease, whereas, excessive 16:0 sphingolipids can be pathological (Turpin et al., 2014). Since the effect of sphingolipid acyl chain length has not been thoroughly investigated, presumably other disease states could also be influenced by changes in ELOVL or CerS protein expression. As the essential role of sphingolipid acyl chain length becomes more widely acknowledged, additional studies will be required to better understand if there is a causative link associated with acyl chain length and other diseases.

From this thesis work, we speculate that changing ELOVL or CerS protein expression would alter the sphingolipid content in the PM and, therefore, lead to changes in lateral organization of the PM. This could alter lipid-protein and protein-protein interactions. It should also be noted, although outside the scope of this work, that sphingolipids have other functions in the cell, other than in the PM. For example, ceramides are in low abundance, however, metabolism of this class of sphingolipids can dynamically regulate important second messenger signalling molecules, such as ceramide-1-phosphate or sphingosine-1-phosphate (Gomez-Munoz, 2004; Spiegel and Kolesnick, 2002). Changes in sphingolipid acyl chain length could potentially alter the second messenger function. Furthermore, ELOVL and/or CerS proteins could, in principle, have secondary enzymatic functions in the cell that regulate other pathways independently of sphingolipid acyl chains. Although we identified that sphingolipid acyl chain length governs PM organization, the full spectrum of effects, in the context of human disease, has yet to be elucidated.

7.8 – Conclusion

The primary objective of this thesis was to characterize the cholesterol transbilayer distribution in the PM of mammalian cells, with the intention of understanding how cholesterol asymmetry influences the lateral organization of the PM. We developed a novel technique capable of analyzing cholesterol in each leaflet of a bilayer. Using this technique, we conclude that cholesterol is concentrated in the inner leaflet of the mammalian cell PM. We further identified a mechanism underlying this distribution. We demonstrated that 24:0 sphingolipid asymmetry is critical for the distribution of cholesterol between leaflets. With this discovery, we reveal that 24:0 sphingolipids interact differently with cholesterol than SM with shorter acyl chains. Since 24:0 sphingolipids are the dominant species in mammalian

cells, we suggest that the classical model of how cholesterol interacts with SM is rather limited and does not apply to the plasma membrane of live mammalian cells. We also conclude that the live cell PM has limited capacity to form microdomains, due to high levels of VLAC sphingolipids exclusively in the outer leaflet, which leads to cholesterol enrichment in the cytoplasm leaflet. When cholesterol asymmetry is reduced, lost or locally manipulated, membrane microdomains may form dynamically and locally. This could serve as a mechanism to regulate lipid-protein and protein-protein interactions in the PM.

Several pathologies have been identified that are caused by or associated with a disruption in sphingolipid acyl chain length (Couttas et al., 2016; Fan et al., 2015; Imgrund et al., 2009; Raichur et al., 2014; Turpin et al., 2014). Currently, it is not known how the principles illustrated in this thesis relate to whole organism disease progression. We speculate that shifting the 16:0/ 24:0 sphingolipid balance would alter many membrane processes at the cellular level that would manifest into larger scale disturbances. A direct link between PM organization and sphingolipid acyl chain pathologies, however, has yet to be established. Future work should focus on how changes in sphingolipid acyl chain length affect downstream signalling pathways, as well as, other established microdomain-regulated processes, such as intracellular membrane trafficking. Nevertheless, this work establishes a broad framework to better understand PM function and highlights the importance of maintaining membrane phospholipid asymmetry. At the very least, we now realize another layer of complexity in the organization of the PM and look forward to seeing if the results presented in this thesis could be the basis for future research and lead to a better understanding human health and disease.

References

Anderson, R.G.W., Brown, M.S., and Goldstein, J.L. (1977). Role of the coated endocytic vesicle in the uptake of receptor-bound low density lipoprotein in human fibroblasts. Cell *10*, 351-364.

Angelova, M.I., and Dimitrov, D.S. (1986). LIPOSOME ELECTROFORMATION. Faraday Discussions *81*, 303-+.

Angelova, M.I., Soleau, S., Meleard, P., Faucon, J.F., and Bothorel, P. (1992). PREPARATION OF GIANT VESICLES BY EXTERNAL AC ELECTRIC-FIELDS - KINETICS AND APPLICATIONS. Trends in Colloid and Interface Science Vi *89*, 127-131.

Ano, Y., Kutsukake, T., Hoshi, A., Yoshida, A., and Nakayama, H. (2015). Identification of a Novel Dehydroergosterol Enhancing Microglial Anti-Inflammatory Activity in a Dairy Product Fermented with Penicillium candidum. Plos One *10*, 16.

Armstrong, C.L., Barrett, M.A., Hiess, A., Salditt, T., Katsaras, J., Shi, A.C., and Rheinstädter, M.C. (2012). Effect of cholesterol on the lateral nanoscale dynamics of fluid membranes. European Biophysics Journal, 1-13.

Arumugam, S., Petrov, E.P., and Schwille, P. (2015). Cytoskeletal Pinning Controls Phase Separation in Multicomponent Lipid Membranes. Biophysical Journal *108*, 1104-1113.

Bagatolli, L.A., and Gratton, E. (1999). Two-photon fluorescence microscopy observation of shape changes at the phase transition in phospholipid giant unilamellar vesicles. Biophysical Journal *77*, 2090-2101.

Bagatolli, L.A., and Gratton, E. (2000). Two photon fluorescence microscopy of coexisting lipid domains in giant unilamellar vesicles of binary phospholipid mixtures. Biophysical Journal *78*, 290-305.

Baker, C.H., Matsuda, S.P.T., Liu, D.R., and Corey, E.J. (1995). MOLECULAR-CLONING OF THE HUMAN GENE ENCODING LANOSTEROL SYNTHASE FROM A LIVER CDNA LIBRARY. Biochemical and Biophysical Research Communications *213*, 154-160.

Baumgart, T., Hammond, A.T., Sengupta, P., Hess, S.T., Holowka, D.A., Baird, B.A., and Webb, W.W. (2007a). Large-scale fluid/fluid phase separation of proteins and lipids in giant plasma membrane vesicles. Proceedings of the National Academy of Sciences of the United States of America *104*, 3165-3170.

Baumgart, T., Hunt, G., Farkas, E.R., Webb, W.W., and Feigenson, G.W. (2007b). Fluorescence probe partitioning between Lo/Ld phases in lipid membranes. Biochimica et Biophysica Acta - Biomembranes *1768*, 2182-2194.

Bennett, W.F.D., MacCallum, J.L., Hinner, M.J., Marrink, S.J., and Tieleman, D.P. (2009). Molecular view of cholesterol flip-flop and chemical potential in different membrane environments. Journal of the American Chemical Society *131*, 12714-12720.

Bjorkhem, I., and Meaney, S. (2004). Brain cholesterol: Long secret life behind a barrier. Arteriosclerosis Thrombosis and Vascular Biology *24*, 806-815.

Bjorkqvist, Y.J.E., Brewer, J., Bagatolli, L.A., Slotte, J.P., and Westerlund, B. (2009). Thermotropic behavior and lateral distribution of very long chain sphingolipids. Biochimica Et Biophysica Acta-Biomembranes *1788*, 1310-1320.

Blau, L., and Bittman, R. (1978). CHOLESTEROL DISTRIBUTION BETWEEN 2 HALVES OF LIPID BILAYER OF HUMAN ERYTHROCYTE GHOST MEMBRANES. Journal of Biological Chemistry *253*, 8366-8368.

Bligh, E.G., and Dyer, W.J. (1959). A rapid method of total lipid extraction and purification. Canadian journal of biochemistry and physiology *37*, 911-917.

Boegheim Jr, J.P.J., Van Linde, M., Op Den Kamp, J.A.F., and Roelofsen, B. (1983). The sphingomyelin pools in the outer and inner layer of the human erythrocyte membrane are composed of different molecular species. Biochimica et Biophysica Acta - Biomembranes *735*, 438-442.

Breslow, D.K. (2013). Sphingolipid Homeostasis in the Endoplasmic Reticulum and Beyond. Cold Spring Harbor Perspectives in Biology *5*, 16.

Bretscher, M.S. (1972a). ASYMMETRICAL LIPID BILAYER STRUCTURE FOR BIOLOGICAL-MEMBRANES. Nature-New Biology *236*, 11-&.

Bretscher, M.S. (1972b). PHOSPHATIDYL-ETHANOLAMINE - DIFFERENTIAL LABELING IN INTACT CELLS AND CELL GHOSTS OF HUMAN ERYTHROCYTES BY A MEMBRANE-IMPERMEABLE REAGENT. Journal of Molecular Biology *71*, 523-&.

Brown, A.J., Sun, L.P., Feramisco, J.D., Brown, M.S., and Goldstein, J.L. (2002). Cholesterol addition to ER membranes alters conformation of SCAP, the SREBP escort protein that regulates cholesterol metabolism. Molecular Cell *10*, 237-245.

Brown, D.A., and London, E. (2000). Structure and function of sphingolipid- and cholesterol-rich membrane rafts. Journal of Biological Chemistry *275*, 17221-17224.

Brown, D.A., and Rose, J.K. (1992). SORTING OF GPI-ANCHORED PROTEINS TO GLYCOLIPID-ENRICHED MEMBRANE SUBDOMAINS DURING TRANSPORT TO THE APICAL CELL-SURFACE. Cell *68*, 533-544.

Brown, M.S., Goldstein, J.L., Krieger, M., Ho, Y.K., and Anderson, R.G.W. (1979). REVERSIBLE ACCUMULATION OF CHOLESTERYL ESTERS IN MACROPHAGES INCUBATED WITH ACETYLATED LIPOPROTEINS. Journal of Cell Biology *82*, 597-613.

Camont, L., Chapman, J., and Kontush, A. (2011). Functionality of HDL particles: Heterogeneity and relationships to cardiovascular disease. Archives of Cardiovascular Diseases Supplements *3*, 258-266.

Campbell, J.M.H. (1925). Critical review - Cholesterol in health and disease. Quarterly Journal of Medicine *18*, 393-422.

Chazotte, B. (2011). Labeling the plasma membrane with TMA-DPH. Cold Spring Harbor Protocols *6*.

Chen, W.L., Chen, G.X., Head, D.L., Mangelsdorf, D.J., and Russell, D.W. (2007). Enzymatic reduction of oxysterols impairs LXR signaling in cultured cells and the livers of mice. Cell Metabolism *5*, 73-79.

Chen, Y.F., Liu, Y., Sullards, M.C., and Merrill, A.H. (2010). An Introduction to Sphingolipid Metabolism and Analysis by New Technologies. Neuromolecular Medicine *12*, 306-319.

Cheng, D., Espenshade, P.J., Slaughter, C.A., Jaen, J.C., Brown, M.S., and Goldstein, J.L. (1999). Secreted site-1 protease cleaves peptides corresponding to luminal loop of sterol regulatory element-binding proteins. Journal of Biological Chemistry *274*, 22805-22812.

Cheng, H.T., and London, E. (2011). Preparation and properties of asymmetric large unilamellar vesicles: Interleaflet coupling in asymmetric vesicles is dependent on temperature but not curvature. Biophysical Journal *100*, 2671-2678.

Cheng, H.T., Megha, and London, E. (2009). Preparation and Properties of Asymmetric Vesicles That Mimic Cell Membranes EFFECT UPON LIPID RAFT FORMATION AND TRANSMEMBRANE HELIX ORIENTATION. Journal of Biological Chemistry *284*, 6079-6092.

Chiantia, S., Klymchenko, A.S., and London, E. (2012). A novel leaflet-selective fluorescence labeling technique reveals differences between inner and outer leaflets at high bilayer curvature. Biochimica Et Biophysica Acta-Biomembranes *1818*, 1284-1290.

Chiantia, S., and London, E. (2012). Acyl Chain Length and Saturation Modulate Interleaflet Coupling in Asymmetric Bilayers: Effects on Dynamics and Structural Order. Biophysical Journal *103*, 2311-2319.

Chiantia, S., Schwille, P., Klymchenko, A.S., and London, E. (2011). Asymmetric GUVs prepared by MβCD-mediated lipid exchange: An FCS study. Biophysical Journal *100*, L01-L03.

Christian, A.E., Byun, H.S., Zhong, N., Wanunu, M., Marti, T., Fürer, A., Diederich, F., Bittman, R., and Rothblat, G.H. (1999). Comparison of the capacity of β-cyclodextrin derivatives and cyclophanes to shuttle cholesterol between cells and serum lipoproteins. Journal of Lipid Research *40*, 1475-1482.

Clark, B.J. (2012). The mammalian START domain protein family in lipid transport in health and disease. Journal of Endocrinology *212*, 257-275.

Clark, B.J., Wells, J., King, S.R., and Stocco, D.M. (1994). THE PURIFICATION, CLONING, AND EXPRESSION OF A NOVEL LUTEINIZING HORMONE-INDUCED MITOCHONDRIAL PROTEIN IN MA-10 MOUSE LEYDIG TUMOR-CELLS - CHARACTERIZATION OF THE STEROIDOGENIC ACUTE REGULATORY PROTEIN (STAR). Journal of Biological Chemistry *269*, 28314-28322.

Clinkenbeard, K.D., Sugiyama, T., Reed, W.D., and Lane, M.D. (1975). CYTOPLASMIC 3-HYDROXY-3-METHYLGLUTARYL COENZYME A SYNTHASE FROM LIVER - PURIFICATION, PROPERTIES, AND ROLE IN CHOLESTEROL-SYNTHESIS. Journal of Biological Chemistry *250*, 3124-3135.

Cooper, R.A. (1978). INFLUENCE OF INCREASED MEMBRANE CHOLESTEROL ON MEMBRANE FLUIDITY AND CELL-FUNCTION IN HUMAN RED BLOOD-CELLS. Journal of Supramolecular Structure *8*, 413-430.

Costet, P., Luo, Y., Wang, N., and Tall, A.R. (2000). Sterol-dependent transactivation of the ABC1 promoter by the liver X receptor/retinoid X receptor. Journal of Biological Chemistry *275*, 28240-28245.

Couttas, T.A., Kain, N., Suchowerska, A.K., Quek, L.E., Turner, N., Fath, T., Garner, B., and Don, A.S. (2016). Loss of ceramide synthase 2 activity, necessary for myelin biosynthesis, precedes tau pathology in the cortical pathogenesis of Alzheimer's disease. Neurobiology of Aging *43*, 89-100.

Crane, J.M., and Tamm, L.K. (2004). Role of cholesterol in the formation and nature of lipid rafts in planar and spherical model membranes. Biophysical Journal *86*, 2965-2979.

Dean, K.M., Roudot, P., Reis, C.R., Welf, E.S., Mettlen, M., and Fiolka, R. (2016). Diagonally Scanned Light-Sheet Microscopy for Fast Volumetric Imaging of Adherent Cells. Biophysical Journal *110*, 1456-1465.

DeBose-Boyd, R.A. (2008). Feedback regulation of cholesterol synthesis: sterol-accelerated ubiquitination and degradation of HMG CoA reductase. Cell Research *18*, 609-619.

DeBose-Boyd, R.A., Brown, M.S., Li, W.P., Nohturfft, A., Goldstein, J.L., and Espenshade, P.J. (1999). Transport-dependent proteolysis of SREBP: Relocation of Site-1 protease from Golgi to ER obviates the need for SREBP transport to Golgi. Cell *99*, 703-712.

Dekruijff, B., Cullis, P.R., and Verkleij, A.J. (1980). NON-BILAYER LIPID STRUCTURES IN MODEL AND BIOLOGICAL-MEMBRANES. Trends in Biochemical Sciences *5*, 79-81.

Demus, H. (1973). SUBCELLULAR FRACTIONATION OF HUMAN LYMPHOCYTES - ISOLATION OF 2 PLASMA-MEMBRANE FRACTIONS AND COMPARISON OF

PROTEIN COMPONENTS OF VARIOUS LYMPHOCYTIC ORGANELLES. Biochimica Et Biophysica Acta *291*, 93-106.

Deng, Y.Q., Rivera-Molina, F.E., Toomre, D.K., and Burd, C.G. (2016). Sphingomyelin is sorted at the trans Golgi network into a distinct class of secretory vesicle. Proceedings of the National Academy of Sciences of the United States of America *113*, 6677-6682.

Devaux, P.F., and Morris, R. (2004). Transmembrane asymmetry and lateral domains in biological membranes. Traffic *5*, 241-246.

Devaux, P.F., and Zachowski, A. (1994). Maintenance and consequences of membrane phospholipid asymmetry. Chemistry and Physics of Lipids *73*, 107-120.

Diekmann, Y., and Pereira-Leal, J.B. (2013). Evolution of intracellular compartmentalization. Biochemical Journal *449*, 319-331.

Dietrich, C., Bagatolli, L.A., Volovyk, Z.N., Thompson, N.L., Levi, M., Jacobson, K., and Gratton, E. (2001). Lipid rafts reconstituted in model membranes. Biophysical Journal *80*, 1417-1428.

Dimitrov, D.S., and Angelova, M.I. (1988). LIPID SWELLING AND LIPOSOME FORMATION MEDIATED BY ELECTRIC-FIELDS. Bioelectrochemistry and Bioenergetics *19*, 323-336.

Doree, C., and Gardner, J.A. (1908). The origin and destiny of cholesterol in the animal organism Part I - On the so-called hippocoprosterol. Proceedings of the Royal Society of London Series B-Containing Papers of a Biological Character *80*, 212-226.

Draberova, L., and Draber, P. (1993). THY-1 GLYCOPROTEIN AND SRC-LIKE PROTEIN-TYROSINE KINASE P53/P56(LYN) ARE ASSOCIATED IN LARGE DETERGENT-RESISTANT COMPLEXES IN RAT BASOPHILIC LEUKEMIA-CELLS. Proceedings of the National Academy of Sciences of the United States of America *90*, 3611-3615.

Egelhaaf, S.U., Wehrli, E., Muller, M., Adrian, M., and Schurtenberger, P. (1996). Determination of the size distribution of lecithin liposomes: A comparative study using freeze fracture, cryoelectron microscopy and dynamic light scattering. Journal of Microscopy-Oxford *184*, 214-228.

Eggeling, C. (2015). Super-resolution optical microscopy of lipid plasma membrane dynamics. In Membrane Nanodomains, I. Parmryd, ed. (London: Portland Press Ltd), pp. 69-80.

Eggeling, C., Ringemann, C., Medda, R., Schwarzmann, G., Sandhoff, K., Polyakova, S., Belov, V.N., Hein, B., Von Middendorff, C., Schönle, A.*, et al.* (2009). Direct observation of the nanoscale dynamics of membrane lipids in a living cell. Nature *457*, 1159-1162.

Eisenberg, S., Shvartsman, D.E., Ehrlich, M., and Henis, Y.I. (2006). Clustering of raft-associated proteins in the external membrane leaflet modulates internal leaflet H-Ras diffusion and signaling. Molecular and Cellular Biology *26*, 7190-7200.

Fahy, E., Subramaniam, S., Brown, H.A., Glass, C.K., Merrill, A.H., Murphy, R.C., Raetz, C.R.H., Russell, D.W., Seyama, Y., Shaw, W.*, et al.* (2005). A comprehensive classification system for lipids. Journal of Lipid Research *46*, 839-861.

Fan, S., Niu, Y., Tan, N., Wu, Z., Wang, Y., You, H., Ke, R., Song, J., Shen, Q., Wang, W.*, et al.* (2013). LASS2 enhances chemosensitivity of breast cancer by counteracting acidic tumor microenvironment through inhibiting activity of V-ATPase proton pump. Oncogene *32*, 1682-1690.

Fan, S.H., Wang, Y.Y., Lu, J., Zheng, Y.L., Wu, D.M., Zhang, Z.F., Shan, Q., Hu, B., Li, M.Q., and Cheng, W. (2015). CERS2 Suppresses Tumor Cell Invasion and is Associated with Decreased V-ATPase and MMP-2/MMP-9 Activities in Breast Cancer. Journal of Cellular Biochemistry *116*, 502-513.

Field, F.J., Born, E., Murthy, S., and Mathur, S.N. (1998). Transport of cholesterol from the endoplasmic reticulum to the plasma membrane is constitutive in CaCo-2 cells and differs from the transport of plasma membrane cholesterol to the endoplasmic reticulum. Journal of Lipid Research *39*, 333-343.

Fisher, K.A. (1976). ANALYSIS OF MEMBRANE HALVES - CHOLESTEROL. Proceedings of the National Academy of Sciences of the United States of America *73*, 173-177.

Fung, B.K.K., and Stryer, L. (1978). SURFACE DENSITY DETERMINATION IN MEMBRANES BY FLUORESCENCE ENERGY-TRANSFER. Biochemistry *17*, 5241-5248.

Garbarino, J., Pan, M.H., Chin, H.F., Lund, F.W., Maxfield, F.R., and Breslow, J.L. (2012). STARD4 knockdown in HepG2 cells disrupts cholesterol trafficking associated with the plasma membrane, ER, and ERC. Journal of Lipid Research *53*, 2716-2725.

Gault, C.R., Obeid, L.M., and Hannun, Y.A. (2010). An Overview of Sphingolipid Metabolism: From Synthesis to Breakdown. In Sphingolipids as Signaling and Regulatory Molecules, C. Chalfant, and M. DelPoeta, eds. (Berlin: Springer-Verlag Berlin), pp. 1-23.

Gerl, M.J., Sampaio, J.L., Urban, S., Kalvodova, L., Verbavatz, J.M., Binnington, B., Lindemann, D., Lingwood, C.A., Shevchenko, A., Schroeder, C.*, et al.* (2012). Quantitative analysis of the lipidomes of the influenza virus envelope and MDCK cell apical membrane. Journal of Cell Biology *196*, 213-221.

Giang, H., and Schick, M. (2014). How cholesterol could be drawn to the cytoplasmic leaf of the plasma membrane by phosphatidylethanolamine. Biophysical Journal *107*, 2337-2344.

Glaser, K.B., Mobilio, D., Chang, J.Y., and Senko, N. (1993). PHOSPHOLIPASE-A2 ENZYMES - REGULATION AND INHIBITION. Trends in Pharmacological Sciences *14*, 92-98.

Gliss, C., Clausen-Schaumann, H., Gunther, R., Odenbach, S., Randl, O., and Bayerl, T.M. (1998). Direct detection of domains in phospholipid bilayers by grazing incidence diffraction of neutrons and atomic force microscopy. Biophysical Journal *74*, 2443-2450.

Gomez-Munoz, A. (2004). Ceramide-1-phosphate: a novel regulator of cell activation. Febs Letters *562*, 5-10.

Grammatikos, G., Dietz, J., Ferreiros, N., Koch, A., Dultz, G., Bon, D., Karakasiliotis, I., Lutz, T., Knecht, G., Gute, P*., et al.* (2016). Persistence of HCV in Acutely-Infected Patients Depletes C24-Ceramide and Upregulates Sphingosine and Sphinganine Serum Levels. International Journal of Molecular Sciences *17*, 12.

Gudheti, M.V., Curthoys, N.M., Gould, T.J., Kim, D., Gunewardene, M.S., Gabor, K.A., Gosse, J.A., Kim, C.H., Zimmerberg, J., and Hess, S.T. (2013). Actin Mediates the Nanoscale Membrane Organization of the Clustered Membrane Protein Influenza Hemagglutinin. Biophysical Journal *104*, 2182-2192.

Hagmann, J., and Fishman, P.H. (1982). DETERGENT EXTRACTION OF CHOLERA-TOXIN AND GANGLIOSIDES FROM CULTURED-CELLS AND ISOLATED MEMBRANES. Biochimica Et Biophysica Acta *720*, 181-187.

Hanada, K., Kumagai, K., Yasuda, S., Miura, Y., Kawano, M., Fukasawa, M., and Nishijima, M. (2003). Molecular machinery for non-vesicular trafficking of ceramide. Nature *426*, 803-809.

Hansson, G.K., and Hermansson, A. (2011). The immune system in atherosclerosis. Nature Immunology *12*, 204-212.

Hartmann, D., Lucks, J., Fuchs, S., Schiffmann, S., Schreiber, Y., Ferreiros, N., Merkens, J., Marschalek, R., Geisslinger, G., and Grosch, S. (2012). Long chain ceramides and very long chain ceramides have opposite effects on human breast and colon cancer cell growth. International Journal of Biochemistry & Cell Biology *44*, 620-628.

Havel, R.J., Eder, H.A., and Bragdon, J.H. (1955). DISTRIBUTION AND CHEMICAL COMPOSITION OF ULTRACENTRIFUGALLY SEPARATED LIPOPROTEINS IN HUMAN SERUM. Journal of Clinical Investigation *34*, 1345-1353.

Helle, S.C.J., Kanfer, G., Kolar, K., Lang, A., Michel, A.H., and Kornmann, B. (2013). Organization and function of membrane contact sites. Biochimica Et Biophysica Acta-Molecular Cell Research *1833*, 2526-2541.

Hiramoto-Yamaki, N., Tanaka, K.A.K., Suzuki, K.G.N., Hirosawa, K.M., Miyahara, M.S.H., Kalay, Z., Tanaka, K., Kasai, R.S., Kusumi, A., and Fujiwara, T.K. (2014). Ultrafast

Diffusion of a Fluorescent Cholesterol Analog in Compartmentalized Plasma Membranes. Traffic *15*, 583-612.

Hoessli, D., and Runggerbrandle, E. (1985). ASSOCIATION OF SPECIFIC CELL-SURFACE GLYCOPROTEINS WITH A TRITON X-100-RESISTANT COMPLEX OF PLASMA-MEMBRANE PROTEINS ISOLATED FROM T-LYMPHOMA CELLS (P1798). Experimental Cell Research *156*, 239-250.

Hoessli, D.C., and Runggerbrandle, E. (1983). ISOLATION OF PLASMA-MEMBRANE DOMAINS FROM MURINE LYMPHOCYTES-T. Proceedings of the National Academy of Sciences of the United States of America-Biological Sciences *80*, 439-443.

Holtta-Vuori, M., Uronen, R.L., Repakova, J., Salonen, E., Vattulainen, I., Panula, P., Li, Z.G., Bittman, R., and Ikonen, E. (2008). BODIPY-Cholesterol: A New Tool to Visualize Sterol Trafficking in Living Cells and Organisms. Traffic *9*, 1839-1849.

Huang, Z., and London, E. (2013). Effect of Cyclodextrin and Membrane Lipid Structure upon Cyclodextrin-Lipid Interaction. Langmuir *29*, 14631-14638.

Hugueney, P., and Camara, B. (1990). PURIFICATION AND CHARACTERIZATION OF FARNESYL PYROPHOSPHATE SYNTHASE FROM CAPSICUM-ANNUUM. Febs Letters *273*, 235-238.

Hussain, M.M. (2014). Intestinal lipid absorption and lipoprotein formation. Current Opinion in Lipidology *25*, 200-206.

Iaea, D.B., and Maxfield, F.R. (2015). Cholesterol trafficking and distribution. In Membrane Nanodomains, I. Parmryd, ed. (London: Portland Press Ltd), pp. 43-55.

Ikonen, E. (2008). Cellular cholesterol trafficking and compartmentalization. Nature Reviews Molecular Cell Biology *9*, 125-138.

Im, Y.J., Raychaudhuri, S., Prinz, W.A., and Hurley, J.H. (2005). Structural mechanism for sterol sensing and transport by OSBP-related proteins. Nature *437*, 154-158.

Imgrund, S., Hartmann, D., Farwanah, H., Eckhardt, M., Sandhoff, R., Degen, J., Gieselmann, V., Sandhoff, K., and Willecke, K. (2009). Adult Ceramide Synthase 2 (CERS2)-deficient Mice Exhibit Myelin Sheath Defects, Cerebellar Degeneration, and Hepatocarcinomas. Journal of Biological Chemistry *284*, 33549-33560.

Israelachvili, J.N., Mitchell, D.J., and Ninham, B.W. (1977). THEORY OF SELF-ASSEMBLY OF LIPID BILAYERS AND VESICLES. Biochimica Et Biophysica Acta *470*, 185-201.

Iwabuchi, K., Nakayama, H., Iwahara, C., and Takamori, K. (2010). Significance of glycosphingolipid fatty acid chain length on membrane microdomain-mediated signal transduction. Febs Letters *584*, 1642-1652.

Jakobsson, A., Westerberg, R., and Jacobsson, A. (2006). Fatty acid elongases in mammals: Their regulation and roles in metabolism. Progress in Lipid Research *45*, 237-249.

Ji, P., Jayapal, S.R., and Lodish, H.F. (2008). Enucleation of cultured mouse fetal erythroblasts requires Rac GTPases and mDia2. Nature Cell Biology *10*, 314-U339.

Juhasz, J., Davis, J.H., and Sharom, F.J. (2010). Fluorescent probe partitioning in giant unilamellar vesicles of 'lipid raft' mixtures. Biochemical Journal *430*, 415-423.

Kabayama, K., Sato, T., Saito, K., Loberto, N., Prinetti, A., Sonnino, S., Kinjo, M., Igarashi, Y., and Inokuchi, J.I. (2007). Dissociation of the insulin receptor and caveolin-1 complex by ganglioside GM3 in the state of insulin resistance. Proceedings of the National Academy of Sciences of the United States of America *104*, 13678-13683.

Kabouridis, P.S., Janzen, J., Magee, A.L., and Ley, S.C. (2000). Cholesterol depletion disrupts lipid rafts and modulates the activity of multiple signaling pathways in T lymphocytes. European Journal of Immunology *30*, 954-963.

Kahlenberg, A., Walker, C., and Rohrlick, R. (1974). Evidence for an asymmetric distribution of phospholipids in the human erythrocyte membrane. Canadian Journal of Biochemistry *52*, 803-806.

Keller, H., Lorizate, M., and Schwille, P. (2009). PI(4,5)P2 Degradation Promotes the Formation of Cytoskeleton-Free Model Membrane Systems. ChemPhysChem *10*, 2805-2812.

Kenworthy, A.K. (2007). Fluorescence recovery after photobleaching studies of lipid rafts. In Methods in Molecular Biology, pp. 179-192.

Kenworthy, A.K., and Edidin, M. (1998). Distribution of a glycosylphosphatidylinositol-anchored protein at the apical surface of MDCK cells examined at a resolution of < 100 angstrom using imaging fluorescence resonance energy transfer. Journal of Cell Biology *142*, 69-84.

Kenworthy, A.K., Nichols, B.J., Remmert, C.L., Hendrix, G.M., Kumar, M., Zimmerberg, J., and Lippincott-Schwartz, J. (2004). Dynamics of putative raft-associated proteins at the cell surface. Journal of Cell Biology *165*, 735-746.

Kilsdonk, E.P.C., Yancey, P.G., Stoudt, G.W., Bangerter, F.W., Johnson, W.J., Phillips, M.C., and Rothblat, G.H. (1995). Cellular cholesterol efflux mediated by cyclodextrins. Journal of Biological Chemistry *270*, 17250-17256.

Kinosian, B., Glick, H., and Garland, G. (1994). CHOLESTEROL AND CORONARY HEART-DISEASE - PREDICTING RISKS BY LEVELS AND RATIOS. Annals of Internal Medicine *121*, 641-647.

Kornberg, R.D., and McConnell, H.M. (1971). INSIDE-OUTSIDE TRANSITIONS OF PHOSPHOLIPIDS IN VESICLE MEMBRANES. Biochemistry *10*, 1111-+.

Kornhuber, J., Rhein, C., Muller, C.P., and Muhle, C. (2015). Secretory sphingomyelinase in health and disease. Biological Chemistry *396*, 707-736.

Kozarsky, K.F., Donahee, M.H., Rigotti, A., Iqbal, S.N., Edelman, E.R., and Krieger, M. (1997). Overexpression of the HDL receptor SR-BI alters plasma HDL and bile cholesterol levels. Nature *387*, 414-417.

Kuhry, J.G., Fonteneau, P., Duportail, G., Maechling, C., and Laustriat, G. (1983). TMA-DPH - A SUITABLE FLUORESCENCE POLARIZATION PROBE FOR SPECIFIC PLASMA-MEMBRANE FLUIDITY STUDIES IN INTACT LIVING CELLS. Cell Biophysics *5*, 129-140.

Lamer, C.D., Henriquez, R.R., Johnson, J.D., and Macfarlane, R.D. (2011). Developing High Performance Lipoprotein Density Profiling for Use in Clinical Studies Relating to Cardiovascular Disease. Analytical Chemistry *83*, 8524-8530.

Lange, Y., Dolde, J., and Steck, T.L. (1981). The rate of transmembrane movement of cholesterol in the human erythrocyte. Journal of Biological Chemistry *256*, 5321-5323.

Lange, Y., Ye, J., and Steck, T.L. (1998). Circulation of cholesterol between lysosomes and the plasma membrane. Journal of Biological Chemistry *273*, 18915-18922.

LaRocca, T.J., Pathak, P., Chiantia, S., Toledo, A., Silvius, J.R., Benach, J.L., and London, E. (2013). Proving Lipid Rafts Exist: Membrane Domains in the Prokaryote Borrelia burgdorferi Have the Same Properties as Eukaryotic Lipid Rafts. Plos Pathogens *9*, 11.

Lasserre, R., Guo, X.J., Conchonaud, F., Hamon, Y., Hawchar, O., Bernard, A.M., Soudja, S.M.H., Lenne, P.F., Rigneault, H., Olive, D.*, et al.* (2008). Raft nanodomains contribute to Akt/PKB plasma membrane recruitment and activation. Nature Chemical Biology *4*, 538-547.

Lev, S. (2010). Non-vesicular lipid transport by lipid-transfer proteins and beyond. Nature Reviews Molecular Cell Biology *11*, 739-750.

Levental, I., Byfield, F.J., Chowdhury, P., Gai, F., Baumgart, T., and Janmey, P.A. (2009). Cholesterol-dependent phase separation in cell-derived giant plasma-membrane vesicles. Biochemical Journal *424*, 163-167.

Levental, K.R., Lorent, J.H., Lin, X.B., Skinkle, A.D., Surma, M.A., Stockenbojer, E.A., Gorfe, A.A., and Levental, I. (2016). Polyunsaturated Lipids Regulate Membrane Domain Stability by Tuning Membrane Order. Biophysical Journal *110*, 1800-1810.

Leventis, R., and Silvius, J.R. (2001). Use of cyclodextrins to monitor transbilayer movement and differential lipid affinities of cholesterol. Biophysical Journal *81*, 2257-2267.

Lewis, G.F., and Rader, D.J. (2005). New insights into the regulation of HDL metabolism and reverse cholesterol transport. Circulation Research *96*, 1221-1232.

Lin, Q., and London, E. (2014). Preparation of artificial plasma membrane mimicking vesicles with lipid asymmetry. PLoS ONE *9*.

Lin, Q.Q., and London, E. (2015). Ordered Raft Domains Induced by Outer Leaflet Sphingomyelin in Cholesterol-Rich Asymmetric Vesicles. Biophysical Journal *108*, 2212-2222.

Lingwood, D., Ries, J., Schwille, P., and Simons, K. (2008). Plasma membranes are poised for activation of raft phase coalescence at physiological temperature. Proceedings of the National Academy of Sciences of the United States of America *105*, 10005-10010.

Lingwood, D., and Simons, K. (2010). Lipid rafts as a membrane-organizing principle. Science *327*, 46-50.

Lipp, A.M., Juhasz, K., Paar, C., Ogris, C., Eckerstorfer, P., Thuenauer, R., Hesse, J., Nimmervoll, B., Stockinger, H., Schutz, G.J.*, et al.* (2014). Lck Mediates Signal Transmission from CD59 to the TCR/CD3 Pathway in Jurkat T Cells. Plos One *9*, 12.

London, E., and Brown, D.A. (2000). Insolubility of lipids in Triton X-100: physical origin and relationship to sphingolipid/cholesterol membrane domains (rafts). Biochimica Et Biophysica Acta-Biomembranes *1508*, 182-195.

Lynen, F., and Ochoa, S. (1953). ENZYMES OF FATTY ACID METABOLISM. Biochimica Et Biophysica Acta *12*, 299-314.

López, C.A., de Vries, A.H., and Marrink, S.J. (2011). Molecular mechanism of cyclodextrin mediated cholesterol extraction. PLoS Computational Biology *7*.

Ma, S., and Chisholm, R.L. (2002). Cytoplasmic dynein-associated structures move bidirectionally in vivo. Journal of Cell Science *115*, 1453-1460.

MacDonald, R.C., MacDonald, R.I., Menco, B.P.M., Takeshita, K., Subbarao, N.K., and Hu, L.-r. (1991). Small-volume extrusion apparatus for preparation of large, unilamellar vesicles. Biochimica et Biophysica Acta (BBA) - Biomembranes *1061*, 297-303.

Macfarlane, R.D., Bondarenko, P.V., Cockrill, S.L., Cruzado, I.D., Koss, W., McNeal, C.J., Spiekerman, A.M., and Watkins, L.K. (1997). Development of a lipoprotein profile using capillary electrophoresis and mass spectrometry. Electrophoresis *18*, 1796-1806.

Marassi, F.M., Shivers, R.R., and Macdonald, P.M. (1993). RESOLVING THE 2 MONOLAYERS OF A LIPID BILAYER IN GIANT UNILAMELLAR VESICLES USING DEUTERIUM NUCLEAR-MAGNETIC-RESONANCE. Biochemistry *32*, 9936-9943.

Mathivet, L., Cribier, S., and Devaux, P.F. (1996). Shape change and physical properties of giant phospholipid vesicles prepared in the presence of an AC electric field. Biophysical Journal *70*, 1112-1121.

Maxfield, F.R., and van Meer, G. (2010). Cholesterol, the central lipid of mammalian cells. Current Opinion in Cell Biology *22*, 422-429.

Mayor, S., and Riezman, H. (2004). Sorting GPI-anchored proteins. Nature Reviews Molecular Cell Biology *5*, 110-120.

McIntosh, T.J., Simon, S.A., Needham, D., and Huang, C.H. (1992). STRUCTURE AND COHESIVE PROPERTIES OF SPHINGOMYELIN CHOLESTEROL BILAYERS. Biochemistry *31*, 2012-2020.

Mei, F., You, J.F., Liu, B.Y., Zhang, M.X., Liu, J.Y., Zhang, B., and Pei, F. (2015). LASS2/TMSG1 inhibits growth and invasion of breast cancer cell in vitro through regulation of vacuolar ATPase activity. Tumor Biology *36*, 2831-2844.

Merrill, A.H., Vanechten, G., Wang, E., and Sandhoff, K. (1993). FUMONISIN-B(1) INHIBITS SPHINGOSINE (SPHINGANINE) N-ACYLTRANSFERASE AND DE-NOVO SPHINGOLIPID BIOSYNTHESIS IN CULTURED NEURONS IN-SITU. Journal of Biological Chemistry *268*, 27299-27306.

Mesmin, B., and Maxfield, F.R. (2009). Intracellular sterol dynamics. Biochimica et Biophysica Acta - Molecular and Cell Biology of Lipids *1791*, 636-645.

Mesmin, B., Pipalia, N.H., Lund, F.W., Ramlall, T.F., Sokolov, A., Eliezer, D., and Maxfield, F.R. (2011). STARD4 abundance regulates sterol transport and sensing. Molecular Biology of the Cell *22*, 4004-4015.

Mombelli, E., Morris, R., Taylor, W., and Fraternali, F. (2003). Hydrogen-bonding propensities of sphingomyelin in solution and in a bilayer assembly: A molecular dynamics study. Biophysical Journal *84*, 1507-1517.

Mondal, M., Mesmin, B., Mukherjee, S., and Maxfield, F.R. (2009). Sterols are mainly in the cytoplasmic leaflet of the plasma membrane and the endocytic recycling compartment in CHO cells. Molecular Biology of the Cell *20*, 581-588.

Montes, L.R., Alonso, A., Goni, F.M., and Bagatolli, L.A. (2007). Giant unilamellar vesicles electroformed from native membranes and organic lipid mixtures under physiological conditions. Biophysical Journal *93*, 3548-3554.

Morris, R.J., Jen, A., and Warley, A. (2011). Isolation of nano-meso scale detergent resistant membrane that has properties expected of lipid 'rafts'. Journal of Neurochemistry *116*, 671-677.

Mukherjee, S., Zha, X., Tabas, I., and Maxfield, F.R. (1998). Cholesterol distribution in living cells: Fluorescence imaging using dehydroergosterol as a fluorescent cholesterol analog. Biophysical Journal *75*, 1915-1925.

Munro, S. (2003). Lipid rafts: Elusive or illusive? Cell *115*, 377-388.

Murate, M., and Kobayashi, T. (2016). Revisiting transbilayer distribution of lipids in the plasma membrane. Chemistry and Physics of Lipids *194*, 58-71.

Naganuma, T., Sato, Y., Sassa, T., Ohno, Y., and Kihara, A. (2011). Biochemical characterization of the very long-chain fatty acid elongase ELOVL7. Febs Letters *585*, 3337-3341.

Needham, D., and Evans, E. (1988). STRUCTURE AND MECHANICAL-PROPERTIES OF GIANT LIPID (DMPC) VESICLE BILAYERS FROM 20-DEGREES-C BELOW TO 10-DEGREES-C ABOVE THE LIQUID-CRYSTAL CRYSTALLINE PHASE-TRANSITION AT 24-DEGREES-C. Biochemistry *27*, 8261-8269.

Ngo, M.H., Colbourne, T.R., and Ridgway, N.D. (2010). Functional implications of sterol transport by the oxysterol-binding protein gene family. Biochemical Journal *429*, 13-24.

Niemelä, P.S., Hyvönen, M.T., and Vattulainen, I. (2006). Influence of chain length and unsaturation on sphingomyelin bilayers. Biophysical Journal *90*, 851-863.

Nordlund, J.R., Schmidt, C.F., Dicken, S.N., and Thompson, T.E. (1981). Transbilayer distribution of phosphatidylethanolamine in large and small unilamellar vesicles. Biochemistry *20*, 3237-3241.

Norman, A.W. (2012). The History of the Discovery of Vitamin D and Its Daughter Steroid Hormone. Annals of Nutrition and Metabolism *61*, 199-206.

Ohno, Y., Suto, S., Yamanaka, M., Mizutani, Y., Mitsutake, S., Igarashi, Y., Sassa, T., and Kihara, A. (2010). ELOVL1 production of C24 acyl-CoAs is linked to C24 sphingolipid synthesis. Proceedings of the National Academy of Sciences of the United States of America *107*, 18439-18444.

Ohvo, H., and Slotte, J.P. (1996). Cyclodextrin-mediated removal of sterols from monolayers: Effects of sterol structure and phospholipids on desorption rate. Biochemistry *35*, 8018-8024.

Ohvo-Rekila, H., Ramstedt, B., Leppimaki, P., and Slotte, J.P. (2002). Cholesterol interactions with phospholipids in membranes. Progress in Lipid Research *41*, 66-97.

Ohvo-Rekilä, H., Åkerlund, B., and Slotte, J.P. (2000). Cyclodextrin-catalyzed extraction of fluorescent sterols from monolayer membranes and small unilamellar vesicles. Chemistry and Physics of Lipids *105*, 167-178.

Okino, N., He, X.X., Gatt, S., Sandhoff, K., Ito, M., and Schuchman, E.H. (2003). The reverse activity of human acid ceramidase. Journal of Biological Chemistry *278*, 29948-29953.

Owen, D.M., and Gaus, K. (2013). Imaging lipid domains in cell membranes: the advent of super-resolution fluorescence microscopy. Frontiers in Plant Science *4*, 9.

Park, J.W., Park, W.J., Kuperman, Y., Boura-Halfon, S., Pewzner-Jung, Y., and Futerman, A.H. (2013). Ablation of Very Long Acyl Chain Sphingolipids Causes Hepatic Insulin Resistance in Mice Due to Altered Detergent-Resistant Membranes. Hepatology *57*, 525-532.

Park, W.J., and Park, J.W. (2015). The effect of altered sphingolipid acyl chain length on various disease models. Biological Chemistry *396*, 693-705.

Pathak, P., and London, E. (2015). The Effect of Membrane Lipid Composition on the Formation of Lipid Ultrananodomains. Biophysical Journal *109*, 1630-1638.

Pewzner-Jung, Y., Ben-Dor, S., and Futerman, A.H. (2006). When do lasses (longevity assurance genes) become CerS (ceramide synthases)? Insights into the regulation of ceramide synthesis. Journal of Biological Chemistry *281*, 25001-25005.

Pewzner-Jung, Y., Brenner, O., Braun, S., Laviad, E.L., Ben-Dor, S., Feldmesser, E., Horn-Saban, S., Amann-Zalcenstein, D., Raanan, C., Berkutzki, T.*, et al.* (2010a). A critical role for ceramide synthase 2 in liver homeostasis II. Insights into molecular changes leading to hepatopathy. Journal of Biological Chemistry *285*, 10911-10923.

Pewzner-Jung, Y., Park, H., Laviad, E.L., Silva, L.C., Lahiri, S., Stiban, J., Erez-Roman, R., Brugger, B., Sachsenheimer, T., Wieland, F.*, et al.* (2010b). A Critical Role for Ceramide Synthase 2 in Liver Homeostasis I. ALTERATIONS IN LIPID METABOLIC PATHWAYS. Journal of Biological Chemistry *285*, 10902-10910.

Pike, L.J. (2006). Rafts defined: A report on the Keystone symposium on lipid rafts and cell function. Journal of Lipid Research *47*, 1597-1598.

Popik, W., Alce, T.M., and Au, W.C. (2002). Human immunodeficiency virus type 1 uses lipid raft-colocalized CD4 and chemokine receptors for productive entry into CD4(+) T cells. Journal of Virology *76*, 4709-4722.

Popjak, G., Goodman, D.S., and Cornforth, J.W. (1961). MECHANISM OF SQUALENE BIOSYNTHESIS FROM MEVALONATE AND FARNESYL PYROPHOSPHATE. Biochemical and Biophysical Research Communications *4*, 138-&.

Pott, T., Bouvrais, H., and Méléard, P. (2008). Giant unilamellar vesicle formation under physiologically relevant conditions. Chemistry and Physics of Lipids *154*, 115-119.

Pourmousa, M., Rog, T., Mikkeli, R., Vattulainen, I., Solanko, L.M., Wustner, D., List, N.H., Kongsted, J., and Karttunen, M. (2014). Dehydroergosterol as an Analogue for Cholesterol: Why It Mimics Cholesterol So Well-or Does It? Journal of Physical Chemistry B *118*, 7345-7357.

Pralle, A., Keller, P., Florin, E.L., Simons, K., and Hörber, J.K.H. (2000). Sphingolipid-cholesterol rafts diffuse as small entities in the plasma membrane of mammalian cells. Journal of Cell Biology *148*, 997-1007.

Quehenberger, O., Armando, A.M., Brown, A.H., Milne, S.B., Myers, D.S., Merrill, A.H., Bandyopadhyay, S., Jones, K.N., Kelly, S., Shaner, R.L.*, et al.* (2010). Lipidomics reveals a remarkable diversity of lipids in human plasma. Journal of Lipid Research *51*, 3299-3305.

Radhakrishnan, A., Ikeda, Y., Kwon, H.J., Brown, M.S., and Goldstein, J.L. (2007). Sterol-regulated transport of SREBPs from endoplasmic reticulum to Golgi: Oxysterols block transport by binding to Insig. Proceedings of the National Academy of Sciences of the United States of America *104*, 6511-6518.

Radhakrishnan, A., Sun, L.P., Kwon, H.J., Brown, M.S., and Goldstein, J.L. (2004). Direct binding of cholesterol to the purified membrane region of SCAP: Mechanism for a sterol-sensing domain. Molecular Cell *15*, 259-268.

Raghupathy, R., Anilkumar, A.A., Polley, A., Singh, P.P., Yadav, M., Johnson, C., Suryawanshi, S., Saikam, V., Sawant, S.D., Panda, A.*, et al.* (2015). Transbilayer lipid interactions mediate nanoclustering of lipid-anchored proteins. Cell *161*, 581-594.

Raichur, S., Wang, S.T., Chan, P.W., Li, Y., Ching, J.H., Chaurasia, B., Dogra, S., Ohman, M.K., Takeda, K., Sugii, S.*, et al.* (2014). CerS2 Haploinsufficiency Inhibits beta-Oxidation and Confers Susceptibility to Diet-Induced Steatohepatitis and Insulin Resistance. Cell Metabolism *20*, 687-695.

Ramstedt, B., and Slotte, J.P. (1999). Interaction of cholesterol with sphingomyelins and acyl-chain-matched phosphatidylcholines: A comparative study of the effect of the chain length. Biophysical Journal *76*, 908-915.

Rao, M., and Mayor, S. (2005). Use of Forster's resonance energy transfer microscopy to study lipid rafts. Biochimica Et Biophysica Acta-Molecular Cell Research *1746*, 221-233.

Reynolds, G.A., Basu, S.K., Osborne, T.F., Chin, D.J., Gil, G., Brown, M.S., Goldstein, J.L., and Luskey, K.L. (1984). HMG COA REDUCTASE - A NEGATIVELY REGULATED GENE WITH UNUSUAL PROMOTER AND 5' UNTRANSLATED REGIONS. Cell *38*, 275-285.

Richmond, D.L., Schmid, E.M., Martens, S., Stachowiak, J.C., Liska, N., and Fletcher, D.A. (2011). Forming giant vesicles with controlled membrane composition, asymmetry, and contents. Proceedings of the National Academy of Sciences of the United States of America *108*, 9431-9436.

Ridsdale, A., Denis, M., Gougeon, P.Y., Ngsee, J.K., Presley, J.F., and Zha, X. (2006). Cholesterol is required for efficient endoplasmic reticulum-to-Golgi transport of secretory membrane proteins. Molecular Biology of the Cell *17*, 1593-1605.

Rilling, H., Tchen, T.T., and Bloch, K. (1958). ON THE MECHANISM OF SQUALENE BIOGENESIS. Proceedings of the National Academy of Sciences of the United States of America *44*, 167-173.

Risley, J.M. (2002). Cholesterol biosynthesis: Lanosterol to cholesterol. Journal of Chemical Education *79*, 377-384.

Rizzo, M.A., Springer, G., Segawa, K., Zipfel, W.R., and Piston, D.W. (2006). Optimization of pairings and detection conditions for measurement of FRET between cyan and yellow fluorescent proteins. Microscopy and Microanalysis *12*, 238-254.

Sakamoto, H., Okamoto, K., Aoki, M., Kato, H., Katsume, A., Ohta, A., Tsukuda, T., Shimma, N., Aoki, Y., Arisawa, M.*, et al.* (2005). Host sphingolipid biosynthesis as a target for hepatitis C virus therapy. Nature Chemical Biology *1*, 333-337.

Sankaram, M.B., and Thompson, T.E. (1991). CHOLESTEROL-INDUCED FLUID-PHASE IMMISCIBILITY IN MEMBRANES. Proceedings of the National Academy of Sciences of the United States of America *88*, 8686-8690.

Sassa, T., and Kihara, A. (2014). Metabolism of Very Long-Chain Fatty Acids: Genes and Pathophysiology. Biomolecules & Therapeutics *22*, 83-92.

Sassa, T., Suto, S., Okayasu, Y., and Kihara, A. (2012). A shift in sphingolipid composition from C24 to C16 increases susceptibility to apoptosis in HeLa cells. Biochimica Et Biophysica Acta-Molecular and Cell Biology of Lipids *1821*, 1031-1037.

Schroeder, F., Nemecz, G., Wood, W.G., Joiner, C., Morrot, G., Ayraut-Jarrier, M., and Devaux, P.F. (1991). Transmembrane distribution of sterol in the human erythrocyte. Biochimica et Biophysica Acta - Biomembranes *1066*, 183-192.

Schroeder, R., London, E., and Brown, D. (1994). INTERACTIONS BETWEEN SATURATED ACYL CHAINS CONFER DETERGENT RESISTANCE ON LIPIDS AND GLYCOSYLPHOSPHATIDYLINOSITOL (GPI)-ANCHORED PROTEINS - GPI-ANCHORED PROTEINS IN LIPOSOMES AND CELLS SHOW SIMILAR BEHAVIOR. Proceedings of the National Academy of Sciences of the United States of America *91*, 12130-12134.

Schwartz, K., Lawn, R.M., and Wade, D.P. (2000). ABC1 gene expression and ApoA-I-mediated cholesterol efflux are regulated by LXR. Biochemical and Biophysical Research Communications *274*, 794-802.

Sever, N., Yang, T., Brown, M.S., Goldstein, J.L., and DeBose-Boyd, R.A. (2003). Accelerated degradation of HMG CoA reductase mediated by binding of Insig-1 to its sterol-sensing domain. Molecular Cell *11*, 25-33.

Sezgin, E., Kaiser, H.J., Baumgart, T., Schwille, P., Simons, K., and Levental, I. (2012). Elucidating membrane structure and protein behavior using giant plasma membrane vesicles. Nature Protocols *7*, 1042-1051.

Sharma, P., Varma, R., Sarasij, R.C., Ira, Gousset, K., Krishnamoorthy, G., Rao, M., and Mayor, S. (2004). Nanoscale Organization of Multiple GPI-Anchored Proteins in Living Cell Membranes. Cell *116*, 577-589.

Shevchenko, A., and Simons, K. (2010). Lipidomics: coming to grips with lipid diversity. Nature Reviews Molecular Cell Biology *11*, 593-598.

Shimshick, E.J., and McConnell, H.M. (1973). LATERAL PHASE SEPARATION IN PHOSPHOLIPID MEMBRANES. Biochemistry *12*, 2351-2360.

Siggia, E.D., Lippincott-Schwartz, J., and Bekiranov, S. (2000). Diffusion in inhomogeneous media: Theory and simulations applied to whole cell photobleach recovery. Biophysical Journal *79*, 1761-1770.

Silva, L.C., Ben David, O., Pewzner-Jung, Y., Laviad, E.L., Stiban, J., Bandyopadhyay, S., Merrill, A.H., Prieto, M., and Futerman, A.H. (2012). Ablation of ceramide synthase 2 strongly affects biophysical properties of membranes. Journal of Lipid Research *53*, 430-436.

Simons, K., and Gerl, M.J. (2010). Revitalizing membrane rafts: New tools and insights. Nature Reviews Molecular Cell Biology *11*, 688-699.

Simons, K., and Ikonen, E. (1997). Functional rafts in cell membranes. Nature *387*, 569-572.

Simons, K., and Van Meer, G. (1988). LIPID SORTING IN EPITHELIAL-CELLS. Biochemistry *27*, 6197-6202.

Singer, S.J., and Nicolson, G.L. (1972). FLUID MOSAIC MODEL OF STRUCTURE OF CELL-MEMBRANES. Science *175*, 720-&.

Singh, J., Khan, M., and Singh, I. (2009). Silencing of Abcd1 and Abcd2 genes sensitizes astrocytes for inflammation: implication for X-adrenoleukodystrophy. Journal of Lipid Research *50*, 135-147.

Slotte, J.P. (2013). Biological functions of sphingomyelins. Progress in Lipid Research *52*, 424-437.

Snyder, B., and Freire, E. (1982). Fluorescence energy transfer in two dimensions. A numeric solution for random and nonrandom distributions. Biophys J *40*, 137-148.

Soccio, R.E., and Breslow, J.L. (2004). Intracellular cholesterol transport. Arteriosclerosis Thrombosis and Vascular Biology *24*, 1150-1160.

Son, M., and London, E. (2013a). The dependence of lipid asymmetry upon phosphatidylcholine acyl chain structure. Journal of Lipid Research *54*, 223-231.

Son, M., and London, E. (2013b). The dependence of lipid asymmetry upon polar headgroup structure. Journal of Lipid Research *54*, 3385-3393.

Son, M.J., and London, E. (2011). Extending Techniques to Prepare Asymmetric Vesicles to Additional Lipid Compositions: Lipid Structure Affects the Ability to Maintain Lipid Asymmetry. Biophysical Journal *100*, 337-337.

Song, B.L., Javitt, N.B., and DeBose-Boyd, R.A. (2005). Insig-mediated degradation of HMG CoA reductase stimulated by lanosterol, an intermediate in the synthesis of cholesterol. Cell Metabolism *1*, 179-189.

Spiegel, S., and Kolesnick, R. (2002). Sphingosine 1-phosphate as a therapeutic agent. Leukemia *16*, 1596-1602.

Steck, T.L., Ye, J., and Lange, Y. (2002). Probing red cell membrane cholesterol movement with cyclodextrin. Biophysical Journal *83*, 2118-2125.

Stryer, L. (1978). FLUORESCENCE ENERGY-TRANSFER AS A SPECTROSCOPIC RULER. Annual Review of Biochemistry *47*, 819-846.

Sun, L.P., Seemann, J., Goldstein, J.L., and Brown, M.S. (2007). Sterol-regulated transport of SREBPs from endoplasmic reticulum to Golgi: Insig renders sorting signal in Scap inaccessible to COPII proteins. Proceedings of the National Academy of Sciences of the United States of America *104*, 6519-6526.

Surma, M.A., Klose, C., and Simons, K. (2012). Lipid-dependent protein sorting at the trans-Golgi network. Biochimica Et Biophysica Acta-Molecular and Cell Biology of Lipids *1821*, 1059-1067.

Takeda, M., Leser, G.P., Russell, C.J., and Lamb, R.A. (2003). Influenza virus hemagglutinin concentrates in lipid raft microdomains for efficient viral fusion. Proceedings of the National Academy of Sciences of the United States of America *100*, 14610-14617.

Thurm, A., Tierney, E., Farmer, C., Albert, P., Joseph, L., Swedo, S., Bianconi, S., Bukelis, I., Wheeler, C., Sarphare, G.*, et al.* (2016). Development, behavior, and biomarker characterization of Smith-Lemli-Opitz syndrome: an update. Journal of Neurodevelopmental Disorders *8*, 10.

Tobert, J.A. (2003). Lovastatin and beyond: The history of the HMG-CoA reductase inhibitors. Nature Reviews Drug Discovery *2*, 517-526.

Trinkle-Mulcahy, L., Chusainow, J., Lam, Y.W., Swift, S., and Lamond, A. (2007). Visualization of intracellular PP1 targeting through transiently and stably expressed fluorescent protein fusions. In Methods in Molecular Biology, pp. 133-154.

Turpin, S.M., Nicholls, H.T., Willmes, D.M., Mourier, A., Brodesser, S., Wunderlich, C.M., Mauer, J., Xu, E., Hammerschmidt, P., Brönneke, H.S.*, et al.* (2014). Obesity-induced CerS6-dependent C16:0 ceramide production promotes weight gain and glucose intolerance. Cell Metabolism *20*, 678-686.

van Gestel, R.A., Brouwers, J.F., Ultee, A., Helms, J.B., and Gadella, B.M. (2016). Ultrastructure and lipid composition of detergent-resistant membranes derived from mammalian sperm and two types of epithelial cells. Cell and Tissue Research *363*, 129-145.

van Meer, G. (2011). Dynamic transbilayer lipid asymmetry. Cold Spring Harbor perspectives in biology *3*.

Van Meer, G., Voelker, D.R., and Feigenson, G.W. (2008). Membrane lipids: Where they are and how they behave. Nature Reviews Molecular Cell Biology *9*, 112-124.

Varma, R., and Mayor, S. (1998). GPI-anchored proteins are organized in submicron domains at the cell surface. Nature *394*, 798-801.

Veatch, S.L., and Keller, S.L. (2003). Separation of Liquid Phases in Giant Vesicles of Ternary Mixtures of Phospholipids and Cholesterol. Biophysical Journal *85*, 3074-3083.

Veatch, S.L., and Keller, S.L. (2005). Seeing spots: Complex phase behavior in simple membranes. Biochimica et Biophysica Acta - Molecular Cell Research *1746*, 172-185.

Verkleij, A.J., Zwaal, R.F.A., Roelofsen, B., Comfurius, P., Kastelijn, D., and van Deenen, L.L.M. (1973). The asymmetric distribution of phospholipids in the human red cell membrane. A combined study using phospholipases and freeze-etch electron microscopy. BBA - Biomembranes *323*, 178-193.

Wang, X.D., Briggs, M.R., Hua, X.X., Yokoyama, C., Goldstein, J.L., and Brown, M.S. (1993). NUCLEAR-PROTEIN THAT BINDS STEROL REGULATORY ELEMENT OF LOW-DENSITY-LIPOPROTEIN RECEPTOR PROMOTER .2. PURIFICATION AND CHARACTERIZATION. Journal of Biological Chemistry *268*, 14497-14504.

Warnock, D.E., Roberts, C., Lutz, M.S., Blackburn, W.A., Young, W.W., and Baenziger, J.U. (1993). DETERMINATION OF PLASMA-MEMBRANE LIPID MASS AND COMPOSITION IN CULTURED CHINESE-HAMSTER OVARY CELLS USING HIGH-GRADIENT MAGNETIC AFFINITY-CHROMATOGRAPHY. Journal of Biological Chemistry *268*, 10145-10153.

Waterham, H.R. (2002). Inherited disorders of cholesterol biosynthesis. Clinical Genetics *61*, 393-403.

Wustner, D., Lund, F.W., Rohrl, C., and Stangl, H. (2016). Potential of BODIPY-cholesterol for analysis of cholesterol transport and diffusion in living cells. Chemistry and Physics of Lipids *194*, 12-28.

Xu, F., Rychnovsky, S.D., Belani, J.D., Hobbs, H.H., Cohen, J.C., and Rawson, R.B. (2005). Dual roles for cholesterol in mammalian cells. Proceedings of the National Academy of Sciences of the United States of America *102*, 14551-14556.

Yesylevskyy, S.O., and Demchenko, A.P. (2012). How cholesterol is distributed between monolayers in asymmetric lipid membranes. European Biophysics Journal with Biophysics Letters *41*, 1043-1054.

Zhang, Y.R., Tuomilehto, J., Jousilahti, P., Wang, Y.J., Antikainen, R., and Hu, G. (2012). Total and High-Density Lipoprotein Cholesterol and Stroke Risk. Stroke *43*, 1768-1774.

Zhang, Z.W., Cheng, J., Xu, F., Chen, Y.E., Du, J.B., Yuan, M., Zhu, F., Xu, X.C., and Yuan, S. (2011). Red Blood Cell Extrudes Nucleus and Mitochondria Against Oxidative Stress. Iubmb Life *63*, 560-565.

Zhu, X.W., Owen, J.S., Wilson, M.D., Li, H.T., Griffiths, G.L., Thomas, M.J., Hiltbold, E.M., Fessler, M.B., and Parks, J.S. (2010). Macrophage ABCA1 reduces MyD88-dependent Toll-like receptor trafficking to lipid rafts by reduction of lipid raft cholesterol. Journal of Lipid Research *51*, 3196-3206.

Zsadon, B., Szilasi, M., Szejtli, J., Seres, G., and Tudos, F. (1978). CHROMATOGRAPHY OF ALPHA-CYCLODEXTRIN, BETA-CYCLODEXTRIN AND GAMMA-CYCLODEXTRIN ON DEXTRAN GEL COLUMNS. Starke *30*, 276-279.

Zurzolo, C., and Simons, K. (2016). Glycosylphosphatidylinositol-anchored proteins: Membrane organization and transport. Biochimica Et Biophysica Acta-Biomembranes *1858*, 632-639.

Contributions of Collaborators

The LUV and GUV data was generated with assistance from Gary (Congyu) Zhang, who was an undergraduate research assistant in the Zha lab. Mass Spectrometry of the asymmetric vesicles was performed in collaboration with Dr. David Ford from Saint Louis University in St. Louis, Missouri.

The FRET data presented in **Chapter 6** was produced in collaboration with Dr. John Presley from McGill University and Dr. Riya Raghupathy, who was briefly a member of the Zha lab. Specifically, the FRET simulation described in **Figure 23** was performed by Dr. Presley who is a co-author on a manuscript. The live cell FRET data, shown in **Figure 21** and **Figure 22** were assisted by Dr. Raghupathy, who optimized the system and performed a portion of the imaging and data analysis.

The data presented in **Appendix 3** was produced by a collaborator with expertise in performing molecular dynamics simulations of membrane bilayers. Although the simulations were designed with guidance by Xiaohui Zha and I, the work was performed and analyzed by Drs. Himanshu Khandelia, Weria Pezeshkian and John Ispen from the MEMPHYS, Center for Biomembrane Physics at the University of Southern Denmark. This work will be publish together with much of the data presented in this thesis, however, since I did not personally perform the experiments, the data was provided as appendix material.

Appendix

A.1 - Detailed cholesterol extraction assay protocol

A primary objective of this thesis was to develop a strategy to quantify the distribution of cholesterol between the leaflets of bilayer membrane. We aimed to develop and test the method in an artificial liposomal system to ensure feasibility, then use the system to quantify cholesterol in live mammalian cells. In a symmetric membrane, where all components are randomly distributed, cholesterol is distributed equally between leaflets. It was demonstrated, for example, that fluorescent sterols are evenly distributed in symmetric large unilamellar vesicles (Mondal et al., 2009). Previous efforts to quantify the cholesterol transbilayer distribution have primarily used indirect methods. For example, the cholesterol distribution can be inferred by quantifying structurally similar fluorescent sterols, or cholesterol conjugated to a fluorescent moiety. Other strategies have involved using cholesterol oxidase, or freeze-fracture.

The strategy to quantify the cholesterol distribution that we developed involves using methyl-β-cyclodextrin (MCD) to extract cholesterol selectively from the outer leaflet of a bilayer. By reducing temperature, the flip-flop of cholesterol between bilayer leaflets is prevented, or greatly reduced, which allows cyclodextrin to remove only outer leaflet cholesterol. After the outer leaflet cholesterol is extracted, the amount of cholesterol present in the media (cyclodextrin bound cholesterol) is quantified. If cholesterol is evenly distributed, 50% cholesterol would be present in the outer leaflet at steady state. To facilitate highly sensitive quantification, radiolabelled (^{3}H) cholesterol is introduced into the membrane prior to cyclodextrin treatment and quantified by scintillation counting. A detailed description of the experimental protocol is described below.

In the case of unilamellar vesicles, ^{3}H-cholesterol can be incorporated into the vesicles during initial vesicle formation, or can be introduced into the vesicles at a later stage by incubation with ^{3}H-cholesterol loaded β-cyclodextrin. Although initial incorporation of ^{3}H-cholesterol involves fewer steps in preparation, this results in contaminating the LUV extruder apparatus with tritium, which in some cases may be better to avoid if the extruder will be used for other purposes. Furthermore, when generating asymmetric LUVs, it is preferable to add ^{3}H-cholesterol at the end to avoid the potential to contaminate common use centrifuges and incubators that are used in the process.

Using POPC as an example, two 1 mM POPC populations are generated; one with 1% biotinylated PE (b-PE) and the other with 100 pmol ^{3}H-cholesterol. The b-PE is used to bind the resulting vesicles to streptavidin coated agarose beads, which facilitates easy washing and separation of the vesicles from the media. The appropriate lipids, stored in chloroform:methanol (95:5) are first dried into a lipid film in a glass tube under nitrogen and then placed in a vacuum desiccator to remove residual solvent. The lipids are then overlaid with 1 mL buffer and vortexed aggressively to resuspend. At this stage, the vesicles are termed multilamellar vesicles (MLV). To assist in breaking up large aggregates, the sample is subjected to repeated freeze-thaw cycles by placing the glass tubes back and forth between warm water and a mixture of dry ice and 95% ethanol. After freeze-thawing, the vesicle population containing the b-PE is extruded through a membrane with 100 nm pores to form a uniform population of unilamellar vesicles using the Avanti mini-extruder system. Depending on the melting temperature of the lipids used, the extruder may need to be heated above room temperature to allow the lipids to pass through the 100 nm membrane. After the b-PE vesicles are extruded, the sample is then incubated overnight at 4 ºC rotating in 3 mL

buffer in the presence of 200 µL of pre-wash streptavidin beads so that the vesicles bind the beads. The ^{3}H-cholesterol labelled vesicles can be frozen for later use and stored at -20 ºC.

After overnight incubation of the b-PE vesicles and the agarose beads, the vesicles that did not bind the beads are removed by washing the beads 3 times. This done by centrifuging the 3 mL buffered solution of vesicles and beads for 1 minute at 1000 rpm to pellet the beads. The supernatant is removed and the sample is resuspended in fresh 3 mL buffer. Once the unbound vesicles are discarded, the ^{3}H-cholesterol can be incorporated. The amount of vesicles that are bound to the beads was once determined to be approximately 10% of the original vesicles.

Incorporation of ^{3}H-cholesterol is done by pre-incubating ^{3}H-cholesterol donor vesicles with 2mM β-cyclodextrin. The ^{3}H-cholesterol donor and β-cyclodextrin complex is then diluted two-fold and incubated with the bead-bound acceptor vesicles for 30 minutes at 37 ºC. After ^{3}H-cholesterol is donated to the acceptor population, the bead-bound vesicles are again washed 3 times by centrifugation, as described above, to remove the cyclodextrin and unincorporated ^{3}H-cholesterol. At this point, it is useful to take 100 µL of the washed bead-bound vesicles to read the scintillation counting values for the sample. By knowing the amount of ^{3}H-cholesterol incorporated, this helps to standardize the concentration of vesicles used in each experiment. For the experiments described in this thesis, the stock vesicle solution was adjusted so that 100 µL produced 2000 counts per minute. The samples are now ready for the cholesterol extraction assay.

The cholesterol extraction assay is performed as a time course experiment in 1.5 mL microcentrifuge tubes in duplicate or triplicate. 100 µL of ^{3}H-cholesterol labelled, bead-bound vesicles are placed into the tubes, often with multiple times points ranging from 0 to 60 minutes. The tubes are then incubated at the desired temperature for at least 60 minutes

prior to adding cyclodextrin to ensure that the temperature is equilibrated. The 0 ºC experiments are achieved by performing the cholesterol extraction procedure in a 4 ºC cold room and pre-incubating all components and tools used in an ice-water bath. An 8.25 mg/mL solution of MCD is also prepared in the same buffer as the vesicles and pre-incubated to the appropriate temperature. Furthermore, two control samples are also made which will receive either buffer or 2% triton X-100 to act as negative and positive controls.

To initiate the cholesterol extraction, 400 μL of MCD are added to the 100 μL vesicles to give a final concentration of 5 mM MCD. At each time point, the tubes are centrifuged at the corresponding temperature for 1 minute at 1000 x g and 200 μL of supernatant (the extracted cholesterol fraction) is removed for scintillation counting. After correcting for background, using the negative control, the amount of cholesterol extracted over time is plotted relative to the total amount of cholesterol in the sample (positive control).

A.2 - Detailed giant unilamellar vesicle protocol

GUVs were prepared by electroformation by following the procedure originally described by Angelova et al. and further modified by Juhasz et al (Angelova and Dimitrov, 1986; Juhasz et al., 2010). For the purpose of examining membrane phase properties, GUVs are commonly prepared using either indium tin oxide (ITO) coated coverslips or parallel platinum wires. In either case, dilute lipid samples in organic solvent are dried onto the apparatus of choice, overlaid with an aqueous solution and subjected to an oscillating electric current to initiate vesicle electroformation.

A.2.1 - Indium tin oxide method

The ITO-coated coverslip method of generating GUVs involves purchasing specialized coverslips that can conduct an electric current. This method uses two ITO-coated coverslips and a 2-3 mm thick silicon spacer to sit between the coverslips. Lipid is dried onto one coverslip, the hollow spacer is placed on top and filled with aqueous solution, followed by sealing the chamber with the second ITO-coated coverslip. An electric current is applied, which alternates between the two coverslips, which causes swelling of the lipid film into vesicles. The ITO-coated coverslip method is an ideal strategy for visualizing active vesiculation. Since the lipids are dried onto a transparent coverslip, which can be fixed to a microscope stage, vesiculation can be monitored in real-time. This is advantageous because altering the parameters of the function generator during vesiculation can promote enlargement or detachment of vesicles. This enables optimizing the vesiculation parameters and can improve GUV yield.

A.2.2 - Platinum wire method

The GUV experiments described in this thesis exclusively used the platinum wire method for vesiculation. This method was selected for its ease of use and construction, as well as, the minimal materials required. Although the ITO method is equally valid, the platinum wire strategy worked well from the beginning and did not require trying an alternative method. A detailed description of the protocol is described below.

3-inches of platinum wire (0.8 mm diameter) were purchased from Omega Engineering and cut in half to act as two parallel electrodes. To assemble the system, one end of a BNC cable was cut off to expose the two internal wires and the 1.5-inch platinum was soldered onto each wire. Each solder point was then sealed with heat-shrink tubing. The wires were arranged so that approximately 1-inch of platinum was exposed from the end of

the BNC cable and the two platinum wires were fixed in place parallel to each other with 3 mm between them. Before and after using the wires, the platinum was thoroughly cleaned with water and chloroform, followed by sonication in methanol for 30 minutes.

For the formation of unilamellar vesicles, the stock lipid solutions used must contain low concentrations of lipids to prevent multiple layers of lipids (multilamellar vesicles). Typically, stock solutions of the desired lipids are prepared in chloroform:methanol (95:5) with a final concentration of 330 μM. 2.5 μL of the lipids are then applied across the entire length of each platinum wire under a stream of nitrogen to assist with rapid evaporation of the organic solvents. After the lipid is dried, the wire is placed in a vacuum desiccator for 1 hour, or overnight, to remove residual solvent.

For electroformation, the platinum wires are submerged in approximately 1 mL of 30 mM sucrose in a glass tube at 70 ºC. The wire is then connected to a digital PM5193 programmable synthesizer/ function generator producing an A/C sine wave at 10 Hz and 3 V for 90 minutes. After electroformation is complete, the vesicles in 1 mL sucrose are concentrated into a low volume by passively filtering the sample through a membrane with 8 μm pores. The 8 μm filter is also used to wash the vesicles in equimolar glucose. This results in vesicles that have sucrose in the interior and glucose in the exterior. This difference in molecular weight causes the vesicles to settle to the bottom of the dish and greatly simplifies image acquisition.

To regulate the temperature of the GUV samples, a custom heating apparatus was built by removing the heating coil from a hair dryer and fixing the coil to an electrical cord with a standard 120 V wall plug connector. The heating coil was arranged circularly to fit inside a 35 mm glass-bottom microscopy dish. The glass bottom dish was modified to have a column in the centre (made from a syringe) that isolates the GUV-containing media over

the glass coverslip from the surrounding media where the heating coil is submerged. The temperature of the solution can then be regulated by heating or cooling the sample, while monitoring small changes in temperature with a digital thermometer.

A.3 – Molecular dynamics simulations of asymmetric membranes

During the process of characterizing how membrane asymmetry regulates the distribution of cholesterol between bilayer leaflets, we established collaboration with a molecular dynamics (MD) simulation research group. The goal of this collaboration was to establish a theoretical basis for the results of our asymmetric membrane experiments and attempt to identify potential mechanisms for the 24:0 SM effect. The results of these simulations will be published in a peer-review journal accompanied by much of the data presented in this thesis.

Our collaborators performed all-atom MD simulations of asymmetric membranes composed of DOPC and DPPC, which also contained 16:0 or 24:0 SM exclusively in the outer leaflet (**Figure A1**) and demonstrated several striking differences. First, cholesterol favours the inner leaflet (5.5 kBT less free energy) if 24:0 SM is in the outer leaflet (**Figure A1A**, ***b***), while the SM containing leaflet is preferred if 16:0 SM is in the outer leaflet (**Figure A1B**, ***b***). Secondly, the energy barrier for cholesterol to flip from the outer to the inner leaflet is significantly smaller when 24:0 SM is in the outer leaflet (6 kBT), compared to that of 16:0 SM (15 kBT). Both factors would favor cholesterol in the inner leaflet if 24:0 SM in the outer leaflet. Moreover, the atom density profile indicates that the 24:0 SM acyl chain significantly penetrates into the opposite leaflet in a bilayer (**Figure A1A**, ***b***, red peak); while 16:0 SM is contained in its own leaflet (**Figure A1B**, ***b***). This interdigitation would increase the density in the inner leaflet near the centre of the bilayer and induce mechanical

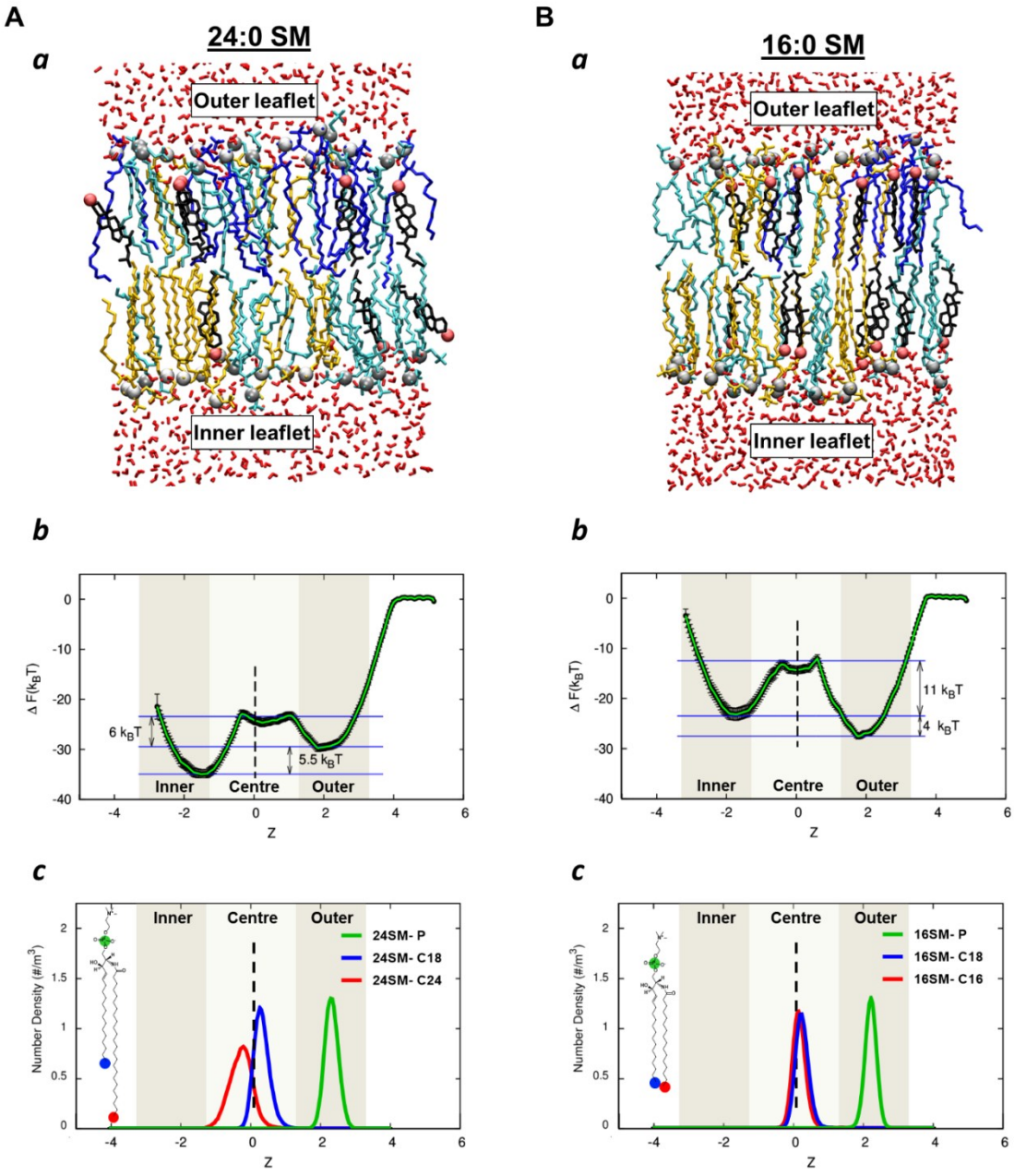
A
24:0 SM
a
Outer leaflet
Inner leaflet
b
ΔF(k_BT)
6 k_BT
5.5 k_BT
Inner
Centre
Outer
Z
c
Number Density (#/m^3)
24SM- P
24SM- C18
24SM- C24
B
16:0 SM
a
Outer leaflet
Inner leaflet
b
ΔF(k_BT)
11 k_BT
4 k_BT
Inner
Centre
Outer
Z
c
Number Density (#/m^3)
16SM- P
16SM- C18
16SM- C16

Figure A1 – Cholesterol displays a preference for the inner bilayer leaflet when very long acyl chain sphingomyelin is in the outer leaflet. A) (*a*) Cross sectional image of asymmetric 24:0 SM membrane at the end of the simulation **(*b*)** Free energy profile of transferring a cholesterol molecule from outer leaflet to the inner leaflet in a 24:0 SM asymmetric membrane shows cholesterol prefers the inner leaflet. The Z-axis refers to the z-distance between the position of the pulled cholesterol molecule relative to the center of the bilayer, Z=0 (see Methods). **(*c*)** Normalized density profile for specific atoms of 24:0 SM in the 24:0 SM membrane system. Only the head group phosphate (green) and terminal acyl chain carbons (blue and red) are displayed to demonstrate the depth of acyl chain penetration into the bilayer. **B) (*a*)** Cross sectional image of asymmetric 16:0 SM membrane at the end of the simulation. **(*b*)** Free energy profile for transferring a cholesterol molecule from outer leaflet to the inner leaflet in a 16:0 SM asymmetric membrane shows cholesterol has a slight preference for the outer leaflet. The Z-axis is the same as in A. **(*c*)** Normalized density profile for specific atoms of 16:0 SM in the 16:0 SM membrane system. Only the head group phosphate (green) and terminal acyl chain carbons (blue and red) are displayed to demonstrate the depth of acyl chain penetration into the bilayer. Lipid composition for both 16:0 and 24:0 SM simulations: 20 SM (blue), 20 DPPC (yellow), 20 DOPC (cyan) and 24 CHL (black) molecules in the upper monolayer and 28 DPPC, 29 DOPC and 24 CHL in the lower monolayer. 5158 water molecules are present. Red and gray spheres are O and P atom of cholesterol and DOPC lipids respectively

instability. To compensate, cholesterol could either move into the inner leaflet to fill the gap or 24:0 SM would be pushed up towards the aqueous phase, which weakens outer leaflet 24:0 SM-cholesterol interactions. Consistent with this notion, the MD simulations indicate that 24:0 SM engages in weaker H-bonding with cholesterol than 16:0 SM (**Figure A2**). Therefore, reduced H-bond capacity in the outer leaflet could add another force to favour cholesterol in the inner leaflet when 24:0 SM is in the outer leaflet, although other factors are likely contributing. Taken together, the MD simulations support our conclusions drawn from the asymmetric LUV experiments (**Figure 12D**). Outer leaflet 24:0 SM has a unique effect of causing cholesterol to concentrate into the inner leaflet of a bilayer membrane.

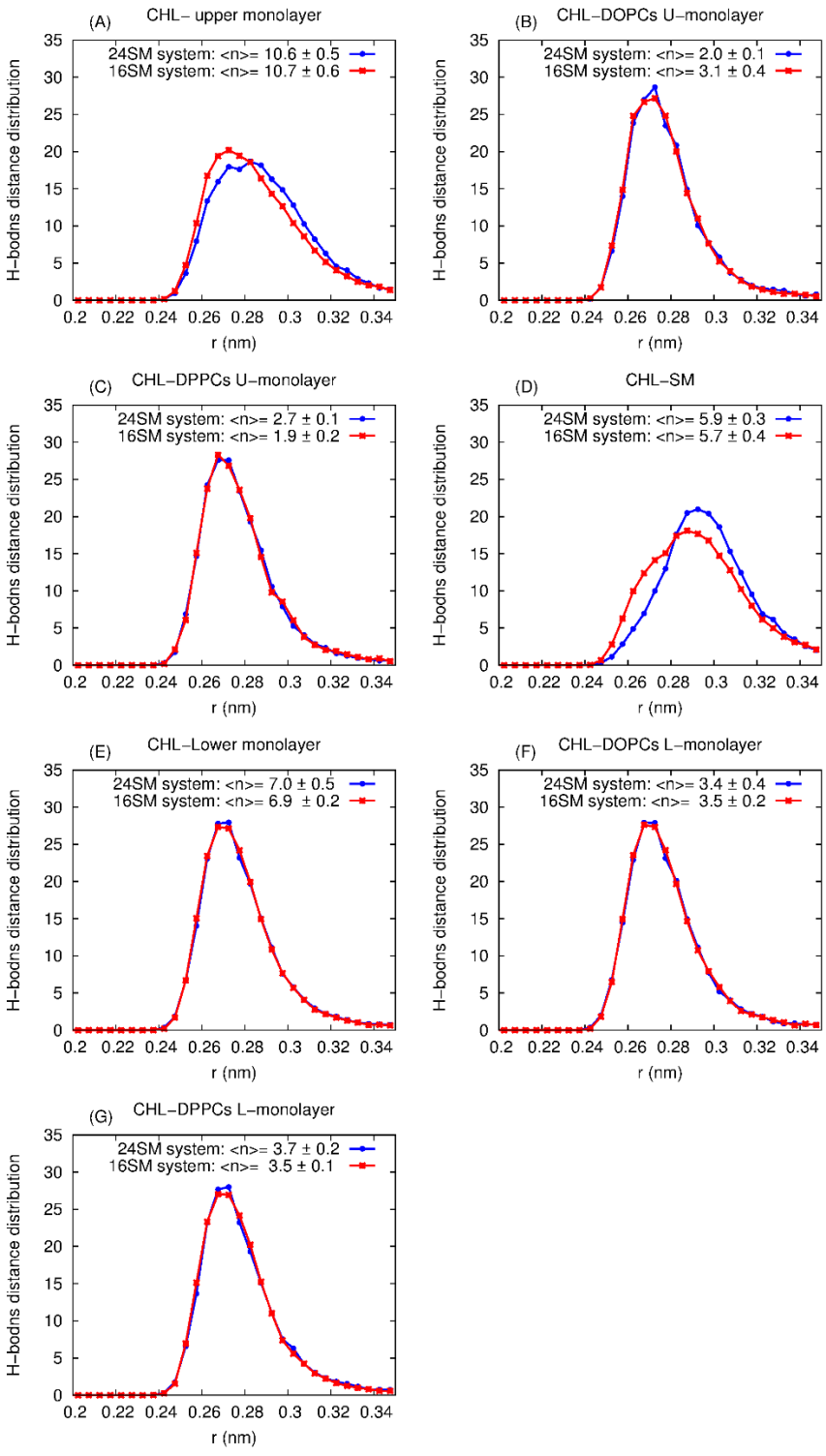
(A)
CHL– upper monolayer
24SM system: <n>= 10.6 ± 0.5
16SM system: <n>= 10.7 ± 0.6
(B)
CHL–DOPCs U–monolayer
24SM system: <n>= 2.0 ± 0.1
16SM system: <n>= 3.1 ± 0.4
(C)
CHL–DPPCs U–monolayer
24SM system: <n>= 2.7 ± 0.1
16SM system: <n>= 1.9 ± 0.2
(D)
CHL–SM
24SM system: <n>= 5.9 ± 0.3
16SM system: <n>= 5.7 ± 0.4
(E)
CHL–Lower monolayer
24SM system: <n>= 7.0 ± 0.5
16SM system: <n>= 6.9 ± 0.2
(F)
CHL–DOPCs L–monolayer
24SM system: <n>= 3.4 ± 0.4
16SM system: <n>= 3.5 ± 0.2
(G)
CHL–DPPCs L–monolayer
24SM system: <n>= 3.7 ± 0.2
16SM system: <n>= 3.5 ± 0.1
H–bodns distance distribution
r (nm)
0 5 10 15 20 25 30 35
0.2 0.22 0.24 0.26 0.28 0.3 0.32 0.34

Figure A2 – Cholesterol exhibits reduced hydrogen bonding strength with 24:0 sphingolipids compared to 16:0 sphingolipids in asymmetric membrane molecular dynamic simulations. Each plot is a distribution of the H-bond distances formed between specific species: **A**) Cholesterol and all upper leaflet lipids. **B**) Cholesterol and upper leaflet DOPC. **C**) Cholesterol and upper leaflet DPPC. **D**) Cholesterol and upper leaflet SM. **E**) Cholesterol and all lower leaflet lipids. **F**) Cholesterol and lower leaflet DOPC. **G**) Cholesterol and lower leaflet DPPC. The value in the upper right corner of each panel refers to the number of H-bonds made by cholesterol in each plot. The data (**A** and **D**) shows that the H-bonding with 16:0 SM (16SM) occurs at shorter distances (corresponding to a stronger H-bond) than with 24:0 SM (24SM). All other distributions are identical.

Curriculum Vitae

KEVIN C. COURTNEY

EDUCATION

2011-Present University of Ottawa, Ottawa, ON

PhD in Biochemistry

Thesis topic: "*Cholesterol transbilayer distribution in mammalian cells*"

2006-2010 University of Guelph, Guelph, ON

Biological Science Degree (B.Sc. Honours)

AWARDS AND SCHOLARSHIPS

2015 Biophysical Society of Canada, Ottawa, ON

Travel award to give a talk at the 2015 Biophysical society meeting in Baltimore, MD

2012 University of Ottawa, Ottawa, ON

Biochemistry, Microbiology and Immunology poster competition (Third place)

2011-Present University of Ottawa, Ottawa, ON

Graduate degree entrance scholarship

2010 University of Guelph, Guelph, ON

NSERC Undergraduate Student Research Award (Sharom lab)

2008 University of Guelph, Guelph, ON

NSERC Undergraduate Student Research Award (Klironomos lab)

EXPERIENCE

2011-Present Ottawa Hospital Research Institute/ University of Ottawa, Ottawa, ON

Lipid metabolism/ Membrane Biochemistry graduate student (Xiaohui Zha lab)

* Examining how membrane lipid composition and organization regulates cell function.

* Novel technique development to characterize cholesterol transbilayer distribution in mammalian cells and model membrane systems.

* Construction of transversely asymmetric large and giant unilamellar vesicles to examine how asymmetric cholesterol transbilayer distribution affects membrane domain formation.

* Fluorescence microscopy, anisotropy, FRET and live cell FRAP to monitor membrane domain assembly and dynamics.

* PCR, molecular cloning, transfection and generation of stable cell lines.

2011 University Health Network/ University of Toronto, Toronto, ON

Structural Biology lab Technician (Mitsu Ikura lab)

* Protein mutagenesis

* Molecular cloning for X-ray crystallography/ NMR analysis

* SDS-PAGE and western blotting

* PCR, DNA sequencing

2009-2011 University of Guelph, Guelph, ON

Membrane Biochemistry Research Assistant (Frances Sharom lab)

* Wildtype and mutant enzyme kinetics experiments involving GPI-anchored protein cleavage from reconstituted proteoliposomes.

* Site-directed mutagenesis on membrane proteins PI-PLC and MsbA.

* Recombinant bacterial culturing and over-expression of His-tagged protein.

* Protein purification by standard affinity chromatographic techniques and Fast Protein Liquid Chromatography (FPLC).

* SDS-PAGE and western blotting to determine protein purity and molecular weight.

* High-speed and ultracentrifugation.

* Various absorbance and fluorometric assays (Bradford, pNPP, Attophos).

2006-2009 University of Guelph, Guelph, ON

Soil Microbiology/ Molecular Fungal Genetics Research Assistant (John Klironomos lab)

* Completed an independently designed and conducted undergraduate thesis project.

* Microscopy, PCR, electrophoresis, and Terminal Restriction Fragment Length Polymorphism (T-TRFLP) analysis to differential fungal species.

* Assisted with graduate study research projects focusing on molecular ecology.

* Performed DNA extractions, PCR and sequencing.

* Collected and taxonomically identified flora from research plots.

PUBLICATIONS

Zha X, Lange Y, **Courtney KC**, Maxfield FR, Steck TL (2017) Correspondence: Plasma Membrane Cholesterol Asymmetry **Nature Chemical Biology** (*submitted*)

Courtney KC, Pezeshkian W, Raghupathy R, Zhang C, Ipsen, JH, Ford DA, Khandelia H, Presley JF, Zha X. (2017) Long acyl chain (C24) sphingolipids play a surprising and central role in governing lateral organization of the live cell plasma membrane. (*submitted*)

Courtney KC, Zhang C, Zha X. (2017) Light-induced lipid peroxidation promotes segregation of ordered and disordered membrane domains. (*in preparation*)

Eid W, Dauner K, **Courtney KC**, Gagnon A, Parks RJ, Sorisky A, Zha X (2017) mTORC1 Activates SREBP-2 by Suppressing Cholesterol Trafficking to the Lysosomes in Mammalian Cells. **Proceedings of the National Academy of Sciences** (*in review*)

Dong F, Mo Z, Eid W, **Courtney KC**, Zha X (2014) Akt Inhibition Promotes ABCA1-Mediated Cholesterol Efflux to ApoA-I through Suppressing mTORC1. PLOS ONE 9(11): e113789. doi:10.1371/journal.pone.0113789

Courtney KC, Bainard LD, Sikes BA, Koch AM, Maherali H, Klironomos JN, Hart MM (2012) Determining a Minimum Detection Threshold in Terminal Restriction Fragment Length Polymorphism Analysis. Journal of microbiological methods, 88(1), 14-18.

PRESENTATIONS / MEETINGS ATTENDED

Courtney KC, Zhang C, Zha X. (2015) Membrane dynamics platform presentation: "Very Long Acyl Chain Sphingolipids Prefer a Tail-to-Tail Interdigitation with Cholesterol, which Restricts Microdomain Formation", Biophysical Society (Feb 7-11, 2015), Baltimore, MD.

Courtney KC, Zha X, (2014) Poster presentation: "Cholesterol transbilayer distribution in mammalian cells", Biophysical Society (Feb 15-19, 2014), San Francisco, CA.

Courtney KC, Zha X, (2012) Poster presentation: "Cholesterol transbilayer distribution in mammalian cells", The American Society of Cell Biology (Dec 15-19, 2012), San Francisco.